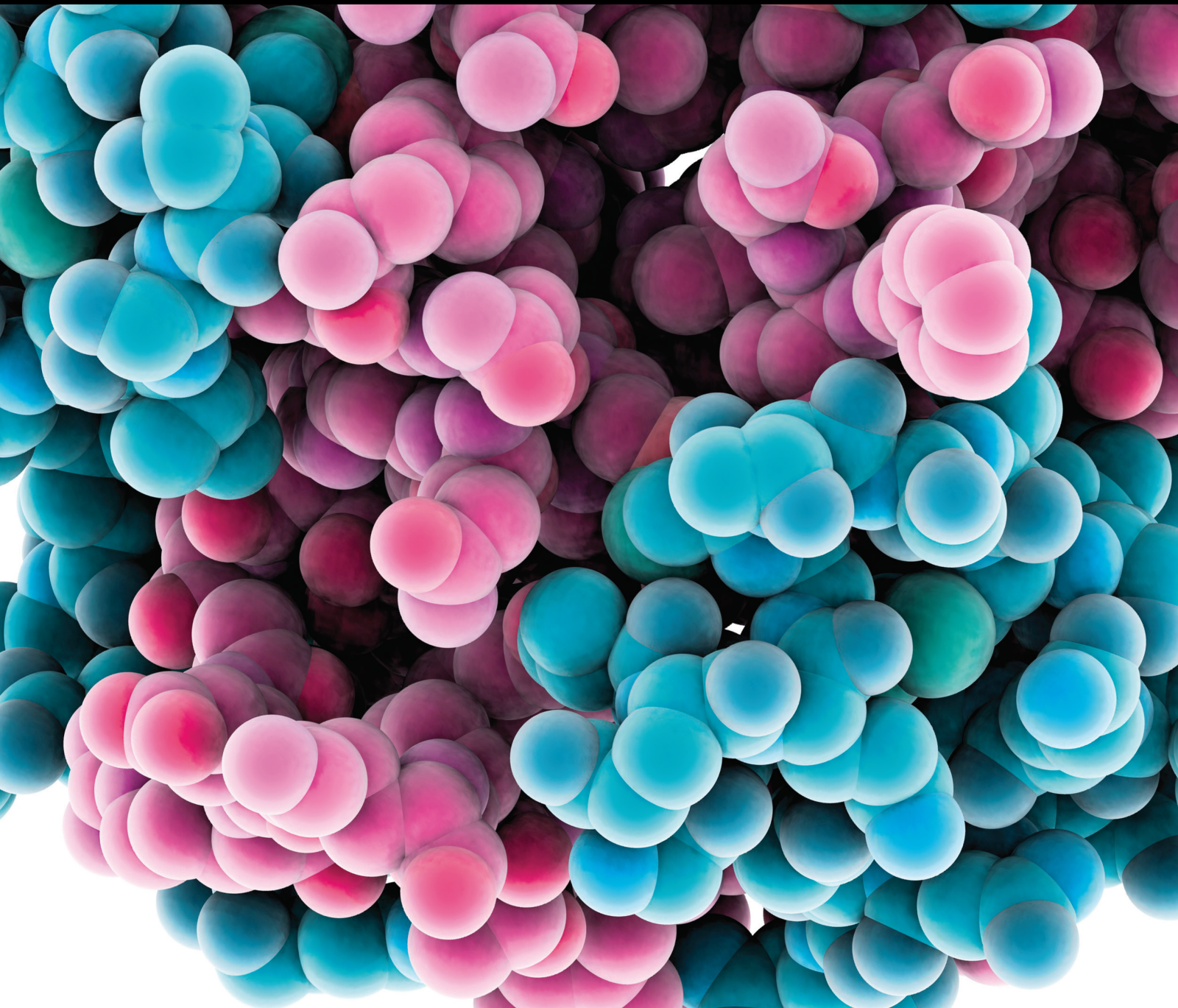# Pathogenesis, Diagnosis, and Treatment of Diabetic Retinopathy

Lead Guest Editor: Rafael Simó
Guest Editors: Alan W. Stitt and Stela Vujosevic

Pathogenesis, Diagnosis, and Treatment of Diabetic Retinopathy

Pathogenesis, Diagnosis, and Treatment of Diabetic Retinopathy

Lead Guest Editor: Rafael Simó
Guest Editors: Alan W. Stitt and Stela Vujosevic

Chief Editor

Contents

Corrigendum

Corrigendum to "Protective Effect of the HIF-1A Pro582Ser Polymorphism on Severe Diabetic Retinopathy"

Neda Rajamand Ekberg,[1,2,3] **Sofie Eliasson,**[2] **Young Wen Li,**[2,4] **Xiaowei Zheng** ⓘ,[2]
Katerina Chatzidionysiou,[1] **Henrik Falhammar** ⓘ,[1,2] **Harvest F. Gu** ⓘ,[5]
and Sergiu-Bogdan Catrina ⓘ[1,2,3]

[1]*Department of Endocrinology Metabolism and Diabetes, Karolinska University Hospital, Stockholm, Sweden*
[2]*Department of Molecular Medicine and Surgery, Karolinska Institutet, Stockholm, Sweden*
[3]*Centrum for Diabetes, Academic Specialist Centrum, Stockholm, Sweden*
[4]*Department of Pharmacology, Guilin Medical University, Guilin, China*
[5]*School of Basic Medicine and Clinical Pharmacy, China Pharmaceutical University, Nanjing, China*

Correspondence should be addressed to Sergiu-Bogdan Catrina; sergiu-bogdan.catrina@ki.se

Received 8 May 2021; Accepted 8 May 2021; Published 26 May 2021

In the article titled "Protective Effect of the HIF-1A Pro582Ser Polymorphism on Severe Diabetic Retinopathy" [1], the sentence "A total of 703 participated in the genetical analysis" in Section 2.1 should be corrected to "A total of 850 patients agreed and gave their informed consent before the enrolment in the study, and a total of 703 participated in the genetical analysis."

The authors clarified that 850 patients were enrolled in the study, but blood samples for the genetic analysis were only available in 703 patients; therefore, the genetic association study was only performed on these 703 patients.

References

[1] N. R. Ekberg, S. Eliasson, Y. W. Li et al., "Protective Effect of the HIF-1A Pro582Ser Polymorphism on Severe Diabetic Retinopathy," *Journal of Diabetes Research*, vol. 2019, Article ID 2936962, 8 pages, 2019.

Research Article

Early Detection of Microvascular Changes in Patients with Diabetes Mellitus without and with Diabetic Retinopathy: Comparison between Different Swept-Source OCT-A Instruments

Stela Vujosevic [iD],[1] **Caterina Toma** [iD],[1] **Edoardo Villani** [iD],[2,3] **Valentina Gatti,**[1]
Marco Brambilla,[4] **Andrea Muraca,**[1] **Maria Chantal Ponziani,**[5] **Gianluca Aimaretti,**[6]
Alessandro Nuzzo,[6] **Paolo Nucci** [iD],[2,3] **and Stefano De Cilla'**[1,7]

[1]*Eye Clinic, University Hospital "Maggiore della Carità", Novara, Italy*
[2]*Department of Clinical Sciences and Community Health, University of Milan, Milan, Italy*
[3]*Eye Clinic, San Giuseppe Hospital, Milan, Italy*
[4]*Department of Medical Physics, University Hospital "Maggiore della Carità", Novara, Italy*
[5]*Diabetology Unit, S.S. Trinità Hospital, Borgomanero, Italy*
[6]*Department of Translational Medicine, Endocrinology, University Hospital "Maggiore della Carità", Novara, Italy*
[7]*Department of Health Sciences, University of East Piedmont "A. Avogadro", Novara, Italy*

Correspondence should be addressed to Stela Vujosevic; stela.vujosevic@gmail.com

Optical coherence tomography angiography (OCT-A) has recently improved the ability to detect subclinical and early clinically visible microvascular changes occurring in patients with diabetes mellitus (DM). The aim of the present study is to evaluate and compare early quantitative changes of macular perfusion parameters in patients with DM without DR and with mild nonproliferative DR (NPDR) evaluated by two different swept-source (SS) OCT-A instruments using two scan protocols (3×3 mm and 6×6 mm). One hundred eleven subjects/eyes were prospectively evaluated: 18 healthy controls (control group), 73 eyes with DM but no DR (no-DR group), and 20 eyes with mild NPDR (DR group). All quantitative analyses were performed using ImageJ and included vessel and perfusion density, area and circularity index of the FAZ, and vascular complexity parameters. The agreement between methods was assessed according to the method of Bland-Altman. A significant decrease in the majority of the considered parameters was found in the DR group versus the controls with both instruments. The results of Bland-Altman analysis showed the presence of a systemic bias between the two instruments with PLEX Elite providing higher values for the majority of the tested parameters when considering 6×6 mm angiocubes and a less definite difference in 3×3 mm angiocubes. In conclusion, this study documents early microvascular changes occurring in the macular region of patients at initial stages of DR, confirmed with both SS OCT-A instruments. The fact that early microvascular alterations could not be detected with one instrument does not necessarily mean that these alterations are not actually present, but this could be an intrinsic limitation of the device itself. Further, larger longitudinal studies are needed to better understand microvascular damage at very early stages of diabetic retinal disease and to define the strengths and weaknesses of different OCT-A devices.

1. Introduction

Diabetic retinopathy (DR) is the most important complication of both type 1 and type 2 diabetes mellitus (DM) [1]. Currently, there is a growing body of scientific evidence indicating that specific neural and vascular retinal modifications can be present even before the onset of clinically visible signs of DR [2–11].

Recent advent of optical coherence tomography angiography (OCT-A), a new noninvasive depth-resolved retinal imaging technique, has allowed a better evaluation of the changes occurring at the macular and peripapillary capillary

networks in patients with DM with or without DR [12–17]. Subclinical and early microvascular changes detected on OCT-A mainly consist of remodeling and enlargement of the foveal avascular zone (FAZ), capillary nonperfusion, and reduced vascular density [10, 12–21], and recently, also venous beading and increased vascular tortuosity were found to be more frequent in the macular region of patients with DM but with no DR versus healthy controls [10].

Several studies were performed using different OCT-A devices, and this could explain some discrepancies in the available results. In fact, even if all OCT-A devices rely on the common principle that erythrocytes could be used as a motion contrast to differentiate vessels from static tissues [22], they use different algorithms for image acquisition and processing and different methods for layer segmentation [23–27]. Recently, Corvi et al. evaluated the reproducibility of quantitative parameters using seven different OCT-A devices in healthy subjects and concluded that the measurements obtained were too different to allow reliable comparisons [28].

The aim of this study is to evaluate and compare early quantitative changes of the macular perfusion parameters in patients with DM without DR and with mild nonproliferative DR (NPDR) by two different swept-source (SS) OCT-A instruments and using two scan protocols (3×3 mm and 6×6 mm).

2. Materials and Methods

2.1. Patients and Study Design. In this prospective cross-sectional comparative case-control study, we consecutively enrolled 111 eyes of 111 subjects, consisting of 18 healthy control eyes (control group), 73 eyes with DM without clinical signs of DR (no-DR group), and 20 eyes with mild NPDR (DR group). The right eye was considered for the analysis, unless a better quality in the left eye images was present. All patients with DM were referred from the Diabetes Unit to the Medical Retina Service, University Hospital "Maggiore della Carità," Novara, Italy, for evaluation. Normal controls were recruited among subjects referring to our clinic for a routine annual examination or for preliminary exams for cataract surgery (the eye that was not planned for surgery was chosen for the study).

Inclusion criteria for the study were as follows: patients over 18 years of age with a diagnosis of type 1 or type 2 DM according to the updated diagnostic criteria by the American Diabetes Association [29] and confirmed by an expert diabetologist (G.A., M.C.P., and A.N.); no signs of DR or signs of mild NPDR on slit-lamp fundus examination with 90D lens (Volk Optical Inc., Mentor, OH, USA) performed by an expert ophthalmologist (S.V.) according to the *International Clinical Diabetic Retinopathy Disease Severity Scale* [30]; and subjects with normal glucose test for the control group. Exclusion criteria were as follows: any retinal disease other than mild NPDR (including diabetic macular edema); any previous intraocular treatment (such as intravitreal injections of anti-VEGF/steroids or retinal laser); cataract surgery within 6 months in the study eye; refractive error of greater than +/−4D; glaucoma or history of

ocular hypertension (IOP > 21 mmHg); neurodegenerative diseases (e.g., multiple sclerosis, Alzheimer's disease, and Parkinson's disease); uncontrolled systemic blood pressure (BP ≥ 120/80 mmHg) [31]; and poor quality of OCT and/or OCT-A images due to significant media opacity or poor patient cooperation.

Anamnestic data were collected for each patient, including type of DM, value of glycated haemoglobin (HbA1c), use of antidiabetic agents (insulin and/or oral hypoglicaemic drugs), use of other drugs for concomitant pathologic conditions (e.g., systemic hypertension, cardiovascular diseases, and rheumatic diseases), and previous ocular or other surgery. Each patient underwent a complete ophthalmologic examination including best-corrected visual acuity (BCVA) determination using the standard Early Treatment Diabetic Retinopathy Study (ETDRS) protocol at 4 meters distance, IOP measurement, slit-lamp dilated fundus examination with 90D lens, and acquisition of color fundus photography of the posterior pole. On the same day, SS-OCT and SS-OCT-A images were acquired with two different instruments.

The study adhered to the tenets of the Declaration of Helsinki and was approved by the institutional Ethics Committee (CE123 2017); each patient approved to participate in the study and signed a written informed consent.

2.2. Imaging

2.2.1. Swept-Source Optical Coherence Tomography and Optical Coherence Tomography Angiography. On the same day, each patient underwent OCT and OCT-A with two different SS instruments, after pupil dilation. The same scanning protocol was used for image acquisition. The devices were prototype PLEX Elite 9000 (Carl Zeiss Meditec Inc., Dublin, California, USA) and DRI OCT-A Triton Plus (Topcon Medical Systems Europe, Milano, Italy). Zeiss PLEX Elite uses a 1,060 nm wavelength, with a scanning speed of 100,000 A-scans/second, and image processing is obtained through the so-called OCT-microangiography complex algorithm (OMAG) [23, 24]. Topcon DRI-OCT uses a 1,050 nm wavelength, with a scanning speed of 100,000 A-scans/second and image processing relying on a motion contrast measure named OCT-A Ratio Analysis (OCTARA) [26]. The acquisition protocol performed included the following scans: a linear 12 mm high-definition B-scan centered on the fovea at 0°, OCT-A maps covering the central 3×3 mm and 6×6 mm macular area. All OCT-A images were carefully reviewed to check automatic segmentations of the superficial capillary plexus (SCP) and deep capillary plexus (DCP), and manual corrections were applied, when necessary, in order to ensure a correct segmentation. For PLEX Elite device, the projections' removal tool was applied for evaluation of DCP. Poor quality images and/or with artifacts were excluded from the analysis.

2.2.2. Quantitative Evaluation of OCT-A Images. Both 3×3 mm and 6×6 mm OCT-A maps were used for quantitative analysis. All images were saved and analyzed in anonymous and masked fashion. The following quantitative parameters

were evaluated: area and circularity index (CI) of the FAZ; perfusion density (PD) and vessel density (VD); and branch analysis including the number of branches (NoB) and total branch length (tBL). All these parameters were evaluated on both SCP and DCP using ImageJ software, version 1.51 (http://imagej.nih.gov/ij/; provided in the public domain by the National Institutes of Health, Bethesda, MD, USA). For DRI-Triton Plus OCT-A, the SCP slab was segmented with an inner boundary at the inner limiting membrane (ILM) +2.6 μm and an outer boundary at the inner plexiform layer (IPL)/inner nuclear layer (INL) +15.6 μm, while the DCP slab was segmented between IPL/INL +15.6 μm and IPL/INL +70.2 μm. For PLEX Elite OCT-A, the SCP slab was segmented between ILM and IPL, while the DCP slab extended from the IPL to the retinal pigment epithelium (RPE fit) −100 μm.

2.2.3. ImageJ Analysis. All DRI-Triton Plus OCT-A images were exported and analyzed with their original resolution of 320×320 pixels (9.4 μm lateral resolution for 3×3 mm images and 18.7 μm lateral resolution for 6×6 mm images). PLEX Elite OCT-A images were exported with their original resolution of 300×300 pixels for 3×3 mm angiocubes (10 μm lateral resolution) and 500×500 pixels for 6×6 mm angiocubes (12 μm lateral resolution) and analyzed after a process of cropping in order to match the DRI-Triton Plus's smaller field of view (images were cropped down by about 10%). All images were then opened in ImageJ analysis software.

The FAZ profile was manually outlined using the freehand selection tool on images of SCP and DCP using a previously published method [32], and the software automatically calculated FAZ perimeter and area. FAZ CI was then measured using the following equation: FAZ CI = $(4\pi \times \text{area})/\text{perimeter}^2$. CI is the expression of the regularity of a shape: the more its value is closer to 1, the more the shape is similar to a perfect circle [31].

Images were then converted into 8-bit files, and the Otsu method of thresholding was applied before automatic measurements were performed, as previously reported [33]. Otsu's method of thresholding uses a bimodal distribution and determines the optimum threshold by minimizing intraclass variance and maximizing interclass variance [34]. PD on SCP and DCP (PDS and PDD) was calculated on binarized images as the ratio between all the perfused area in pixels and the total area of the image in pixels. VD on SCP and DCP (VDS and VDD) was calculated after skeletonization of the binarized image; it is a measure of the statistical length of moving the blood column, as previously described [35]. The process of skeletonization reduces all vessel diameter to 1 pixel; therefore, VD has the advantage of not being influenced by vessel dimension (Figures 1 and 2).

The Analyze Skeleton function of ImageJ was then applied to skeletonized images. This plugin tags all pixels in a skeleton image, counts all their junctions, triple and quadruple points, and branches and then measures the average and maximum lengths [36, 37]. When activating this function, a results table called "Branch information" is created; from this table, we considered only two parameters: tBL

(total sum of the single branches' length in the area) and NoB (number of branches in the area), as previously described in the peripapillary region of patients with DM [17].

2.3. Statistical Analysis. The clinical and demographic variables were compared among the three subject groups using one-way ANOVA. The means of populations were estimated as least square means, which are the best linear estimates for the marginal means in the ANOVA design. In case of an overall statistically significant difference among subject groups, pairwise comparisons among the three groups were done using Scheffé's test.

The ANOVA analyses were performed using statistical version software 6.0 (StatSoft, Inc., Tulsa, OK, USA), using a two-sided type I error rate of $p \leq 0.002$, after Bonferroni's correction for multiple comparisons.

The agreement between methods was assessed according to the method of Bland-Altman [38]. The mean of the differences (bias), the 95% limits of agreement (LAs), and the 95% confidence intervals for the bias and the LAs were calculated. The distribution of the differences was compared with a Kolmogorov-Smirnoff test to check for normality, as a prerequisite for the Bland-Altman method applicability.

3. Results

Of 111 examined subjects/eyes, 73 had no DR (mean age: 51 ± 20.4 years), 20 had mild DR (mean age: 63 ± 14.5 years), and 18 were healthy controls (mean age: 50 ± 21.1 years). There was no significant difference in the mean age among the three groups (one-way ANOVA, $p = 0.06$). Of 93 patients with DM, 38 had type 1 DM and 55 had type 2 DM.

Mean duration of DM was 12.7 ± 10.7 years in the DM with no DR group and 18.3 ± 11.4 in the DR group ($p = 0.049$). Mean value of HbA1c was 7.1 ± 1.1 in the DM with no DR group and 7.6 ± 1.2 in the DR group ($p = 0.055$). Mean BCVA value was 85 ± 0.0 ETDRS letters in the control group, 84.8 ± 1.2 in the DM with no DR group, and 84.3 ± 1.6 in the DR group ($p = 0.15$).

Table 1 shows the mean values of the significant parameters evaluated on 6×6 mm angiocubes in different groups. The following parameters were significantly decreased in the DR group versus controls with both instruments: CI and tBL in the SCP and VD and NoB in the DCP. The FAZ area in the DCP was significantly greater with both instruments in the DR group versus the controls. The following parameters were significantly decreased in the DR group versus controls only with PLEX Elite OCT-A: PD and VD in the SCP and PD, FAZ CI, NoB, and tBL in the DCP. The following parameters were significantly different in the no-DR group versus controls: a decrease in PD and tBL in the DCP and an increase in FAZ area in the DCP detected only with PLEX Elite and a decrease in FAZ CI in the SCP detected only with DRI-Triton Plus.

Table 2 shows the mean values of significant parameters evaluated on 3×3 mm angiocubes in different groups. The following parameters were significantly decreased in the DR group versus controls: PD, VD, CI, and tBL in the DCP with both instruments; NoB in the DCP with only PLEX Elite; and
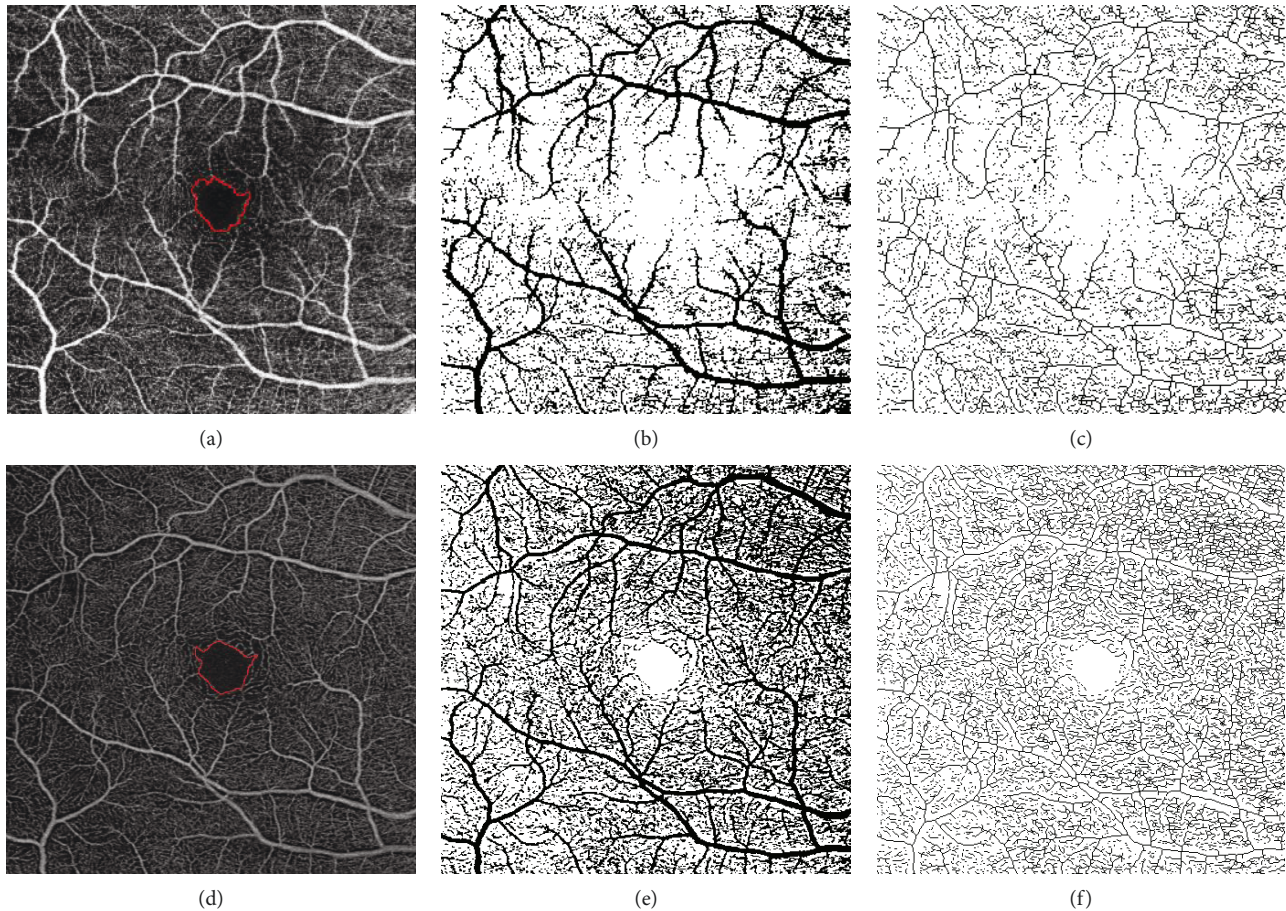
FIGURE 1: ImageJ analysis of 6×6 mm images at the SCP of a patient with DM and without DR. (a–c) SCP image obtained with DRI OCT-A Triton Plus (Topcon Medical Systems Europe, Milano, Italy). (d–f) SCP image obtained with prototype PLEX Elite 9000 (Carl Zeiss Meditec, Inc., Dublin, California, USA). (a, d) Original SCP slabs in which the FAZ profile was manually outlined using the freehand selections tool. (b, e) Binarized images. (c, f) Skeletonized images. SCP: superficial capillary plexus; DM: diabetes mellitus; DR: diabetic retinopathy; OCT-A: OCT angiography; FAZ: foveal avascular zone.

CI in the SCP with only DRI-Triton Plus. FAZ area in the DCP was significantly greater only with PLEX Elite. FAZ CI in the DCP was significantly reduced only with PLEX Elite in no-DR group versus controls.

Table 3 summarizes the results of Bland-Altman analysis for PD, VD, FAZ, NoB, and tBL, showing comparison between the two OCT-A instruments. A systemic bias exists between the two instruments with PLEX Elite providing higher values for all tested parameters, except for FAZ CI in the SCP, when considering 6×6 mm angiocubes. However, when evaluating the 3×3 mm angiocube, the difference between the two instruments is less clear, with PLEX Elite providing higher values only for PD and FAZ area. As representative examples, Figure 3 shows the Bland-Altman plot for VD in 3×3 mm angiocube scans evaluated at the DCP. The width of the LA's interval is quite narrow, amounting to only 31.5% of the mean value, thus indicating a good agreement between the two instruments. Figure 4 shows the Bland-Altman plot for the FAZ area in 6×6 mm angiocube scans evaluated at the DCP. The width of the LAs' interval is wide, amounting to 197.8% of the mean value, thus indicating a poor agreement between the two instruments.

4. Discussion

In the present study, a quantitative evaluation of microvascular changes occurring in the macula in patients with DM with and without clinical signs of DR was performed, using two different SS OCT-A devices and two different angiocube scan sizes. A significant alteration of specific OCT-A parameters was confirmed with both instruments in patients with initial signs of DR when compared to healthy controls.

OCT-A is a method recently introduced in clinical practice that allows for a detailed characterization of retinal microvasculature through the segmentation of individual retinal vascular layers. Recently, Gildea published a review focusing on the diagnostic value of OCT-A in the evaluation of a number of microvascular parameters in patients with diabetes and highlighting the usefulness of this technique in the identification and localization of microaneurysms; visualization of preretinal neovascularization and areas of capillary nonperfusion; detection of FAZ enlargement; and remodeling and quantification of vascular perfusion and branching complexity [39]. However, different OCT-A devices and segmentation methods that have been used as well as different
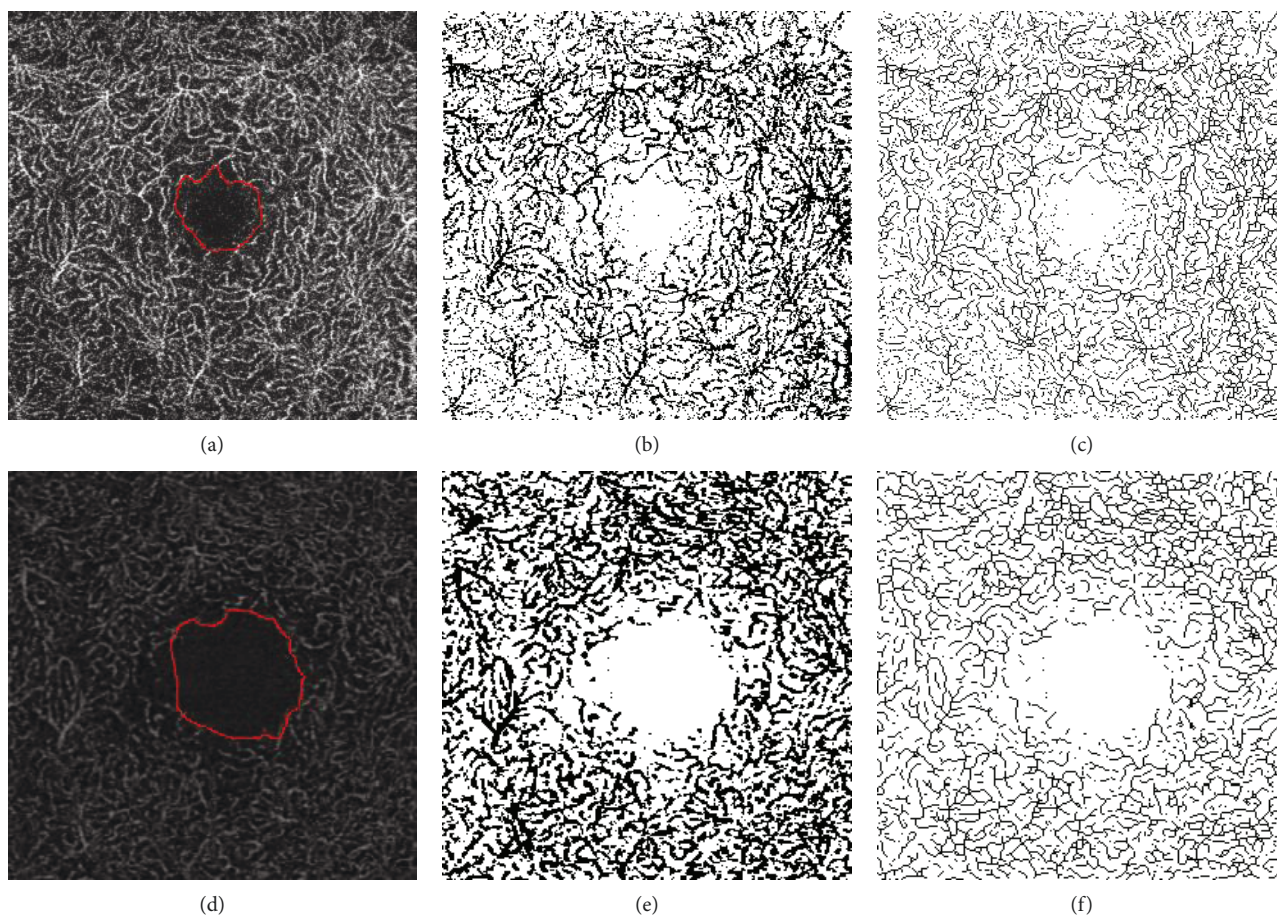
FIGURE 2: ImageJ analysis of 3×3 mm images at the DCP of a patient with DR. (a–c) DCP image obtained with DRI OCT-A Triton Plus (Topcon Medical Systems Europe, Milano, Italy). (d–f) DCP image obtained with prototype PLEX Elite 9000 (Carl Zeiss Meditec, Inc., Dublin, California, USA). (a, d) Original DCP slabs in which the FAZ profile was manually outlined using the freehand selections tool. (b, e) Binarized images. (c, f) Skeletonized images. DCP: deep capillary plexus; DR: diabetic retinopathy; OCT-A: OCT angiography; FAZ: foveal avascular zone.

regions of interest have been analyzed in these studies, making it difficult to draw final conclusions, especially when considering quantitative vascular perfusion parameters such as VD and PD [39]. In particular, the majority of available data are obtained with spectral domain OCT-A devices and just few studies were performed with SS-OCT-A. Swept-source OCT-A devices use a longer wavelength (1050 nm), thus having a better ability to penetrate deeper into the tissues than spectral domain devices that use a shorter wavelength. While many studies reported high intra- and interoperator reproducibility in the evaluation of different OCT-A parameters, both in normal and pathologic eyes, using the same scan type and the same device (in particular, FAZ area evaluation at the SCP and perfusion parameters) [40–47], concerns remain on the results interchangeability when using different scan sizes and devices. Rabiolo et al. recently published a study performed with PLEX Elite, comparing FAZ area and VD measurements in different angiocube scan sizes (3×3, 6×6, and 12×12 mm) after cropping original images to obtain the same size. The authors concluded that FAZ area is a robust parameter even if measured on different angiocubes, while VD depends on image size [47].

Different studies performed with OCT-A focused on FAZ measurement as a marker of microvascular damage, documenting that patients with DM had larger FAZ areas versus healthy controls [10, 12–15, 48]. Different methods for quantitative evaluation of FAZ circularity in DM have been recently proposed [49, 50]. In the present study, CI turned out to be an early parameter showing FAZ changes both in the SCP and DCP. Indeed, a clear decreasing trend was documented from controls to no-DR and DR groups, meaning that FAZ regularity was gradually lost as retinal microvascular damage, induced by DM, progressed.

Moreover, the present study documents a significant decrease in VD and PD in patients with initial signs of DR versus healthy controls. This difference was detected with both instruments. These data are in agreement with previously published studies reporting a significant decrease in VD in the macular region in patients with DR compared to healthy controls [51, 52]. In the present study, both angiocube scans (3×3 mm and 6×6 mm) detected a significant difference in VD and PD evaluated in DCP, while significant differences in the SCP were found only in 6×6 mm scans, in particular, using PLEX Elite OCT-A. Hirano et al. evaluated

TABLE 1: Significant quantitative macular parameters evaluated on 6×6 mm angiocubes.

Parameter	Swept-source OCT-A	Controls ($n = 18$)	no-DR ($n = 73$)	DR ($n = 20$)	p value*
VDD	DRI-Triton	11.2 ± 0.7	10.9 ± 0.7	$10.1 \pm 1.0^{\dagger}$	0.0006
	PLEX Elite	16.2 ± 1.2	14.7 ± 2.8	$13.3 \pm 1.0^{\ddagger}$	0.002
FAZ area DCP	DRI-Triton	0.60 ± 0.17	0.42 ± 0.17	$0.60 \pm 0.25^{\S}$	<0.0001
	PLEX Elite	0.78 ± 0.23	$1.22 \pm 0.32^{\P}$	$1.37 \pm 0.55^{\P}$	<0.0001
FAZ CI SCP	DRI-Triton	0.90 ± 0.04	$0.80 \pm 0.109^{\ddagger}$	$0.68 \pm 0.19^{\P}$	<0.0001
	PLEX Elite	0.83 ± 0.07	0.73 ± 0.09	$0.64 \pm 0.21^{\P}$	<0.0001
NoB SCP	DRI-Triton	3523 ± 341	3232 ± 488	2801 ± 532	0.002
	PLEX Elite	6691 ± 343	6278 ± 631	$5813 \pm 794^{\P}$	0.0002
tBL SCP	DRI-Triton	$1.9 \times 10^7 \pm 4.5 \times 10^6$	$2.4 \times 10^7 \pm 5.7 \times 10^6$	$1.6 \times 10^7 \pm 3.5 \times 10^6$	<0.0001
	PLEX Elite	$4.3 \times 10^7 \pm 3.5 \times 10^6$	$3.9 \times 10^7 \pm 6.3 \times 10^6$	$3.5 \times 10^7 \pm 7.6 \times 10^{6\Delta}$	0.0004
PDS	PLEX Elite	0.39 ± 0.02	0.37 ± 0.04	$0.34 \pm 0.05^{\#}$	0.0004
PDD	PLEX Elite	0.44 ± 0.03	$0.39 \pm 0.03^{\P}$	$0.36 \pm 0.03^{\P,\Delta}$	<0.0001
VDS	PLEX Elite	13.2 ± 0.8	12.4 ± 1.4	$11.4 \pm 1.8^{\dagger}$	0.001
FAZ CI DCP	PLEX Elite	0.83 ± 0.06	0.76 ± 0.10	$0.69 \pm 0.10^{\P}$	<0.0001
NoB DCP	PLEX Elite	8064 ± 944	7621 ± 413	$7128 \pm 469^{\P,\ddagger}$	<0.0001
tBL DCP	PLEX Elite	$5.8 \times 10^7 \pm 8.5 \times 10^6$	$4.9 \times 10^7 \pm 5.3 \times 10^{6\P}$	$4.3 \times 10^7 \pm 4.3 \times 10^{6\P,\|}$	<0.0001

*One-way ANOVA analyses: comparison among controls, patients with DM without DR, and patients with DR. Statistical significance was set at $p = 0.002$ after Bonferroni's correction. Comparison versus controls: †Scheffé's test, $p = 0.001$; ‡Scheffé's test, $p = 0.002$; ¶Scheffé's test, $p < 0.0001$; $^{\#}$Scheffé's test, $p = 0.0004$. Comparison versus patients with DM without DR: §Scheffé's test, $p = 0.002$; $^{\int}$Scheffé's test, $p = 0.0002$; $^{\Delta}$Scheffé's test, $p < 0.0001$; $^{\|}$Scheffé's test, $p = 0.0003$. VDD: vessel density at the deep capillary plexus; FAZ: foveal avascular zone; DCP: deep capillary plexus; CI: circularity index; SCP: superficial capillary plexus; NoB: number of branches; tBL: total branches length; PDS: perfusion density at the superficial capillary plexus; PDD: perfusion density at the deep capillary plexus; VDS: vessel density at the superficial capillary plexus.

TABLE 2: Significant quantitative macular parameters evaluated on 3×3 mm angiocubes.

Parameter	Swept-source OCT-A	Controls ($n = 18$)	no-DR ($n = 73$)	DR ($n = 20$)	p value*
PDD	DRI-Triton	0.31 ± 0.02	0.32 ± 0.02	$0.30 \pm 0.03^{\S}$	0.0001
	PLEX Elite	0.37 ± 0.05	0.36 ± 0.04	$0.31 \pm 0.05^{\#,\ddagger}$	0.0001
VDD	DRI-Triton	18.0 ± 1.3	18.2 ± 1.2	$16.8 \pm 1.4^{\int}$	0.0001
	PLEX Elite	13.5 ± 1.9	12.8 ± 1.4	$11.2 \pm 1.8^{\dagger,\|}$	0.0001
FAZ CI DCP	DRI-Triton	0.75 ± 0.08	0.75 ± 0.09	$0.65 \pm 0.19^{**}$	0.001
	PLEX Elite	0.82 ± 0.05	$0.67 \pm 0.13^{\P}$	$0.64 \pm 0.11^{\P}$	<0.0001
tBL DCP	DRI-Triton	$2.1 \times 10^7 \pm 1.9 \times 10^6$	$2.2 \times 10^7 \pm 2.1 \times 10^6$	$2.0 \times 10^7 \pm 2.4 \times 10^{6\int\int}$	0.0007
	PLEX Elite	$1.3 \times 10^7 \pm 2.3 \times 10^6$	$1.2 \times 10^7 \pm 1.7 \times 10^6$	$1.1 \times 10^7 \pm 1.8 \times 10^{6\ddagger\ddagger}$	0.0007
FAZ CI SCP	DRI-Triton	0.72 ± 0.09	0.73 ± 0.12	$0.57 \pm 0.20^{**,\Delta}$	0.002
FAZ area DCP	PLEX Elite	1.06 ± 0.25	1.37 ± 0.32	$1.54 \pm 0.54^{\#}$	0.0003
NoB DCP	PLEX Elite	1861 ± 282	1765 ± 220	$1551 \pm 216^{\P\P,\S}$	0.0002

*One-way ANOVA analyses: comparison among controls, patients with DM without DR and patients with DR. Statistical significance was set at $p = 0.002$ after Bonferroni's correction. Comparison versus controls: $^{\#}$Scheffé's test, $p = 0.0003$; †Scheffé's test, $p = 0.0001$; **Scheffé's test, $p = 0.002$; ¶Scheffé's test, $p < 0.0001$; ‡‡Scheffé's test, $p = 0.001$; ¶¶Scheffé's test, $p = 0.0004$. Comparison versus patients with DM without DR: §Scheffé's test, $p = 0.002$; ‡Scheffé's test, $p = 0.0006$; $^{\int}$Scheffé's test, $p = 0.0001$; $^{\|}$Scheffé's test, $p = 0.001$; $^{\int\int}$Scheffé's test, $p = 0.0009$; $^{\Delta}$Scheffé's test, $p < 0.0001$. PDD: perfusion density at the deep capillary plexus; VDD: vessel density at the deep capillary plexus; FAZ: foveal avascular zone; CI: circularity index; DCP: deep capillary plexus; tBL: total branches length; SCP: superficial capillary plexus; NoB: number of branches.

PD and VD on different scan sizes (3×3, 6×6, and 12×12 mm) using PLEX Elite [53]. The results are partially in agreement with our data, reporting a significant decrease in both PD and VD on all scan sizes between healthy controls and eyes with DR, but no significant differences between healthy and diabetic eyes without DR. However, different from what we found, these differences were described both in the DCP and SCP even on 3×3 mm images [53].

We would like to point out that two aspects should be considered when discussing the findings reported in the

TABLE 3: Results of Bland-Altman analysis for PD, VD, FAZ, NoB, and tBL for comparisons between methods A (DRI-Triton) and B (PLEX Elite).

Parameter	Bias* [95% CI]	Lower LA [95% CI]	Upper LA [95% CI]	LA interval (%)**
PD				
3 × 3 SCP	0.091 [0.083, 0.098]	0.01 [0.00, 0.03]	0.17 [0.15, 0.20]	47.8
3 × 3 DCP	0.033 [0.026, 0.041]	-0.04 [-0.06, -0.03]	0.11 [0.10, 0.12]	44.8
6 × 6 SCP	0.11 [0.097, 0.114]	0.02 [0.004, 0,03]	0.19 [0.18, 0.21]	53.9
6 × 6 DCP	0.087 [0.080, 0.094]	0.01 [0.00, 0.03]	0.16 [0.15, 0.20]	42.3
VD				
3 × 3 SCP	-0.6 [-0.95, -0.25]	-4.2 [-4.8, -3.6]	3.0 [2.4, 3.6]	51.5
3 × 3 DCP	-5.3 [-5.5, -5.1]	-7.7 [-8.1, -7.3]	-2.9 [-3.3, -2.5]	31.5
6 × 6 SCP	4.5 [4.3,4.7]	2.3 [2.0, 2.7]	6.6 [6.3, 7.0]	42.7
6 × 6 DCP	3,8 [3.6,4.0]	1.5 [1.1, 1.9]	6.1 [5.7, 6.4]	36.1
FAZ				
Area 3 × 3 SCP	0.03 [0.00, 0.6]	-0.28 [-0.33, -0.22]	0.33 [0.28, 0.38]	191.1
Area 3 × 3 DCP	0.85 [0.78, 0.91]	0.20 [0.09, 0.31]	1.49 [1.38, 1.60]	138.9
Area 6 × 6 SCP	0.01 [-0.01, 0.03]	-0.19 [-0.22, -0.16]	0.020 [0.17, 0.24]	125.2
Area 6 × 6 DCP	0.69 [0.61, 0.77]	-0.14 [-0.28, 0.00]	1.51 [1.37, 1.65]	197.8
CI 3 × 3 SCP	-0.05 [-0.07, -0.02]	-0.31 [-0.36, -0.27]	0.22 [0.17, 0.26]	76.7
CI 3 × 3 DCP	-0.06 [-0.09, -0.03]	-0.36 [-0.41, -0.31]	0.24 [0.19, 0.30]	83.8
CI 6 × 6 SCP	-0.06 [-0.08, -0.05]	-0.27 [-0.30, -0.23]	0.14 [0.10, 0.17]	51.8
CI 6 × 6 DCP	0.04 [0.00, 0.07]	-0.29 [-0.34, -0.23]	0.36 [0.30, 0.41]	87.2
NoB				
3x3 SCP	-732 [-795, -669]	-1378 [-1487, -1269]	-85 [-194, 24]	57.2
3 × 3 DCP	-1681 [-1713, -1648]	-2015 [-2072, -1959]	-1346 [-1403, -1290]	25.9
6 × 6 SCP	3104 [3006, 3202]	2098 [1929, 2268]	4110 [3940, 4279]	42.7
6 × 6 DCP	3029 [2902, 3157]	1717 [1496, 1938]	0.36 [4120, 4562]	43.0
tBL				
3 × 3 SCP	-2.9×10^6 [-3.4×10^6, -2.4×10^6]	-7.7×10^6 [-8.5×10^6, -6.9×10^6]	1.9×10^6 [$1.1 \times 10^6, 2.7 \times 10^6$]	68.7
3 × 3 DCP	-9.5×10^6 [-9.9×10^6, -9.1×10^6]	-13.6×10^6 [-14.3×10^6, -12.9×10^6]	-5.4×10^6 [-6.1×10^6, -4.7×10^6]	49.3

TABLE 3: Continued.

Parameter	Bias* [95% CI]	Lower LA [95% CI]	Upper LA [95% CI]	LA interval (%)**
6×6 SCP	17.5×10^6 $[15.9 \times 10^6, 19.1 \times 10^6]$	1.1×10^6 $[-1.6 \times 10^6, 3.9 \times 10^6]$	33.9×10^6 $[31.1 \times 10^6, 36.6 \times 10^6]$	107.3
6×6 DCP	16.1×10^6 $[14.3 \times 10^6, 17.8 \times 10^6]$	-2.3×10^6 $[-5.4 \times 10^6, 0.8 \times 10^6]$	33.9×10^6 $[31.3 \times 10^6, 37.5 \times 10^6]$	88.3

*Comparisons were always performed considering the difference between method B (PLEX Elite) and method A (DRI-Triton). Thus, a positive bias means PLEX Elite mean values are greater than those of DRI-Triton's. **LA interval was calculated and the ratio between the amplitude of the interval (difference between upper LA and lower LA) and the mean value of the considered parameter in percentage. PD: perfusion density; SCP: superficial capillary plexus; DCP: deep capillary plexus; VD: vessel density; FAZ: foveal avascular zone; CI: circularity index; NoB: number of branches; tBL: total branches length; LA: limits of agreement.
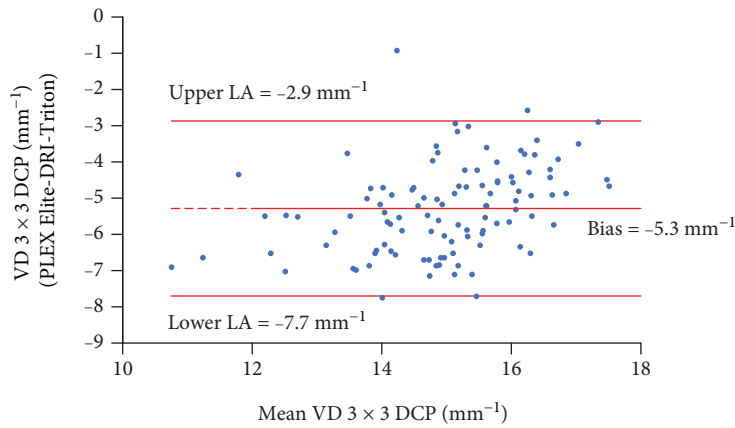
FIGURE 3: Bland-Altman plot for VD in 3×3 mm angiocube scans evaluated at the DCP measured with PLEX Elite and DRI-Triton. The central line indicates the mean of the differences or bias; the upper and lower lines indicate the upper and lower limits of agreement (LA), respectively. VD: vessel density; DCP: deep capillary plexus.
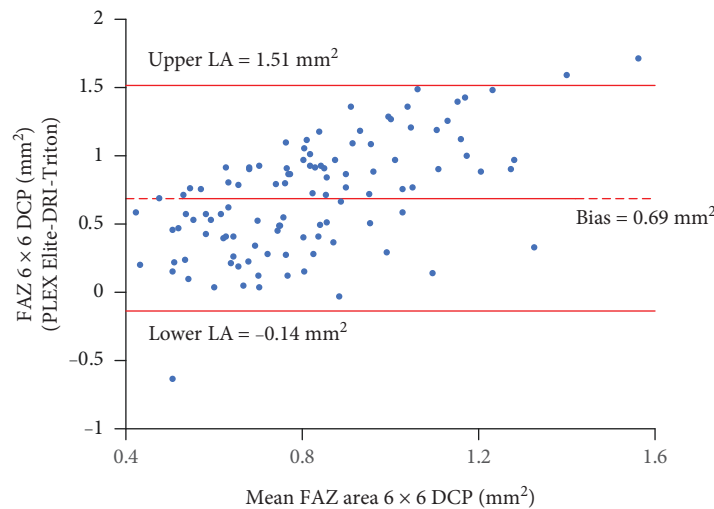
FIGURE 4: Bland-Altman plot for the FAZ area in 6×6 mm angiocube scans evaluated at the DCP measured with PLEX Elite and DRI-Triton. The central line indicates the mean of the differences or bias; the upper and lower lines indicate the upper and lower limits of agreement (LA), respectively. DCP: deep capillary plexus.

present study. First of all, the two devices use different segmentation methods and have different resolutions. In particular, lateral resolution of the two instruments is similar for the 3×3 mm images, while the lateral resolution of PLEX Elite's 6×6 mm images is significantly higher compared to that of 6×6 mm images acquired

with DRI-Triton Plus device. This could explain why PLEX Elite was able to detect significant changes not only in 3×3 mm but also in 6×6 mm images.

Another important consideration that should be made is that our analysis of 6×6 mm images (obtained with PLEX Elite) allowed detecting changes occurring not only in the DCP but also in the SCP. Recent studies performed with OCT-A suggest that changes induced by DM first occur in the DCP and then involve the SCP with disease progression [54–56]. This may be due to a higher density of smaller vessels (more susceptible to hypoxic damage) in the DCP compared to the SCP [57, 58]. Based on our results, we could confirm that lesions induced by diabetes were firstly detectable at the DCP and secondly at the SCP. As the decrease in macular perfusion parameters at SCP level was detected, only on 6×6 mm angiocubes and not on 3×3 mm angiocubes, we may hypothesize that lesions at the SCP start from a more peripheral macular area and then involve into the inner perifoveal region (more central area). This would need to be confirmed with further studies.

Lastly, in this study, we found a significant reduction in NoB and tBL in patients with DR compared to healthy controls in the macular region. To the best of our knowledge, this is the first study to perform this kind of automatic evaluation of vessel complexity in the macular region. Previously, the same method was used to investigate the peripapillary region of patients with diabetes, finding a significant reduction also in patients with DM without clinical signs of DR when compared to healthy controls [17]. It is hypothesized that NoB and tBL reduction could be a consequence of loss of small branching vessels resulting in reduced branching complexity of retinal vasculature [17, 38]. Previously published studies on OCT-A used a different method, called fractal dimension (FD), to analyze the complexity of retinal microvasculature in the macular region [35, 51, 55, 59–62]. FD was significantly altered in patients with DM when compared to healthy subjects and seemed to be associated with increasing severity of DR [35, 51, 55, 59–62]. Therefore, these studies support the hypothesis that the complexity of microvascular network progressively decreases with increasing severity of DR [35, 51, 55, 59–62].

We performed a Bland-Altman analysis to assess the agreement between the two OCT-A devices used in the present study. We found that the agreement between the two instruments was extremely variable depending on the parameter taken into account. Indeed, LA intervals ranged from acceptable values of ≤50% for some parameters (such as PD and VD) to very high values for some other parameters. In particular, LA intervals > 100% were detected for FAZ area and were probably due to the fact that this was the only parameter evaluated in a noncompletely automatic way (FAZ profile was manually outlined using ImageJ). In addition, the two instruments use different segmentation boundaries to delineate SCP and DCP.

The major limitations of this study include the small sample size of patients with multiple comparisons and the lack of homogeneity in the number of different study groups. However, we decided to use Bonferroni's correction for multiple comparisons in order to reduce the risk of having false-positive results, strengthening the validity of our results. In addition, the power of the study is given by the size of the smallest group (control group); thus, the difference in the group numbers should not influence the final results.

In conclusion, this study documents early microvascular changes occurring in the macular region of patients at the initial stages of DR. These changes were confirmed with both SS OCT-A instruments. Based on these results, we would suggest to perform 3×3 mm macular angiocube scans when using DRI-Triton Plus OCT-A, due to its higher resolution. On the other hand, PLEX Elite 6×6 mm angiocube scans seem to detect earlier vascular perfusion changes. Therefore, we should be careful in the evaluation of OCT-A results obtained with different devices: the fact that early microvascular alterations could not be seen does not necessarily mean that these alterations are not actually present, but this could be an intrinsic limitation of the device itself. Further, larger longitudinal studies are needed to better understand the exact extent of microvascular damage in very early stages of diabetic retinal disease and to precisely define the strengths and weaknesses of different OCT-A devices and different scan protocols.

Data Availability

The data used to support the findings of this study are included within the article.

Disclosure

This study was partially presented at the 29th EASDec Annual Meeting 2019, 16th-18th of May, Amsterdam, Netherlands.

Conflicts of Interest

The authors declare that there is no conflict of interest regarding the publication of this paper.

References

[1] J. W. Y. Yau, S. L. Rogers, R. Kawasaki et al., "Global prevalence and major risk factors of diabetic retinopathy," *Diabetes Care*, vol. 35, no. 3, pp. 556–564, 2012.

[2] T. W. Gardner, S. F. Abcouwer, A. J. Barber, and G. R. Jackson, "An integrated approach to diabetic retinopathy research," *Archives of Ophthalmology*, vol. 129, no. 2, pp. 230–235, 2011.

[3] A. M. Joussen, V. Poulaki, W. Qin et al., "Retinal vascular endothelial growth factor induces intercellular adhesion molecule-1 and endothelial nitric oxide synthase expression and initiates early diabetic retinal leukocyte adhesion in vivo," *The American Journal of Pathology*, vol. 160, no. 2, pp. 501–509, 2002.

[4] P. M. Martin, P. Roon, T. K. van Ells, V. Ganapathy, and S. B. Smith, "Death of retinal neurons in streptozotocin-induced diabetic mice," *Investigative Opthalmology & Visual Science*, vol. 45, no. 9, pp. 3330–3336, 2004.

[5] A. Lecleire-Collet, L. H. Tessier, P. Massin et al., "Advanced glycation end products can induce glial reaction and neuronal

degeneration in retinal explants," *British Journal of Ophthalmology*, vol. 89, no. 12, pp. 1631–1633, 2005.

[6] D. A. Antonetti, A. J. Barber, S. K. Bronson et al., "Diabetic retinopathy: seeing beyond glucose-induced microvascular disease," *Diabetes*, vol. 55, no. 9, pp. 2401–2411, 2006.

[7] J. C. Y. Lung, P. G. Swann, D. S. H. Wong, and H. H. L. Chan, "Global flash multifocal electroretinogram: early detection of local functional changes and its correlations with optical coherence tomography and visual field tests in diabetic eyes," *Documenta Ophthalmologica*, vol. 125, no. 2, pp. 123–135, 2012.

[8] S. Vujosevic, A. Micera, S. Bini, M. Berton, G. Esposito, and E. Midena, "Proteome analysis of retinal glia cells-related inflammatory cytokines in the aqueous humour of diabetic patients," *Acta Ophthalmologica*, vol. 94, no. 1, pp. 56–64, 2016.

[9] S. Vujosevic, A. Micera, S. Bini, M. Berton, G. Esposito, and E. Midena, "Aqueous humor biomarkers of Müller cell activation in diabetic eyes," *Investigative Opthalmology & Visual Science*, vol. 56, no. 6, pp. 3913–3918, 2015.

[10] S. Vujosevic, A. Muraca, M. Alkabes et al., "Early microvascular and neural changes in patients with type 1 and type 2 diabetes mellitus without clinical signs of diabetic retinopathy," *Retina*, vol. 39, no. 3, pp. 435–445, 2019.

[11] E. H. Sohn, H. W. van Dijk, C. Jiao et al., "Retinal neurodegeneration may precede microvascular changes characteristic of diabetic retinopathy in diabetes mellitus," *Proceedings of the National Academy of Sciences of the United States of America*, vol. 113, no. 19, pp. E2655–E2664, 2016.

[12] T. E. de Carlo, A. T. Chin, M. A. Bonini Filho et al., "Detection of microvascular changes in eyes of patients with diabetes but not clinical diabetic retinopathy using optical coherence tomography angiography," *Retina*, vol. 35, no. 11, pp. 2364–2370, 2015.

[13] G. Dimitrova, E. Chihara, H. Takahashi, H. Amano, and K. Okazaki, "Quantitative retinal optical coherence tomography angiography in patients with diabetes without diabetic retinopathy," *Investigative Opthalmology & Visual Science*, vol. 58, no. 1, pp. 190–196, 2017.

[14] G. Di, Y. Weihong, Z. Xiao et al., "A morphological study of the foveal avascular zone in patients with diabetes mellitus using optical coherence tomography angiography," *Graefe's Archive for Clinical and Experimental Ophthalmology*, vol. 254, no. 5, pp. 873–879, 2016.

[15] N. Takase, M. Nozaki, A. Kato, H. Ozeki, M. Yoshida, and Y. Ogura, "Enlargement of foveal avascular zone in diabetic eyes evaluated by en face optical coherence tomography angiography," *Retina*, vol. 35, no. 11, pp. 2377–2383, 2015.

[16] D. Cao, D. Yang, Z. Huang et al., "Optical coherence tomography angiography discerns preclinical diabetic retinopathy in eyes of patients with type 2 diabetes without clinical diabetic retinopathy," *Acta Diabetologica*, vol. 55, no. 5, pp. 469–477, 2018.

[17] S. Vujosevic, A. Muraca, V. Gatti et al., "Peripapillary microvascular and neural changes in diabetes mellitus: an OCT-angiography study," *Investigative Opthalmology & Visual Science*, vol. 59, no. 12, pp. 5074–5081, 2018.

[18] D.-H. Lee, H. C. Yi, S. H. Bae, J. H. Cho, S. W. Choi, and H. Kim, "Risk factors for retinal microvascular impairment in type 2 diabetic patients without diabetic retinopathy," *PLoS One*, vol. 13, no. 8, article e0202103, 2018.

[19] K. Kim, E. S. Kim, and S. Y. Yu, "Optical coherence tomography angiography analysis of foveal microvascular changes and inner retinal layer thinning in patients with diabetes," *British Journal of Ophthalmology*, vol. 102, no. 9, pp. 1226–1231, 2018.

[20] F. Scarinci, F. Picconi, G. Virgili et al., "Single retinal layer evaluation in patients with type 1 diabetes with no or early signs of diabetic retinopathy: the first hint of neurovascular crosstalk damage between neurons and capillaries?," *Ophthalmologica*, vol. 237, no. 4, pp. 223–231, 2017.

[21] J. M. Simonett, F. Scarinci, F. Picconi et al., "Early microvascular retinal changes in optical coherence tomography angiography in patients with type 1 diabetes mellitus," *Acta Ophthalmologica*, vol. 95, no. 8, pp. e751–e755, 2017.

[22] A. Rabiolo, A. Carnevali, F. Bandello, and G. Querques, "Optical coherence tomography angiography: evolution or revolution?," *Expert Review of Ophthalmology*, vol. 11, no. 4, pp. 243–245, 2016.

[23] P. J. Rosenfeld, M. K. Durbin, L. Roisman et al., "ZEISS Angioplex™ spectral domain optical coherence tomography angiography: technical aspects," *Developments in Ophthalmology*, vol. 56, pp. 18–29, 2016.

[24] A. R. Miller, L. Roisman, Q. Zhang et al., "Comparison between spectral-domain and swept-source optical coherence tomography angiographic imaging of choroidal neovascularization," *Investigative Opthalmology & Visual Science*, vol. 58, no. 3, pp. 1499–1505, 2017.

[25] D. Huang, Y. Jia, S. S. Gao, B. Lumbroso, and M. Rispoli, "Optical coherence tomography angiography using the Optovue device," *Developments in Ophthalmology*, vol. 56, pp. 6–12, 2016.

[26] Y. Huang, Q. Zhang, M. R. Thorell et al., "Swept-source OCT angiography of the retinal vasculature using intensity differentiation-based optical microangiography algorithms," *Ophthalmic Surgery, Lasers and Imaging Retina*, vol. 45, no. 5, pp. 382–389, 2014.

[27] G. Coscas, M. Lupidi, and F. Coscas, "Heidelberg spectralis optical coherence tomography angiography: technical aspects," *Developments in Ophthalmology*, vol. 56, pp. 1–5, 2016.

[28] F. Corvi, M. Pellegrini, S. Erba, M. Cozzi, G. Staurenghi, and A. Giani, "Reproducibility of vessel density, fractal dimension, and foveal avascular zone using 7 different optical coherence tomography angiography devices," *American Journal of Ophthalmology*, vol. 186, pp. 25–31, 2018.

[29] American Diabetes Association, "2. Classification and diagnosis of diabetes: standards of medical care in diabetes—2019," *Diabetes Care*, vol. 42, Supplement 1, pp. S13–S28, 2018.

[30] C. P. Wilkinson, F. L. Ferris 3rd, R. E. Klein et al., "Proposed international clinical diabetic retinopathy and diabetic macular edema disease severity scales," *Ophthalmology*, vol. 110, no. 9, pp. 1677–1682, 2003.

[31] G. Mancia, R. Fagard, K. Narkiewicz et al., "2013 ESH/ESC guidelines for the management of arterial hypertension: the Task Force for the management of arterial hypertension of the European Society of Hypertension (ESH) and of the European Society of Cardiology (ESC)," *European Heart Journal*, vol. 34, no. 28, pp. 2159–2219, 2013.

[32] J. Choi, J. Kwon, J. W. Shin, J. Lee, S. Lee, and M. S. Kook, "Quantitative optical coherence tomography angiography of macular vascular structure and foveal avascular zone in glaucoma," *PloS One*, vol. 12, no. 9, article e0184948, 2017.

[33] M. Al-Sheikh, N. Phasukkijwatana, R. Dolz-Marco et al., "Quantitative OCT angiography of the retinal microvasculature and the choriocapillaris in myopic eyes," *Investigative Opthalmology & Visual Science*, vol. 58, no. 4, pp. 2063–2069, 2017.

[34] C. A. Schneider, W. S. Rasband, and K. W. Eliceiri, "NIH Image to ImageJ: 25 years of image analysis," *Nature Methods*, vol. 9, no. 7, pp. 671–675, 2012.

[35] R. Reif, J. Qin, L. An, Z. Zhi, S. Dziennis, and R. Wang, "Quantifying optical microangiography images obtained from a spectral domain optical coherence tomography system," *International Journal of Biomedical Imaging*, vol. 2012, Article ID 509783, 11 pages, 2012.

[36] I. Arganda-Carreras, R. Fernández-González, A. Muñoz-Barrutia, and C. Ortiz-De-Solorzano, "3D reconstruction of histological sections: application to mammary gland tissue," *Microscopy Research and Technique*, vol. 73, no. 11, pp. 1019–1029, 2010.

[37] G. Polder, H. L. E. Hovens, A. J. Zweers, A. Jahnen, C. Moll, and A. J. F. Kennedy, "Measuring shoot length of submerged aquatic plants using graph analysis," in *Proceedings of the ImageJ User and Developer Conference 2010*, pp. 172–177, Luxembourg, October 2010.

[38] J. M. Bland and D. G. Altman, "Statistical methods for assessing agreement between two methods of clinical measurement," *The Lancet*, vol. 1, no. 8476, pp. 307–310, 1986.

[39] D. Gildea, "The diagnostic value of optical coherence tomography angiography in diabetic retinopathy: a systematic review," *International Ophthalmology*, pp. 1–21, 2018.

[40] M. Al-Sheikh, T. C. Tepelus, T. Nazikyan, and S. V. R. Sadda, "Repeatability of automated vessel density measurements using optical coherence tomography angiography," *British Journal of Ophthalmology*, vol. 101, no. 4, pp. 449–452, 2017.

[41] P. Carpineto, R. Mastropasqua, G. Marchini, L. Toto, M. Di Nicola, and L. Di Antonio, "Reproducibility and repeatability of foveal avascular zone measurements in healthy subjects by optical coherence tomography angiography," *British Journal of Ophthalmology*, vol. 100, no. 5, pp. 671–676, 2016.

[42] J. Guo, X. She, X. Liu, and X. Sun, "Repeatability and reproducibility of foveal avascular zone area measurements using AngioPlex spectral domain optical coherence tomography angiography in healthy subjects," *Ophthalmologica*, vol. 237, no. 1, pp. 21–28, 2017.

[43] C. La Spina, A. Carnevali, A. Marchese, G. Querques, and F. Bandello, "Reproducibility and reliability of optical coherence tomography angiography for foveal avascular zone evaluation and measurement in different settings," *Retina*, vol. 37, no. 9, pp. 1636–1641, 2017.

[44] R. Mastropasqua, L. Toto, P. A. Mattei et al., "Reproducibility and repeatability of foveal avascular zone area measurements using swept-source optical coherence tomography angiography in healthy subjects," *European Journal of Ophthalmology*, vol. 27, no. 3, pp. 336–341, 2017.

[45] A. Shahlaee, M. Pefkianaki, J. Hsu, and A. C. Ho, "Measurement of foveal avascular zone dimensions and its reliability in healthy eyes using optical coherence tomography angiography," *American Journal of Ophthalmology*, vol. 161, pp. 50–55.e1, 2016.

[46] Q. You, W. R. Freeman, R. N. Weinreb et al., "Reproducibility of vessel density measurement with optical coherence tomography angiography in eyes with and without retinopathy," *Retina*, vol. 37, no. 8, pp. 1475–1482, 2017.

[47] A. Rabiolo, F. Gelormini, A. Marchese et al., "Macular perfusion parameters in different angiocube sizes: does the size matter in quantitative optical coherence tomography angiography?," *Investigative Opthalmology & Visual Science*, vol. 59, no. 1, pp. 231–237, 2018.

[48] M. Al-Sheikh, H. Akil, M. Pfau, and S. V. R. Sadda, "Swept-source OCT angiography imaging of the foveal avascular zone and macular capillary network density in diabetic retinopathy," *Investigative Opthalmology & Visual Science*, vol. 57, no. 8, pp. 3907–3913, 2016.

[49] M. Alam, Y. Zhang, J. I. Lim, R. V. P. Chan, M. Yang, and X. Yao, "Quantitative optical coherence tomography angiography features for objective classification and staging of diabetic retinopathy," *Retina*, p. 1, 2018.

[50] B. D. Krawitz, S. Mo, L. S. Geyman et al., "Acircularity index and axis ratio of the foveal avascular zone in diabetic eyes and healthy controls measured by optical coherence tomography angiography," *Vision Research*, vol. 139, pp. 177–186, 2017.

[51] A. Y. Kim, Z. Chu, A. Shahidzadeh, R. K. Wang, C. A. Puliafito, and A. H. Kashani, "Quantifying microvascular density and morphology in diabetic retinopathy using spectral-domain optical coherence tomography angiography," *Investigative Opthalmology & Visual Science*, vol. 57, no. 9, pp. OCT362–OCT370, 2016.

[52] S. A. Agemy, N. K. Scripsema, C. M. Shah et al., "Retinal vascular perfusion density mapping using optical coherence tomography angiography in normals and diabetic retinopathy patients," *Retina*, vol. 35, no. 11, pp. 2353–2363, 2015.

[53] T. Hirano, J. Kitahara, Y. Toriyama, H. Kasamatsu, T. Murata, and S. Sadda, "Quantifying vascular density and morphology using different swept-source optical coherence tomography angiographic scan patterns in diabetic retinopathy," *British Journal of Ophthalmology*, vol. 103, no. 2, pp. 216–221, 2019.

[54] M. Kim, S. Y. Choi, and Y. H. Park, "Quantitative analysis of retinal and choroidal microvascular changes in patients with diabetes," *Scientific Reports*, vol. 8, no. 1, article 12146, 2018.

[55] Q. Chen, Q. Ma, C. Wu et al., "Macular vascular fractal dimension in the deep capillary layer as an early indicator of microvascular loss for retinopathy in type 2 diabetic patients," *Investigative Opthalmology & Visual Science*, vol. 58, no. 9, pp. 3785–3794, 2017.

[56] M. Ashraf, P. L. Nesper, L. M. Jampol, F. Yu, and A. A. Fawzi, "Statistical model of optical coherence tomography angiography parameters that correlate with severity of diabetic retinopathy," *Investigative Opthalmology & Visual Science*, vol. 59, no. 10, pp. 4292–4298, 2018.

[57] M. C. Savastano, B. Lumbroso, and M. Rispoli, "In vivo characterization of retinal vascularization morphology using optical coherence tomography angiography," *Retina*, vol. 35, no. 11, pp. 2196–2203, 2015.

[58] S. McLenachan, A. L. Magno, D. Ramos et al., "Angiography reveals novel features of the retinal vasculature in healthy and diabetic mice," *Experimental Eye Research*, vol. 138, pp. 6–21, 2015.

[59] S. Zahid, R. Dolz-Marco, K. B. Freund et al., "Fractal dimensional analysis of optical coherence tomography angiography in eyes with diabetic retinopathy," *Investigative Opthalmology & Visual Science*, vol. 57, no. 11, pp. 4940–4947, 2016.

[60] F. Y. Tang, D. S. Ng, A. Lam et al., "Determinants of quantitative optical coherence tomography angiography metrics in

patients with diabetes," *Scientific Reports*, vol. 7, no. 1, article 2575, 2017.

[61] S. Bhardwaj, E. Tsui, S. Zahid et al., "Value of fractal analysis of optical coherence tomography angiography in various stages of diabetic retinopathy," *Retina*, vol. 38, no. 9, pp. 1816–1823, 2018.

[62] T. Zhu, J. Ma, J. Li et al., "Multifractal and lacunarity analyses of microvascular morphology in eyes with diabetic retinopathy: a projection artifact resolved optical coherence tomography angiography study," *Microcirculation*, vol. 26, no. 3, article e12519, 2019.

Research Article

Protective Effect of the *HIF-1A* Pro582Ser Polymorphism on Severe Diabetic Retinopathy

Neda Rajamand Ekberg,[1,2,3] **Sofie Eliasson,**[2] **Young Wen Li,**[2,4] **Xiaowei Zheng,**[2]
Katerina Chatzidionysiou,[1] **Henrik Falhammar** (ID) **,**[1,2] **Harvest F. Gu,**[5]
and Sergiu-Bogdan Catrina (ID)[1,2,3]

[1]*Department of Endocrinology Metabolism and Diabetes, Karolinska University Hospital, Stockholm, Sweden*
[2]*Department of Molecular Medicine and Surgery, Karolinska Institutet, Stockholm, Sweden*
[3]*Centrum for Diabetes, Academic Specialist Centrum, Stockholm, Sweden*
[4]*Department of Pharmacology, Guilin Medical University, Guilin, China*
[5]*School of Basic Medicine and Clinical Pharmacy, China Pharmaceutical University, Nanjing, China*

Correspondence should be addressed to Sergiu-Bogdan Catrina; sergiu-bogdan.catrina@ki.se

Received 21 January 2019; Accepted 18 April 2019; Published 12 May 2019

Guest Editor: Rafael Simó

Objective. Hypoxia is central in the pathogenesis of diabetic retinopathy (DR). Hypoxia-inducible factor-1 (HIF-1) is the key mediator in cellular oxygen homeostasis that facilitates the adaptation to hypoxia. HIF-1 is repressed by hyperglycemia contributing by this to the development of complications in diabetes. Recent work has shown that the *HIF-1A* Pro582Ser polymorphism is more resistant to hyperglycemia-mediated repression, thus protecting against the development of diabetic nephropathy. In this study, we have investigated the effect of the *HIF-1A* Pro582Ser polymorphism on the development of DR and further dissected the mechanisms by which the polymorphism confers a relative resistance to the repressive effect of hyperglycemia. *Research Design and Method*. 703 patients with type 1 diabetes mellitus from one endocrine department were included in the study. The degree of retinopathy was correlated to the *HIF-1A* Pro582Ser polymorphism. The effect of glucose on a stable *HIF-1A* construct with a Pro582Ser mutation was evaluated *in vitro*. *Results*. We identified a protective effect of *HIF-1A* Pro582Ser against developing severe DR with a risk reduction of 95%, even when adjusting for known risk factors for DR such as diabetes duration, hyperglycemia, and hypertension. The Pro582Ser mutation does not cancel the destabilizing effect of glucose but is followed by an increased transactivation activity even in high glucose concentrations. *Conclusion*. The *HIF-1A* genetic polymorphism has a protective effect on the development of severe DR. Moreover, the relative resistance of the *HIF-1A* Pro582Ser polymorphism to the repressive effect of hyperglycemia is due to the transactivation activity rather than the protein stability of HIF-1α.

1. Introduction

Diabetes retinopathy (DR) is one of the most prevalent microvascular complications of diabetes and the leading cause of blindness in working-age adults [1]. Insufficient blood glucose control, duration of diabetes disease, and ineffective blood pressure control are the major risk factors for DR [2]. DR progresses from mild, nonproliferative diabetes retinopathy (NPDR) to moderate and severe NPDR before the occurrence of proliferative diabetes retinopathy (PDR).

In parallel, at any stage of retinopathy patients may also develop diabetic macular edema (DME) [3]. The incidence of DR and progression to severe DR among patients with similar metabolic control may vary substantially [4]. DR affects all races and ethnicities, but some populations might have greater risk for developing DR [5]. There is a familial clustering of DR [6–8], and the heritability has been estimated to contribute with 27% for the risk of DR and with 52% for the risk of PDR [9, 10]. Even though there is a clear evidence for strong genetic influences on DR, there is no

confirmed association with any risk allele despite extensive candidate gene studies or systematic genome-wide association studies [11, 12]. A potential explanation for the negative results is that the candidate genes investigated either did not have a clear pathogenic role in DR or that the investigated polymorphisms did not have a special functional property.

Hypoxia plays a central role in the development of DR. The retina is physiologically exposed to very low levels of oxygen, and oxygen levels drop even further early in the evolution of diabetes (i.e., 3 weeks after experimental diabetes induction) [13]. This can partly be explained by the decreased retinal perfusion caused by the constriction of major arteries and arterioles [14] and by a reduced oxygen extraction [15]. The decreased oxygen tension leads to a series of biochemical and metabolic alterations that result in chronic, low-grade inflammation; increased oxidative stress; vascular dysfunction; pericyte loss; and pathological neovascularization, maintaining a vicious circle that has as a consequence a progressive retinal hypoxia [14].

Hypoxia-inducible factor-1 (HIF-1) is the key mediator in cellular oxygen homeostasis that facilitates the adaptation to oxygen deprivation by regulating the expression of genes that are involved in cellular energy metabolism and glucose transport, angiogenesis, and erythropoiesis, among others [16]. HIF-1 is a heterodimeric transcription factor composed of two subunits, HIF-1α and HIF-1β, both constitutively expressed in mammalian cells. The regulation of HIF-1 activity is critically dependent on the degradation of the HIF-1α subunit in normoxia. The molecular basis of its degradation is oxygen-dependent hydroxylation of at least one of the two proline residues (Pro402 and Pro564) [17] that makes HIF-1α accessible to the von Hippel-Lindau tumor-suppressor (VHL) protein that acts as an E3 ubiquitin ligase and targets HIF-1α for proteasomal degradation [16]. Several additional noncanonical pathways for HIF-1α regulation have also been described [18]. Under hypoxic conditions, HIF-1 is stabilized and translocated to the nuclei where it binds to hypoxic responsive elements (HRE), recruits coactivators CREB-binding protein (CBP)/p300, and transactivates a series of genes essential for the adaptation of the tissues to hypoxia [19]. Hyperglycemia in diabetes has a complex repressive effect on the stabilization and transactivation of HIF-1α, precluding its optimal reaction to hypoxia [20]. The effect of hyperglycemia on protein stability is dependent on VHL [21] but not always restricted to the canonical proline hydroxylation [22].

HIF-1A (for HIF-1α) genetic polymorphisms are associated with diseases for which the response to oxygen deprivation plays a central pathogenic role, i.e., cancer and cardiovascular diseases. The HIF-1A Pro582Ser (dbSNP ID rs11549465) polymorphism, where a C is changed for a T generating the amino acid serine instead of proline, seems to be of particular functional importance and has been intensely studied for its association with various diseases (recently reviewed in [23]). In previous work, we found that the HIF-1A Pro582Ser polymorphism was protective for diabetes nephropathy by conferring a relative resistance of the encoded HIF-1α to the repressive effects of hyperglycemia on the transactivation level [24]. Having in mind the central role of hypoxia for DR, we conducted a genetic association study of the HIF-1A Pro582Ser polymorphism in type 1 diabetic patients with and without DR. We have also continued to explore in vitro the molecular mechanisms that confer the relative resistance of this polymorphism towards the repressive effect of glucose.

2. Research Design and Methods

2.1. Subjects. Subjects were recruited from the Department of Endocrinology, Metabolism, and Diabetes at the Karolinska University Hospital Solna site, Sweden, where all patients with type 1 diabetes ($n = 1492$) (October, 2011–May, 2014) without any exclusion criteria were invited to participate. A total of 703 patients participated in the genetical analysis. The Regional Ethical Review Board in Stockholm, Sweden, approved the study.

All patients underwent dilated eye examination with a fundus photography, which was judged by ophthalmologists at the St. Erik Eye Hospital, Stockholm, Sweden, during the study period. The ophthalmologists were blinded from the genotyping results. The severity of DR was categorized according to the International Clinical Diabetic Retinopathy Severity Scale (ICDRSS) into one of the five following categories: no DR, mild NPDR, moderate NPDR, severe NPDR, and PDR [25]. The patients were classified according to the most advanced DR if discordance was present between the eyes.

For all patients, fasting blood samples were drawn upon study enrolment. HbA1c was measured with high-performance liquid chromatography (Bio-Rad, 36 mmol/mol CV 2.5%, 85 mmol/mol CV 2.5%). An enzymatic colorimetric method (Roche Diagnostics) was used to measure total cholesterol (3 mmol/L CV 4%, 7 mmol/L CV 4%), triglycerides (1 mmol/L CV 6%, 2.5 mmol/L CV 6%), and high-density lipoprotein (HDL) (0.65 mmol/lLCV 7%, 1.5 mmol/L CV 7%). The concentration of low-density lipoprotein (LDL) was calculated according to Friedewald's formula. All blood samples were analyzed at the routine hospital laboratory at Karolinska University Hospital.

Blood samples for analysis of the HIF-1A Pro582Ser polymorphism were available in 703 patients. Genetic analysis was carried out with TaqMan Allelic Discrimination assay by using the ABI 7300 system (Applied Biosystems, Foster City, CA). Negative controls were included on each plate. Patients' genotypes were classified into the groups CC (non-mutated HIF-1A), CT (one allele mutated), and TT (both alleles mutated).

2.2. Plasmid Constructs. Plasmid-encoded FLAG-fused mouse HIF-1α that is stabilized against canonical degradation (by P402A/P564A mutations) was further mutated at Proline 583 (which is the mouse equivalent of the human Proline 582) to serine (pFLAG/mHIF-1a (P/S)) using the QuickChange site-directed mutagenesis kit (Stratagene) according to the manufacturer's instructions. Positive mutants were screened by sequencing using the DYEnamic sequencing kit (Amersham Biosciences Corp.). The Renilla luciferase reporter vector (pRL-TK) was obtained from

Promega Corp. The plasmid encoding a hypoxia response element- (HRE-) driven firefly luciferase reporter (pT81/HRE-luc) has been described previously [22].

2.3. Cell Culture. Human embryonic kidney 293A (HEK293A) cells were maintained in a 1:1 mixture of DMEM and F-12 medium. Transient transfections were performed using Lipofectamine (Invitrogen) according to the manufacturer's instructions. After 16 hours, the cells were cultured in medium containing either a normal (5.5 mM) or high (30 mM) concentration of glucose and exposed to normoxia (21% O_2) or hypoxia (1% O_2). Media were supplemented with FCS (10%), penicillin (50 IU/mL), and streptomycin sulfate (50 mg/mL). Medium and other products for cell culture were purchased from Invitrogen.

2.4. Transcriptional Activity. After 48-hour exposure to different glucose concentrations and oxygen tensions, the transcriptional activity was evaluated in a dual-luciferase reporter assay where the hypoxia response element- (HRE-) driven luciferase reporter gene was coexpressed together with stabilized HIF-1α (P402A/P564A) or stabilized with mutated Pro583 (which is the mouse equivalent of the human Proline 582) (P402A/P564A/P583S) HIF-1A. The Renilla luciferase activity was used as internal control.

2.5. Whole Cell Extraction and Western Blot. After 48-hour exposure to different glucose concentrations and 6-hour oxygen tensions, cells were washed with PBS, collected by centrifugation, and lysed in a high-salt buffer containing 50 mmol/L Tris-HCl (pH 7.4), 500 mmol/L NaCl, 0.2% NP-40, 20% glycerol, 0.5 mmol/L phenylmethylsulfonyl fluoride, 5 mmol/L beta-mercaptoethanol, and a protease inhibitor mix (cOmplete, Mini; Roche Applied Science). The lysates were then cleared by centrifugation for 30 min at 20,000 g at 4°C. The whole-cell extracts were separated by SDS-PAGE and blotted onto nitrocellulose membranes. After blocking in TBS buffer (50 mmol/L Tris-HCl (pH 7.4), 150 mmol/L NaCl) containing 5% nonfat milk, the membranes were incubated with anti-FLAG M2 (F3165, Sigma-Aldrich) or anti-β-actin (ab6276, Abcam) antibodies in TBS buffer containing 1% nonfat milk. After several washes with TBS buffer containing 0.5% Tween 20, the membranes were incubated with anti-mouse or anti-rabbit IgG-horseradish peroxidase conjugate (Amersham Biosciences Corp.) in TBS buffer containing 1% nonfat milk. After several washes, proteins were visualized using enhanced chemiluminescence (Amersham Biosciences Corp.) according to the manufacturer's recommendations.

2.6. Statistical Analysis. The differences between the DR groups were tested using the Kruskal-Wallis test. Initially, we performed univariate logistic regression analyses with DR as the dependent variable and several demographic and disease variables considered to be clinically important as independent variables, such as age, sex, diabetes duration, systolic blood pressure, HbA1c, smoking (yes vs. no), level of triglycerides, LDL, and HDL. The results from these analyses ($p < 0.05$ as the criterion) and correlation analyses (Pearson's and Spearman's correlations) guided the selection

of variables for the multivariate logistic regression analyses. Multivariate logistic regression analysis was performed using the Enter method. Appropriate tests for linearity, interactions, and goodness of fit were performed. Statistical analyses were done with SPSS IBM Statistics 24.

3. Results

3.1. Genetic Association of the HIF-1A Pro582Ser Polymorphism and Diabetic Retinopathy. Of the 703 patients with type 1 diabetes participating in the analysis, 148 (21%) had no sign of DR, 373 (53%) had mild or moderate NPDR, and 182 (26%) had severe NPDR or PDR. Patients' characteristics are shown in Table 1. The observed minor allele frequency for HIF-1A C>T was 0.071. The proportional relationship between different stages of DR was found to vary between the genotypes, so that the genotype CC had the highest incidence of severe NPDR/PDR, while the genotype TT had the lowest incidence (Figure 1). However, there was no difference in the presence of traditional risk factors for DR between the patients when they were grouped by genotype (Table 2).

The results of the univariate analyses are summarized in Table 3. There was a significant negative association between the TT genotype and severe DR (OR = 0.16, 95% CI: 0.03-0.76) (Table 3). Other variables significantly associated to DR were age, diabetes duration, HbA1c, systolic BP, triglycerides, and HDL (Table 3). In the multivariate analysis, a significant negative association between the TT genotype and the risk for severe DR was observed (OR = 0.05, 95% CI: 0.003-0.91) (Table 3). There was no protective effect of the TT genotype on the development of mild-moderate NPDR.

3.2. Biological Effects of the HIF-1A Pro582Ser Polymorphism. Having in account the above genetic association, we have further investigated the potential functional relevance of the HIF-1A Pro582Ser polymorphism for the reaction of cells to hypoxia in hyperglycemia.

As shown in a previous work by our group [24], the protein stability of the HIF-1α Pro582Ser polymorphism was also diminished in the presence of hyperglycemia [24]. Since the oxygen-dependent degradation of HIF-1α is largely dependent on the hydroxylation of two conserved prolines (Pro402 and Pro564), we wanted to investigate if the mutation Pro582Ser has a separate role on the noncanonical regulation of HIF-1 stability by investigating the behavior of a mutated HIF-1α Pro402Ala/Pro564Ala/-Pro582Ser in high glucose. Transfected HEK293A cells were exposed to normoxia or hypoxia and cultured in different glucose concentrations. We found that HIF-1α Pro402Ala/-Pro564Ala/Pro582Ser has the same stability as HIF-1α Pro402Ala/Pro564Ala (Figure 2(a)) and that it is still sensitive to the hyperglycemia-dependent destabilization of HIF-1α in hypoxia (Figure 2(b)).

The HIF-1α Pro582Ser polymorphism has been shown to be more transcriptionally active than wild type HIF-1α [24]. We have further analyzed the effect of Pro582Ser on the transcriptional activity of a canonic stabilized HIF-1α Pro402Ala/Pro564Ala/Pro582Ser in different glucose concentrations

TABLE 1: Characteristics of the patients.

	Patients with no DR ($n = 148$)	Patients with mild-moderate NPDR ($n = 373$)	Patients with severe NPDR/PDR ($n = 182$)	P value
Women/men (n)	68/80	156/217	81/101	0.65
Ethnic origin, Caucasian vs. other (n), (%)	145 (98.0)	370 (99.2)	179 (98.3)	0.47
Age (years)	44.9 ± 1.3 (19-86)	46.2 ± 0.8 (20-86)	52.8 ± 1.0 (25-86)	<0.001
BMI (kg/m^2)	25.8 ± 0.4 (15.5-40.0)	25.6 ± 0.2 (16.4-45.3)	25.8 ± 0.3 (18.3-42.5)	0.55
Diabetes duration (years)	21.2 ± 1.0 (3-66)	27.1 ± 0.6 (8-73)	36.1 ± 0.9 (12-69)	<0.001
HbA1c (%)	7.7 ± 0.09 (5.5-12.5)	8.1 ± 0.0.5 (5.6-12.1)	8.6 ± 0.1 (4.7-12.7)	<0.001
HbA1c (mmol/mol)	61.1 ± 1.0 (37-113)	65.4 ± 0.6 (38-109)	70.7 ± 1.1 (28-115)	
e-GFR (mL/min/1.73 m^2)	97.4 ± 1.6 (23.6-133)	96.9 ± 1.1 (18-140)	83.4 ± 1.7 (7.2-140)	<0.001
TG (mmol/L)	0.9 ± 0.06 (0.18-7.7)	0.9 ± 0.0 (0.2-5.5)	1.1 ± 0.1 (0.3-6.7)	<0.001
Cholesterol (mmol/L)	4.8 ± 0.07 (2.7-8.4)	4.7 ± 0.0 (2.0-7.7)	4.7 ± 0.1 (2.6-8)	0.45
LDL (mmol/L)	2.7 ± 0.06 (1.1-5.2)	2.7 ± 0.0 (1.1-5.4)	2.7 ± 0.1 (1.0-5.8)	0.38
HDL (mmol/L)	1.7 ± 0.04 (0.8-3.8)	1.6 ± 0.0 (0.6-4.2)	1.6 ± 0.0 (0.5-3.7)	0.032
Systolic blood pressure (mmHg)	125.9 ± 1.2 (90-170)	127.2 ± 0.8 (85-180)	132.6 ± 1.2 (90-180)	<0.001
Diastolic blood pressure (mmHg)	73.2 ± 0.7 (50-95)	74.2 ± 0.5 (40-100)	72.2 ± 0.8 (40-100)	0.083

Data are presented as mean ± SEM (range). The differences between the three groups were tested using the Kruskal-Wallis test. DR, diabetic retinopathy; NPDR, nonproliferative diabetic retinopathy; PDR, proliferative diabetic retinopathy; BMI, body mass index; HbA1c, glycated hemoglobin; e-GFR, estimated glomerular filtration rate; TG, triglycerides; LDL, low-density lipoprotein; HDL, high-density lipoprotein.
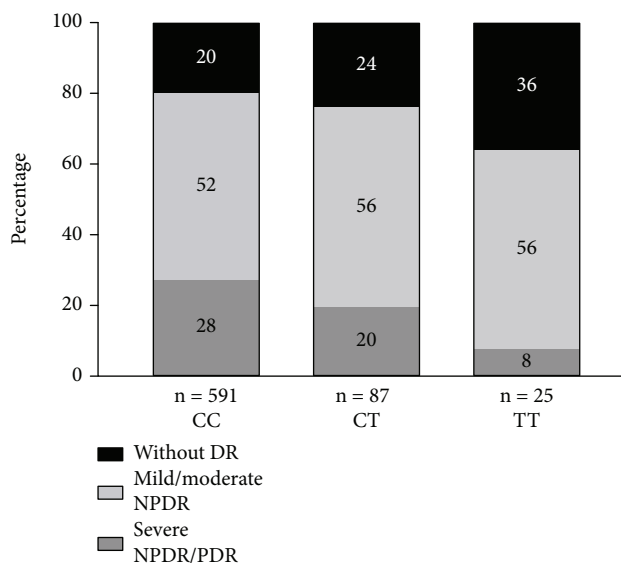
FIGURE 1: Distribution of different grades of DR according to HIF-1A variants in patients with type 1 diabetes. The severity of DR was categorized according to the International Clinical Diabetic Retinopathy Severity Scale. Blood samples were analyzed for the HIF-1A Pro582Ser polymorphism and patients' genotypes were classified into the groups CC, CT, and TT. DR, diabetic retinopathy; NPDR, nonproliferative diabetic retinopathy; PDR, proliferative diabetic retinopathy.

using cotransfection with the HRE-reporter gene. Despite the preserved destabilizing effect of glucose on HIF-1α Pro402Ala/Pro564Ala/Pro582Ser (Figure 2(a)), the Pro582Ser polymorphism has a stimulating effect on transactivation in all glucose concentrations compared to canonically stabilized HIF-1α Pro402Ala/Pro564Ala (Figure 2(c)). These results

indicate that even though the HIF-1α Pro582Ser polymorphism is subject to degradation by the noncanonical proline hydroxylation pathway in high glucose, it has a higher transcriptional activity.

4. Discussion

We have for the first time identified an association between severe NPDR or PDR and the HIF-1A Pro582Ser polymorphism. Moreover, we have brought further mechanistic insight into the function of the HIF-1A Pro582Ser polymorphism in hyperglycemia.

Hypoxia is central in the pathogenesis of DR [14], and HIF-1α has a key role in the tissue response to hypoxia [16]. The HIF-1α function is repressed in diabetes [22], which contributes to an inappropriate reaction to hypoxic injury [22]. Induction of HIF-1α function attenuates progression in animal models of diabetic foot ulcers [21, 26], diabetic nephropathy [27], and diabetic cardiomyopathy [28]. The HIF-1A Pro582Ser polymorphism has been shown to be more active in diabetes, due to a relative resistance to the hyperglycemia-induced repression of HIF-1α transactivation activity [24]. Therefore, a protective effect of the HIF-1A Pro582Ser polymorphism on the risk of developing severe NPDR or PDR is not unexpected. These results are in line with previous studies showing a protective effect of the HIF-1A Pro582Ser polymorphism on other diabetes complications, such as lowered risk of developing foot ulcers [29] and diabetes nephropathy [24].

The canonical oxygen-dependent regulation of HIF-1α is dependent on the hydroxylation of at least two critical prolines (Pro402/Pro564) that makes it accessible to VHL-dependent degradation, which is central for the effect of hyperglycemia on HIF [21]. However, here we show that the Pro582Ser variant is still destabilized in hyperglycemia

TABLE 2: Characteristics of patients with different *HIF-1A* variants.

	Total	CC	CT	TT	*P* value
N	703	591	87	25	
Women/men (*n*)	305/398	260/331	34/53	11/14	0.688
Age (years)	47.6 ± 0.6	48.8 ± 0.6	47.0 ± 1.8	45.7 ± 2.3	0.586
BMI (kg/m^2)	25.5 ± 0.1	25.5 ± 0.2	25.8 ± 0.5	25.6 ± 0.9	0.752
Diabetes duration (years)	28.2 ± 0.5	28.2 ± 0.5	28.1 ± 1.4	26.8 ± 3.0	0.638
HbA1c (mmol/mol)	65.9 ± 0.5	65.8 ± 0.5	65.7 ± 1.4	66.8 ± 3.3	0.895
e-GFR (mL/min/1.73 m^2)	92.6 ± 0.9	93.9 ± 0.9	90.9 ± 2.5	92.5 ± 5.3	0.376
Height (cm)	174.0 ± 0.4	173.9 ± 0.4	174.7 ± 1.1	175.6 ± 2.4	0.762
Systolic blood pressure (mmHg)	128.3 ± 0.6	128.2 ± 0.6	128.9 ± 1.7	130.1 ± 3.5	0.898
Diastolic blood pressure (mmHg)	73.4 ± 0.4	73.4 ± 0.4	73.3 ± 1.0	74.2 ± 1.8	0.828
TG (mg/dL)	0.92 ± 0.03	0.94 ± 0.03	0.8 ± 0.04	0.9 ± 0.08	0.730
Cholesterol (mmol/L)	4.7 ± 0.03	4.7 ± 0.04	4.7 ± 0.09	4.8 ± 0.2	0.966
LDL (mmol/L)	2.7 ± 0.03	2.7 ± 0.03	2.7 ± 0.07	2.8 ± 0.1	0.252
HDL (mmol/L)	1.6 ± 0.02	1.6 ± 0.02	1.6 ± 0.06	1.5 ± 0.09	0.242
Smoking (*n*)	85 (12%)	74 (13%)	9 (10%)	2 (8%)	0.689
Antihypertensive treatment (*n*)	321 (46%)	276 (47%)	34 (39%)	11 (44%)	0.511

Data are shown as mean ± SEM. The differences between the three groups were tested using the Kruskal-Wallis test. CC, CT, and TT are the genotypes of the *HIF-1A* Pro582Ser polymorphism. ns, nonsignificant; BMI, body mass index; HbA1c, glycated hemoglobin; e-GFR, estimated glomerular filtration rate; TG, triglycerides; LDL, low-density lipoprotein; HDL, high-density lipoprotein.

even when the canonical degradation is inhibited by mutations of the Pro402Ala/Pro564Ala. Despite the preserved sensitivity to the destabilizing effect of hyperglycemia (Figure 2(b)), the transactivation activity of HIF-1α Pro582Ser is increased even in high glucose concentration (Figure 2(c)), which might explain the protective effect of the *HIF-1A* Pro582Ser polymorphism for the risk for severe NPDR/PDR. The protective effect of the *HIF-1A* Pro582Ser polymorphism against severe DR remains after adjustment for several known risk factors for severe NPDR/PDR (Table 3) pointing out on the relevance of the special biological behavior of this polymorphism to hypoxia that is central for the pathogenesis of the late stages of DR.

HIF-1 target genes are essential for normal retinal development, vasculature stability, proper retinal function, and vision maintenance. Several HIF-1 target genes are crucial for the protection of the retina in DR [30]. HIF-1 target genes promote oxygen and glucose supply, neovascularization, antioxidization, anti-inflammation, antiapoptosis, and neurotrophy [19]. Patients with the *HIF-1A* Pro582Ser polymorphism, which is more resistant to the repressive effect of hyperglycemia, may therefore have a better adaptation and responses to the retinal hypoxia even from an early period of diabetes that will preclude the progression to severe DR.

This is in contradiction with the noxious effect of the tremendously high HIF-1 signaling induced by the profound hypoxic environment in the late stages of DR [3]. This is also illustrated by the classical observation of the increase of the amount of VEGF (HIF-1 target gene) in ocular fluids that is noticed just in late proliferative stages of DR [31]. This double opposing effect of HIF-1 function in early and late DR is mirrored even for other HIF-1 target genes. For example,

early replenishment of the HIF-1 target gene EPO improves retinal vascular stability and protects retinal neurons from hypoxia-induced apoptosis, but elevated EPO levels during the proliferation stage contribute to neovascularization and ocular disease [32, 33].

This indicates that the manipulation of HIF-1 signaling needs to be carefully considered regarding timing and dosage in order to balance favorable versus detrimental effects. Relatively few attempts have been made to address retinal hypoxia in DR, despite its key pathogenic role [34], but our observation warrants further investigation.

Diabetes duration, blood pressure, dyslipidemia, and glycemic control are well-known risk factors for DR [2]. The logistic regression that includes these risk factors still showed a significant risk reduction for severe DR in patients with the *HIF-1A* Pro582Ser polymorphism that indicates an independent protective effect of the polymorphism. As already shown, the *HIF-1A* Pro582Ser polymorphism is also protective for diabetic nephropathy (DN) [24]. DR and DN share most of the risk factors but not all [35–37]. The *HIF-1A* Pro582Ser polymorphism seems to be a common protective risk for DR and DN since inclusion of microalbuminuria (that strongly correlates with severe DR with OR 14.77, p < 0.0001) in the multiple logistic regression model drops the significance of the protective effect of the *HIF-1A* Pro582Ser polymorphism for severe DR ($p = 0.051$) (data not presented).

A limitation of our study is the relatively small number of patients with the genotype TT, due to the low frequency of this polymorphism. Future research would benefit from multicenter pooling of data in order to acquire a larger sample size.

TABLE 3: Association in patients with type 1 diabetes between various demographic and disease factors and risk for severe NPDR/PDR (comparing no retinopathy ($n = 185$) vs. severe NPDR/PDR ($n = 230$)).

Univariate logistic regression analysis	OR (95% CI)	P value	N
Age	1.03 (1.02-1.05)	<0.0001	415
Sex (female vs. male)	0.96 (0.65-1.41)	0.821	415
Systolic blood pressure	1.03 (1.02-1.04)	<0.0001	414
Diastolic blood pressure	0.99 (0.97-1.01)	0.425	414
Duration	1.11 (1.09-1.13)	<0.0001	415
BMI (kg/m^2)	1.01 (0.96-1.06)	0.616	414
HbA1c	1.06 (1.04-1.08)	<0.0001	415
Smoking (n)	1.26 (0.70-2.27)	0.438	415
TG	1.79 (1.24-2.59)	0.002	415
HDL	0.68 (0.47-0.99)	0.046	414
LDL	0.99 (0.78-1.25)	0.929	412
Cholesterol	1.00 (0.82-1.23)	0.977	415
HIF-1A			330
CC	REF		
CT	0.59 (0.30-1.16)	0.13	
TT	0.16 (0.03-0.76)	0.02	
Multivariate logistic regression analysis	OR (95% CI)	P value	N
Duration	1.11 (1.09-1.15)	<0.0001	328
HbA1c	1.08 (1.06-1.11)	<0.0001	328
Systolic blood pressure	1.03 (1.01-1.05)	0.01	328
HDL	0.60 (0.34-1.07)	0.08	328
HIF1A			328
CC	REF		
CT	0.79 (0.30-2.05)	0.62	
TT	0.05 (0.003-0.91)	0.04	

Univariate and multivariate logistic regression analyses were performed. BMI, body mass index; HbA1c, glycated hemoglobin; TG, triglycerides. CC, CT, and TT are the genotypes of the *HIF-1A* Pro582Ser polymorphism; REF, reference group.

In conclusion, for the first time, we have shown that the *HIF-1A* Pro582Ser polymorphism protects against the development of severe DR. Furthermore, we have provided new mechanistic insights into the regulation of HIF-1α Pro582Ser in hyperglycemia. We speculate that patients with this polymorphism are able to respond better to the hypoxic insults, thus halting the progression of retinal hypoxia and DR pathogenesis. Additional interventional experiments need to be performed to dissect the mechanisms behind this finding. Our study points out a new possible direction in the pursuit of therapeutic strategies for the treatment of DR.

5. Conclusions

The *HIF-1A* Pro582Ser polymorphism has a protective effect on the development of severe DR independently of traditional risk factors for DR. The relative resistance of the *HIF-1A* Pro582Ser polymorphism to the repressive effect of
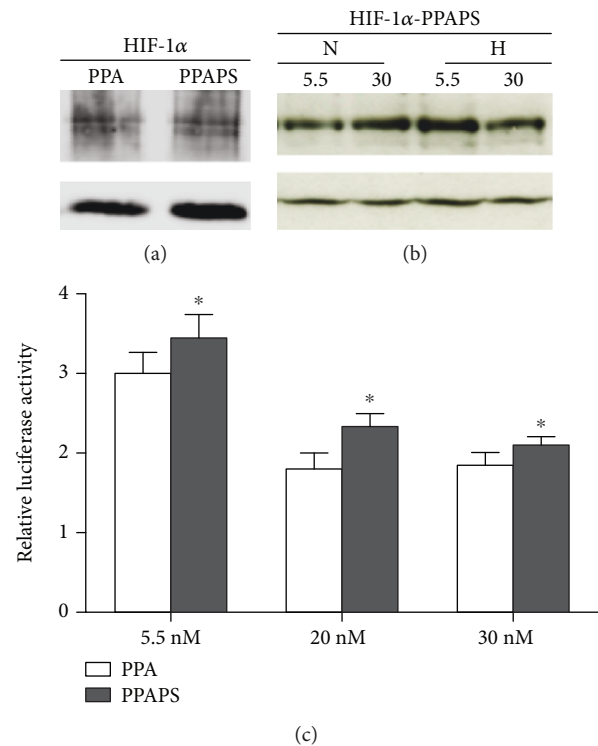
FIGURE 2: (a) HIF-1α (P402A/P564A/P582S) is as stable as HIF-1α (P402A/P564A). Human embryonic kidney 293A (HEK293A) cells were transiently transfected with hypoxia-inducible factor-1α (HIF-1α) (P402A/P564A) or HIF-1α (P402A/P564A/P582S). They were maintained in hypoxia (1% O$_2$) for 16 h before harvest. HIF-1α (P402A/P564A) and HIF-1α (P402A/P564A/P582S) were detected using a FLAG antibody. The HIF-1 constructs are equally expressed. α-Tubulin is shown as internal control. PPA, HIF-1α (P402A/P564A); HIF-1α-PPAPS, hypoxia-inducible factor-1α (P402A/P564A/P582S). (b) HIF-1α (P402A/P564A/P582S) is destabilized in hyperglycemic hypoxic conditions. Human embryonic kidney 293A (HEK293A) cells were transiently transfected with hypoxia-inducible factor-1α (HIF-1α) (P402A/P564A/P582S). They were exposed to 5.5 mM or 30 mM glucose and maintained in normoxia (N) (21% O$_2$) or hypoxia (H) (1% O$_2$) for 6 h before harvest. HIF-1α (P402A/P564A/P582S) was detected using a FLAG antibody. HIF-1α (P402A/P564A/P582S) was destabilized in hyperglycemic hypoxic conditions. HIF-1α-PPAPS, hypoxia-inducible factor-1α (P402A/P564A/P582S); N, normoxia; H, hypoxia. (c) HIF-1α (P402A/P564A/P582S) had a higher transactivation activity than HIF-1α (P402A/P564A). Human embryonic kidney 293A (HEK293A) cells were transiently transfected with hypoxia-inducible factor-1α (HIF-1α) (P402A/P564A/P582S) or HIF-1α (P402A/P564A) together with reporter plasmids in a dual-luciferase reporter assay. The cells were cultured in media containing 5.5, 20, and 30 mM of glucose for 48 h and maintained in hypoxia (1% O$_2$) for 6 h before harvest. PPA, HIF-1α (P402A/P564A); PPAPS, HIF-1α (P402A/P564A/P582S). The transactivation activity was significantly increased in HEK293A cells transfected with HIF-1α (P402A/P564A/P582S) compared to HIF-1α (P402A/P564A) ($p < 0.05$). Data are expressed as mean ± SEM after two-way ANOVA with repeated measures, $n = 4$ per group.

hyperglycemia is due to the transactivation activity rather than the protein stability of HIF-1α.

Data Availability

The data used to support the findings of this study are available from the corresponding author upon request.

Conflicts of Interest

The authors declare that there is no conflict of interest regarding the publication of this paper.

Authors' Contributions

Neda Rajamand Ekberg and Sofie Eliasson contributed equally to this work.

Acknowledgments

References

[1] G. A. Lutty, "Effects of diabetes on the eye," *Investigative Opthalmology & Visual Science*, vol. 54, no. 14, pp. ORSF81–ORSF87, 2013.

[2] J. W. Y. Yau, S. L. Rogers, R. Kawasaki et al., "Global prevalence and major risk factors of diabetic retinopathy," *Diabetes Care*, vol. 35, no. 3, pp. 556–564, 2012.

[3] T. Y. Wong, C. M. G. Cheung, M. Larsen, S. Sharma, and R. Simó, "Diabetic retinopathy," *Nature Reviews Disease Primers*, vol. 2, p. 16012, 2016.

[4] S. E. Moss, R. Klein, and B. E. K. Klein, "Ten-year incidence of visual loss in a diabetic population," *Ophthalmology*, vol. 101, no. 6, pp. 1061–1070, 1994.

[5] S. Sivaprasad, B. Gupta, R. Crosby-Nwaobi, and J. Evans, "Prevalence of diabetic retinopathy in various ethnic groups: a worldwide perspective," *Survey of Ophthalmology*, vol. 57, no. 4, pp. 347–370, 2012.

[6] The Diabetes Control and Complications Trial Research Group, "Clustering of long-term complications in families with diabetes in the diabetes control and complications trial," *Diabetes*, vol. 46, no. 11, pp. 1829–1839, 1997.

[7] D. M. Hallman, J. C. Huber, V. H. Gonzalez, B. E. K. Klein, R. Klein, and C. L. Hanis, "Familial aggregation of severity of diabetic retinopathy in Mexican Americans from Starr County, Texas," *Diabetes Care*, vol. 28, no. 5, pp. 1163–1168, 2005.

[8] K. Uhlmann, P. Kovacs, Y. Boettcher, H. P. Hammes, and R. Paschke, "Genetics of diabetic retinopathy," *Experimental and Clinical Endocrinology & Diabetes*, vol. 114, no. 06, pp. 275–294, 2006.

[9] N. H. Arar, B. I. Freedman, S. G. Adler et al., "Heritability of the severity of diabetic retinopathy: the FIND-Eye study," *Investigative Opthalmology & Visual Science*, vol. 49, no. 9, pp. 3839–3845, 2008.

[10] K. Hietala, C. Forsblom, P. Summanen, P.-H. Groop, and on behalf of the FinnDiane Study Group, "Heritability of proliferative diabetic retinopathy," *Diabetes*, vol. 57, no. 8, pp. 2176–2180, 2008.

[11] B. M. Hampton, S. G. Schwartz, M. A. Brantley Jr, and H. W. Flynn Jr, "Update on genetics and diabetic retinopathy," *Clinical Ophthalmology*, vol. 9, pp. 2175–2193, 2015.

[12] O. Simó-Servat, C. Hernández, and R. Simó, "Genetics in diabetic retinopathy: current concepts and new insights," *Current Genomics*, vol. 14, no. 5, pp. 289–299, 2013.

[13] S. Lee, G. A. Morgan, and N. R. Harris, "Ozagrel reverses streptozotocin-induced constriction of arterioles in rat retina," *Microvascular Research*, vol. 76, no. 3, pp. 217–223, 2008.

[14] M. Capitao and R. Soares, "Angiogenesis and inflammation crosstalk in diabetic retinopathy," *Journal of Cellular Biochemistry*, vol. 117, no. 11, pp. 2443–2453, 2016.

[15] K. Fondi, P. A. Wozniak, K. Howorka et al., "Retinal oxygen extraction in individuals with type 1 diabetes with no or mild diabetic retinopathy," *Diabetologia*, vol. 60, no. 8, pp. 1534–1540, 2017.

[16] N. R. Prabhakar and G. L. Semenza, "Oxygen sensing and homeostasis," *Physiology*, vol. 30, no. 5, pp. 340–348, 2015.

[17] M. Ivan, K. Kondo, H. Yang et al., "HIFalpha targeted for VHL-mediated destruction by proline hydroxylation: implications for O_2 sensing," *Science*, vol. 292, no. 5516, pp. 464–468, 2001.

[18] L. Iommarini, A. M. Porcelli, G. Gasparre, and I. Kurelac, "Non-canonical mechanisms regulating hypoxia-inducible factor 1 alpha in cancer," *Frontiers in Oncology*, vol. 7, p. 286, 2017.

[19] G. L. Semenza, "Oxygen homeostasis," *Wiley Interdisciplinary Reviews: Systems Biology and Medicine*, vol. 2, no. 3, pp. 336–361, 2010.

[20] S. B. Catrina, "Impaired hypoxia-inducible factor (HIF) regulation by hyperglycemia," *Journal of Molecular Medicine*, vol. 92, no. 10, pp. 1025–1034, 2014.

[21] I. R. Botusan, V. G. Sunkari, O. Savu et al., "Stabilization of HIF-1alpha is critical to improve wound healing in diabetic mice," *Proceedings of the National Academy of Sciences*, vol. 105, no. 49, pp. 19426–19431, 2008.

[22] S. B. Catrina, K. Okamoto, T. Pereira, K. Brismar, and L. Poellinger, "Hyperglycemia regulates hypoxia-inducible factor-1alpha protein stability and function," *Diabetes*, vol. 53, no. 12, pp. 3226–3232, 2004.

[23] I. Gladek, J. Ferdin, S. Horvat, G. A. Calin, and T. Kunej, "HIF1A gene polymorphisms and human diseases: graphical review of 97 association studies," *Genes, Chromosomes and Cancer*, vol. 56, no. 6, pp. 439–452, 2017.

[24] H. F. Gu, X. Zheng, N. Abu Seman et al., "Impact of the Hypoxia-Inducible Factor-1 (HIF1A) Pro582Ser Polymorphism on Diabetes Nephropathy," *Diabetes Care*, vol. 36, no. 2, pp. 415–421, 2013.

[25] C. P. Wilkinson, Ferris FL 3rd, R. E. Klein et al., "Proposed international clinical diabetic retinopathy and diabetic macular edema disease severity scales," *Ophthalmology*, vol. 110, no. 9, pp. 1677–1682, 2003.

[26] H. Thangarajah, D. Yao, E. I. Chang et al., "The molecular basis for impaired hypoxia-induced VEGF expression in diabetic tissues," *Proceedings of the National Academy of Sciences*, vol. 106, no. 32, pp. 13505–13510, 2009.

[27] S. Ohtomo, M. Nangaku, Y. Izuhara, S. Takizawa, C. v. Y. d. Strihou, and T. Miyata, "Cobalt ameliorates renal injury in

an obese, hypertensive type 2 diabetes rat model," *Nephrology Dialysis Transplantation*, vol. 23, no. 4, pp. 1166–1172, 2007.

[28] W. Xue, L. Cai, Y. Tan et al., "Cardiac-Specific Overexpression of HIF-1α Prevents Deterioration of Glycolytic Pathway and Cardiac Remodeling in Streptozotocin-Induced Diabetic Mice," *The American Journal of Pathology*, vol. 177, no. 1, pp. 97–105, 2010.

[29] S. Pichu, J. Sathiyamoorthy, E. Krishnamoorthy, D. Umapathy, and V. Viswanathan, "Impact of the hypoxia inducible factor-1α (HIF-1α) pro582ser polymorphism and its gene expression on diabetic foot ulcers," *Diabetes Research and Clinical Practice*, vol. 109, no. 3, pp. 533–540, 2015.

[30] L. Cheng, H. Yu, N. Yan, K. Lai, and M. Xiang, "Hypoxia-inducible factor-1α target genes contribute to retinal neuro-protection," *Frontiers in Cellular Neuroscience*, vol. 11, 2017.

[31] L. P. Aiello, R. L. Avery, P. G. Arrigg et al., "Vascular endothelial growth factor in ocular fluid of patients with diabetic retinopathy and other retinal disorders," *New England Journal of Medicine*, vol. 331, no. 22, pp. 1480–1487, 1994.

[32] T. Coleman and M. Brines, "Science review: recombinant human erythropoietin in critical illness: a role beyond anemia?," *Critical Care*, vol. 8, no. 5, pp. 337–341, 2004.

[33] J. Chen, K. M. Connor, C. M. Aderman, and L. E. Smith, "Erythropoietin deficiency decreases vascular stability in mice," *Journal of Clinical Investigation*, vol. 118, no. 2, pp. 526–533, 2008.

[34] Q. D. Nguyen, S. M. Shah, E. Van Anden, J. U. Sung, S. Vitale, and P. A. Campochiaro, "Supplemental oxygen improves diabetic macular edema: a pilot study," *Investigative Opthalmology & Visual Science*, vol. 45, no. 2, pp. 617–624, 2004.

[35] K. J. Cruickshanks, L. L. Ritter, R. Klein, and S. E. Moss, "The association of microalbuminuria with diabetic retinopathy. The Wisconsin Epidemiologic Study of Diabetic Retinopathy," *Ophthalmology*, vol. 100, no. 6, pp. 862–867, 1993.

[36] P. Romero, M. Salvat, J. Fernandez, M. Baget, and I. Martinez, "Renal and retinal microangiopathy after 15 years of follow-up study in a sample of type 1 diabetes mellitus patients," *Journal of Diabetes and its Complications*, vol. 21, no. 2, pp. 93–100, 2007.

[37] E. Ahlqvist, N. R. van Zuydam, L. C. Groop, and M. I. McCarthy, "The genetics of diabetic complications," *Nature Reviews Nephrology*, vol. 11, no. 5, pp. 277–287, 2015.

Research Article

Analysis of Retinal Perfusion in Children, Adolescents, and Young Adults with Type 1 Diabetes Using Optical Coherence Tomography Angiography

Chiara Mameli [1], **Alessandro Invernizzi,**[2,3] **Alice Bolchini,**[1] **Giorgio Bedogni** [4]
Elisa Giani,[1] **Maddalena Macedoni,**[1] **Gianvincenzo Zuccotti,**[1] **Chiara Preziosa,**[2]
and Marco Pellegrini[2]

[1]*Department of Pediatrics, Vittore Buzzi Children's Hospital, Department of Biomedical and Clinical Science, University of Milan, Milan, Italy*
[2]*Eye Clinic, Department of Biomedical and Clinical Science, Luigi Sacco Hospital, University of Milan, Milan, Italy*
[3]*Save Sight Institute, University of Sydney, Sydney, Australia*
[4]*Clinical Epidemiology Unit, Liver Research Center, Basovizza, Trieste, Italy*

Correspondence should be addressed to Chiara Mameli; chiara.mameli@unimi.it

We performed a cross-sectional study to analyze the retinal vasculature in children, adolescent, and young adults with type 1 diabetes using optical coherence tomography angiography (OCTA). Patients underwent funduscopic examination for diabetic retinopathy (DR) screening during an annual visit for the screening of diabetes-related complications which included the evaluation of glycated hemoglobin (HbA1c), microalbuminuria, lipid profile, arterial pressure, and neurological assessment. In addition, OCTA of the retinal vasculature was performed. Quantitative analysis of the OCTA images evaluated the vessel density at the superficial (SCP) and deep (DCP) capillary plexus of the retina. Structural vascular alterations were evaluated qualitatively. Results were compared to those obtained in a group of healthy age-, sex-, and pubertal stage-matched controls. The effect of age, disease duration, age at the disease onset, mean HbA1c since the onset, and lipid profile on vascular density was tested. Fifty-three patients (median age 15.5, IQR 12.4-19.4 years; 57% females) with type 1 diabetes and 48 controls were enrolled. The median (IQR) HbA1c was 7.6% (60 mmol/mol) (6.9-8.1%, 52-65 mmol/mol), and the median (IQR) duration of disease was 6.0 (3.3-10.3) years. Mean vessel density measured with OCTA was lower in patients compared to controls with the temporal sector showing the highest difference both in the SCP (0.55 vs. 0.57, $p < 0.001$) and the DCP (0.63 vs. 0.65, $p < 0.001$). None of the predictors was associated with the superficial and deep vascular densities. Only 2 patients had clinically detectable DR. Microvascular structural changes were found on OCTA in both of these patients and in one without funduscopic alterations. In conclusion, patients with type 1 diabetes without clinically detectable DR had decreased capillary density compared to controls on OCTA images. These findings may provide useful information for the screening and the management of patients with type 1 diabetes. Further studies are needed to confirm our results and their clinical relevance.

1. Introduction

Type 1 diabetes is the most common metabolic disorder of childhood and adolescence. Its onset in pediatric age together with suboptimal metabolic control puts patients at a greater risk of developing diabetes-related complications [1].

Diabetic retinopathy (DR) is one of the most feared complications of diabetes, leading to visual impairment and blindness if untreated. DR is uncommon before puberty, especially in children aged less than 15 years [2]. The reported prevalence of DR in children and young adults ranges from 10% to 58% depending on the studied population [3–7].

The development and progression of DR depend on several modifiable (glucose control, smoking, arterial hypertension, dyslipidemia, and obesity) and nonmodifiable (age, duration of disease, pubertal status, and genetic predisposition) factors [8]. The pathogenesis of DR is far from being completely elucidated. Changes in retinal blood vessel morphology and retinal blood flow have been reported in DR, but little is known about blood flow alterations during preclinical stages. Functional alterations such as increased vascular permeability and leukostasis have been shown to precede pericyte loss and vascular remodeling [9].

The only available imaging technique to evaluate retinal vasculature before 2000s was fluorescein angiography. This is an invasive examination, requiring an intravenous dye injection, with the risk of local and systemic adverse events. Over the last 4 years, a novel noninvasive technique named optical coherence tomography angiography (OCTA) has been introduced in the clinical practice [10]. OCTA provides a noninvasive, rapid, high-resolution assessment of retinal vascular layers with no need for dye injection. Since its introduction in the clinical practice, OCTA has been applied to several eye diseases offering pathogenetic and prognostic insights. A great advantage of OCTA vs. fluorescein angiography is its ability to study separately the different retinal vascular layers and split the superficial (SCP) from deep (DCP) retinal capillary plexus [10].

Recent studies using OCTA have shown that adults affected by diabetes have low capillary density and that adult patients with type 1 diabetes without clinically evident DR have SCP and DCP anomalies [11–15]. To the best of our knowledge, only one study used OCTA to evaluate retinal vessel density in children affected by type 1 diabetes and found no alterations of SCP, DCP, and the fovea avascular zone [16].

The aim of the present cross-sectional study was to use OCTA to evaluate the retinal perfusion of children, adolescents, and young adults with type 1 diabetes and to compare OCTA findings of these patients with a group of age- and sex-matched healthy controls.

2. Materials and Methods

2.1. Subjects.
This cross-sectional study was performed between May 1st, 2017, and July 31st, 2017, on consecutive patients affected by type 1 diabetes followed up at the Diabetes Clinic of the Vittore Buzzi Children's Hospital (ASST Fatebenefratelli-Sacco, Milan, Italy). The patients were being regularly followed up at our clinic since the diagnosis of type 1 diabetes, and the data for the present study were collected during an annual visit for the screening of diabetes-related complications.

The inclusion criteria were diagnosis of type 1 diabetes, intensive insulin therapy, age between 6 and 25 years, and diabetes duration for at least 6 months. The exclusion criteria were type 2 diabetes mellitus, maturity onset diabetes of the young and syndromic diabetes (e.g., diabetes associated with Down syndrome), myopia exceeding 6.00 diopters, history of nondiabetic retinal disease, previous ocular surgery or laser treatments, ocular media opacities, and poor cooperation.

Healthy sex-, pubertal stage-, and age-matched controls were recruited at the Eye Clinic in Luigi Sacco Hospital Milan. The exclusion criteria for controls were myopia exceeding 6.00 diopters, history of any retinal disease, previous ocular surgery or laser treatment, ocular media opacities, and poor cooperation.

Each patient affected by type 1 diabetes underwent a medical, neurological, and comprehensive ophthalmological examination including best-corrected visual acuity (BCVA) assessment, fundus examination, and OCTA as described in detail below [17]. The healthy control underwent BVCA assessment, fundus examination, and OCTA.

All procedures were free of charge and paid by the National Health System.

The study was conducted according to the Declaration of Helsinki and was approved by the local Ethical Committee. Written informed consent was obtained from the subjects aged 18 years or older or from the parents of those younger than 18 years.

2.2. Clinical Assessment.
The following data were collected for each patient at the time of OCTA: gender, ethnicity, age, height, weight, body mass index (BMI), age at diagnosis of type 1 diabetes, disease duration, type of insulin therapy (multiple daily injections or MDI; continuous subcutaneous insulin infusion or CSII), and insulin requirement (unit/kg/day).

The standard deviation scores (SDS) of weight, height, and BMI were calculated using the World Health Organization (WHO) [18] and the Italian reference data [19]. The pubertal stage was assessed according to Tanner and Whitehouse [20]. Tanner stages 1 and 2 were combined as prepubertal/early pubertal, stages 3 and 4 as pubertal, and stage 5 as postpubertal development.

Systolic blood pressure and diastolic blood pressure were measured following international guidelines [21].

Blood samples were obtained after a 10-hour overnight fast. Creatinine, total cholesterol (TC), high-density lipoprotein cholesterol (HDL), low-density lipoprotein cholesterol (LDL), and triglycerides (TG) were measured using standard laboratory methods. We used standard cut-off values for levels of total cholesterol (hypercholesterolemia ≥ 200 mg per deciliter), HDL cholesterol (hypoHDL < 40 mg per deciliter and <50 mg/dl for females > 16 years), LDL cholesterol (hyperLDL ≥ 130 mg per deciliter), and triglycerides (hyperTG ≥ 150 mg per deciliter) [22].

HbA1c was measured using a fully automated high-performance liquid chromatography system (Variant II, Bio-Rad Laboratories, Munich, Germany).

A first morning urine sample was obtained in all patients to evaluate microalbuminuria.

All samples were analyzed by the laboratory of ASST-Fatebenefratelli Sacco.

The following data were obtained from the medical charts: glycated hemoglobin (HbA1c) at diagnosis and every 3 months, number of hospital admissions for diabetic ketoacidosis (DKA), number of severe hypoglycemic episodes, and presence of diabetes-related complications.

2.3. Ophthalmological Assessment. All study subjects underwent a complete ophthalmological examination including BCVA assessment, slit lamp examination, and funduscopic examination performed by a senior ophthalmologist (MP). Pupils were dilated with 1% tropicamide before funduscopic examination and OCTA image collection.

OCTA images were obtained using the split-spectrum amplitude-decorrelation angiography algorithm (SSADA) on the AngioVue OCT-A system version 2017.1.0.15 (Optovue RTVue XR Avanti, Optovue Inc., Freemont, California, USA). This device uses an 840 nm wavelength laser to capture 70,000 A-scans per second; 304 A-scans made up a B-scan, while 304 vertical and horizontal lines were sampled in the scanning area to obtain a 3D data cube. 3×3 and 6×6 mm volume scans centered onto the fovea were performed in both eyes for each patient.

Automated segmentation of SCP and DCP was performed using the inbuilt software algorithm which sets the inner margin of SCP at 3 μm below the internal limiting membrane of the retina and the outer boundary at 15 μm beneath the inner plexiform layer (IPL), with the DCP top boundary set at 15 μm beneath the IPL and the bottom margin at 71 μm under the IPL.

Vascular density was calculated with the AngioVue Analytics software, which reports the relative density of flow as percentage of the total area. In detail, the vessel density was defined as the percentage of area occupied by vessel lumens after binary reconstruction of images. In the present study, vessel density was calculated for different sectors (superior, nasal, inferior, and temporal) based on the Early Treatment Diabetic Retinopathy Study (ETDRS) chart with the fovea position automatically determined from OCTA. The parafovea was defined as the area within an annulus located between 1 and 2.5 mm from the central fovea.

The SCP and DCP vascular data were analyzed separately. For statistical analysis, we collected the SCP and DCP foveal and parafoveal data from 3×3 mm volumetric scans, and the superior, nasal, inferior, and temporal data from 6×6 mm images. Data from both eyes of all subjects were considered for analysis (see below).

A qualitative evaluation of the OCTA images was also performed by two double-masked ophthalmologists (MP and CP). For each image, the following DR angiographic features were evaluated on both SPC and DPC OCTA images: presence of microaneurysms, rarefaction of perifoveal capillaries, capillary tortuosity, and disruption of the perifoveolar capillary arcades.

2.4. Statistical Analysis. Most continuous variables were not Gaussian-distributed, and all are reported as median and interquartile range (IQR). Discrete variables are reported as the number and proportion of subjects with the characteristic of interest. Between-group comparisons were performed using a fractional generalized linear model (GLM) with a logit link and cluster confidence intervals [23, 24]. The outcome of the fractional GLM was the vascular density (fraction, with theoretical limits from 0 to 1) of the regions of interest (SCP and DCP foveal, parafoveal, temporal, superior, nasal, and inferior areas), and the predictor was type 1

diabetes (discrete: 0 = no; 1 = yes). For each subject, we analyzed both the eyes of each subject in the same model using cluster confidence intervals to take into account the fact that every subject contributed two eyes to the analysis [23]. Because of the 14 multiple comparisons involving SCP and DCP, a significant p value was set at $p < 0.003$ (0.05/14). The effect of age, disease duration, age at disease onset, mean HbA1c, LDL, HDL, TG, and TC on vascular density was tested adding each predictor to the fractional GLM.

3. Results

3.1. Patients. Fifty-five consecutive patients affected by type 1 diabetes were eligible for the study, but two refused to participate. Fifty-three patients with type 1 diabetes were hence included in the analysis. The median (IQR) age was 15.5 (12.4-19.4) years. Thirty (57%) patients were female, and 27 (51%) were being treated with CSII. The median (IQR) HbA1c was 7.6% (60 mmol/mol) (6.9-8.1%, 52-65 mmol/mol), and the median (IQR) duration of disease was 6.0 (3.3-10.3) years. No patient had arterial hypertension, and all patients had a normal neurological evaluation. Two patients had microalbuminuria, i.e., >30 mg/g creatinine/day. The median (IQR) HbA1c from the onset to OCTA was 7.5% (58 mmol/mol) (IQR 7.0-8.0%/53-64 mmol/mol). HyperTC and hyperLDL were detected in 3 patients. Two patients had hyperTG and 6 patients hypoHDL. Detailed data about the 53 patients with type 1 diabetes at the time of OCTA are reported in Table 1.

Forty-eight healthy subjects with a median (IQR) age of 13.7 (11.0-18.9) years served as controls. Forty-five (94%) of them were Caucasians, and 26 (54%) were girls.

3.2. Eyes. A total of 106 (53×2) eyes from patients with type 1 diabetes and 96 (48×2) eyes from healthy controls were analyzed. Tables S1 and S2 report the vascular densities of the SCP and DCP plexus for the right and left eyes of patients with type 1 diabetes and healthy controls. These tables are reported only for descriptive purposes because the comparison between the vascular densities of the SCP and DCP plexus of patients with type 1 diabetes and healthy controls was performed on both eyes using a fractional GLM treating the eyes as clusterized in a given subject (see Statistical Analysis for details).

Vascular density was decreased in patients affected by type 1 diabetes compared to healthy subjects in all the regions of interest in both the superficial and deep plexus with the exception of the fovea. After Bonferroni correction, in the superficial plexus, the mean difference in vascular density between diabetics and controls was significant only in the temporal and the superior regions (0.57 vs. 0.55%, $p < 0.001$ and 0.57 vs. 0.55%, $p = 0.002$, respectively). In the deep plexus, the difference was significant only in the temporal region (0.65 vs. 0.63%, $p < 0.001$). Table 2 gives the mean (95% confidence intervals (95% CI)) vascular densities for the SCP and DCP in patients with type 1 diabetes and healthy controls estimated by the fractional GLM model described under Statistical Analysis. As shown in Table S3, none of the additional predictors was associated in a clinically

Table 1: Patient characteristics.

	Patient with type 1 diabetes		Healthy controls	
	N (%)	Median (IQR)	N (%)	Median (IQR)
Gender	53		48	
Female	30 (57%)		26 (54%)	
Male	23 (43%)		22 (46%)	
Age (years)	53	15.5 (12.4; 19.4)	48	13.7 (11.8-18.9)
Caucasian	53		48	
No	7 (13%)		3 (6%)	
Yes	46 (87%)		45 (94%)	
Weight (kg)	52	59 (45; 65)		
Height (m)	52	1.62 (1.54; 1.71)		
BMI (kg/m^2)	52	21.4 (19.3; 23.8)		
Weight (SDS Cacciari)	38	0.02 (-0.54; 0.86)		
Height (SDS Cacciari)	38	0.23 (-0.41; 0.95)		
BMI (SDS Cacciari)	38	-0.08 (-0.51; 0.58)		
Prepubertal	10		10	
Pubertal	12		12	
Postpubertal	31		26	
Diabetes duration (years)	53	6.0 (3.3; 10.3)		
Insulin treatment	53			
Multiple daily injections	26 (49%)			
CSII	27 (51%)			
HbA1c (%)	53	7.6 (6.9; 8.1)		
HbA1c (mmol/mol)	53	60 (52; 65)		
Microalbuminuria (mg/g creatinine/day)	43	6.0 (5.0; 10.0)		
Cholesterol (mg/dl)	53	169 (151; 182)		
HDL cholesterol (mg/dl)	53	51 (45; 60)		
LDL cholesterol (mg/dl)	53	102 (80; 115)		
Triglycerides (mg/dl)	53	58 (47; 75)		

Data are reported as median (interquartile range) for continuous measures and n (%) for categorical measure. BMI = body mass index; Cacciari = Italian reference data; CSII: continuous subcutaneous insulin infusion; HbA1c = glycated hemoglobin; HDL = high-density lipoprotein; IQR = interquartile range; LDL = low-density lipoprotein; SDS = standard deviation score.

relevant way with the superficial and deep vascular densities evaluated by OCTA. (The presence of statistical significance for few predictors was expected by chance alone because of the number of tested models [96] and is clearly irrelevant because the contribution was always negligible on clinical grounds).

OCTA images were reviewed by 2 masked operators with good agreement, and vascular abnormalities were detected in 3 cases (Figure 1).

4. Discussion

DR has long been considered extremely rare in pediatric age. However, a recent large US study has shown an increase of 20% (95% CI 6 to 35%) of the hazard of DR for every 1-point increase of HbA1c in children with type 1 diabetes [25]. Moreover, DR seems to progress rapidly in children with type 1 diabetes, so its early detection can be beneficial [25].

The worldwide increase in the incidence of type 1 diabetes mandates the consideration of strategies for the early

detection of DR. OCTA may be one of such strategies as studies of diabetic adults have shown that OCTA can detect alterations of retinal blood flow in the presence of normal fundus examinations [14, 15].

In the present study, we found that OCTA was able to detect significantly lower retinal vessel density in temporal SCP (0.55 vs. 0.57) and DCP (0.63 vs. 0.65) in both eyes of patients with type 1 diabetes mostly with no clinically detectable DR compared to healthy children. Reduced vessel density was also detected in the other regions of interest of both SCP and DCP of the same eyes except for the foveal region. This partially confirms recent studies reporting vascular changes in the DCP of patients affected by type 1 diabetes [12, 13].

Our results are intriguing since they demonstrate that OCTA can identify early microvascular changes that occur in the retina before the DR becomes clinically visible and that are consequently not detectable with the standard screening procedures. However, the clinical significance of the differences we found in capillary density between patients affected by type 1 diabetes and controls is unclear because

TABLE 2: Vascular densities of the superficial and deep plexus in patients with type 1 diabetes and healthy controls.

	Healthy controls ($n = 96$ eyes)			Patients with type 1 diabetes ($n = 106$ eyes)			p value
	Mean	95% LCI	95% UCI	Mean	95% LCI	95% UCI	
S-Fovea	0.31	0.30	0.32	0.32	0.31	0.33	0.3025
S-Parafovea	0.58	0.57	0.58	0.57	0.56	0.57	0.0054
S-Temporal	0.57	0.56	0.57	0.55	0.54	0.55	<0.001
S-Superior	0.57	0.56	0.58	0.55	0.54	0.56	0.0028
S-Nasal	0.57	0.56	0.58	0.56	0.55	0.56	0.0068
S-Inferior	0.56	0.55	0.57	0.55	0.54	0.56	0.0229
D-Fovea	0.31	0.29	0.32	0.33	0.31	0.35	0.0404
D-Parafovea	0.65	0.65	0.65	0.64	0.64	0.65	0.0036
D-Temporal	0.65	0.64	0.65	0.63	0.63	0.64	<0.001
D-Superior	0.66	0.65	0.66	0.65	0.65	0.66	0.7267
D-Nasal	0.65	0.65	0.66	0.65	0.64	0.65	0.5897
D-Inferior	0.65	0.65	0.66	0.65	0.65	0.66	0.8462

Comparison of the vascular densities of the superficial and deep plexus in patients with type 1 diabetes and healthy controls. Values are means and 95% confidence intervals estimated from a fractional generalized linear model (see Statistical Analysis for details). LCI = lower confidence interval; UCI = upper confidence interval; S- = superficial plexus; D- = deep plexus.

of their size even when statistically significant. For instance, the mean (SD) difference estimated by the fractional GLM for S-Superior is -0.02 (95% CI -0.03 to -0.01) for patients with type 1 diabetes vs. healthy subjects. Although statistically significant, a reduction of 0.02 is about 4% of the density (0.57) of the control group. Nevertheless, it is interesting to note that in our analysis, the temporal macular sectors resulted to be primarily affected in both the SCP and DCP. This is in agreement with previous findings from other researches evidencing this sector as a particularly susceptible portion of the macula [26]. Han et al. in 2017 described OCTA changes in patients affected by various sickle cell genotypes describing greater flow loss in the temporal subfields [26]. One of the main explanations for this finding was that the temporal macular vessels are located within the watershed zones along the horizontal raphe and consequently nearby terminal vessels. This anatomical configuration may lead to increase susceptibility of vascular damage for this sector. Also, these results confirm previous researches showing retinal thinning to be more prominent in the temporal sectors in the same subset of patients.

Our results could suggest that in a cohort of well-controlled children and young adults with short duration of disease, alterations in retinal vessel density occur very early and before the onset of other diabetes-related complications. We could speculate that retina is one of the most sensitive target tissues. The lack of correlation with median HbA1c value since the disease onset could suggest that we should try to look over hemoglobin A1C and search for new metrics in the clinical practice to estimate the risk of diabetes-related chronic complications. In this field, the role "time in range" is emergent. In adults affected by type 2 diabetes, the lowest percentage of time in range is associated with an increased risk to have diabetic retinopathy and an increased severity of eye damage [27, 28].

The prevalence of clinically detectable DR was very low in our population, i.e., 3‰ (2/53 patients). The low frequency and the mild form in our population of DR are not surprising owing to the low median duration of disease of our patients (6 years). It must also be pointed out that the median (IQR) HbA1c at the time of OCTA was 7.6% (60 mmol/mol) (6.9-8.1; 52-65 mmol/mol), which is compatible with a reasonably good metabolic control in the last three months.

In our series, we performed both a qualitative and a quantitative assessment of retinal vascular alterations occurring in both populations. OCTA qualitative analysis showed vascular abnormalities (microaneurysms, remodeling, and capillary loss) in patients that had clinically detectable DR. Similar qualitative microvascular abnormalities were also detected on OCTA in a patient with long duration of disease and suboptimal metabolic control since diagnosis but with a normal fundus. Interestingly, all the three patients with OCTA-detected retinal alterations had disease duration above the median, i.e., 8, 11, and 20 years.

Even if this is one of the first studies to investigate the role of OCTA in detecting early alterations of the macular capillary network in pediatric patients with type 1 diabetes, it has several limitations. First, this is a cross-sectional study, and as such, it can evaluate the retinal vasculature status only at a specific time point. A prospective evaluation of these children will help us to describe the evolution of our findings. Second, the population recruited is relatively small. The main reason is the difficulty in recruiting children especially in prepubertal age because OCTA requires patient's collaboration. However, considering the available studies published so far on the use of OCTA in pediatric population affected by type 1 diabetes without diabetic retinopathy, our cohort was one of the largest.

Third, recent updates in OCTA software are looking for the possibility to further split the DCP in two separate vascular structures, and the recently described intermediate
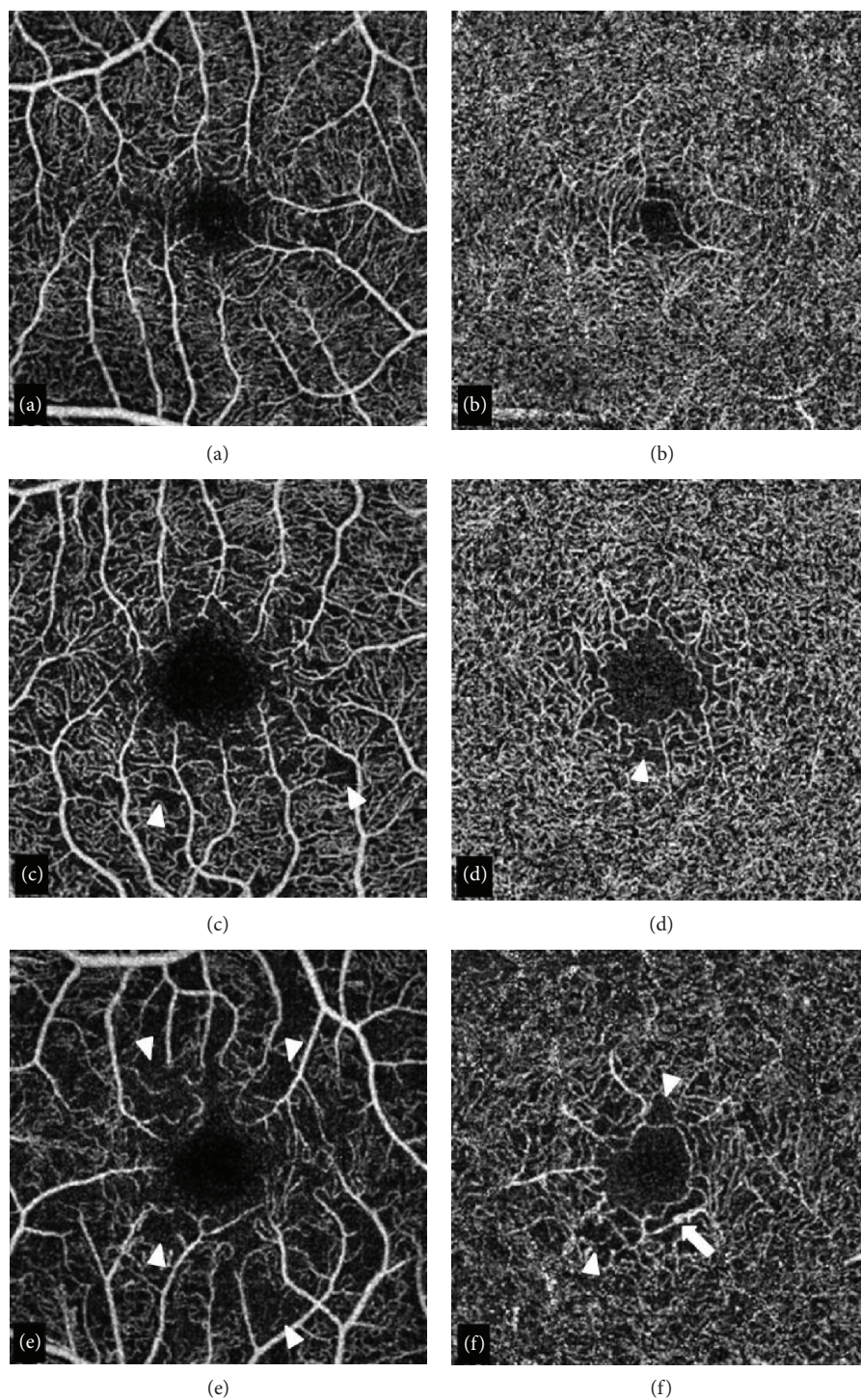
Figure 1: Optical coherence tomography angiography images. (a, b) Optical coherence tomography angiography (OCTA) in a healthy control showing the typical spider web appearance of the superficial capillary plexus (SCP) (a) and the sea fan pattern of the deep capillary plexus (DCP) (b). (c–f) SCP (c and e) and DCP (d and f) in two patients (c and d) patient #40; (e and f) patient #28) showing early vascular changes at the level of both retinal plexus. In these cases, indeed mild capillary loss with reduced vascular density was better visible at the level of the SCP whereas microaneurysms could be recognized at the level of the deep vascular structures. Arrow: microaneurysm; arrowhead: areas of capillary drop-out.

plexus may be primarily affected in the very early phases of the disease.

5. Conclusions

This study investigates the role of OCTA in detecting early vascular changes in pediatric patients with type 1 diabetes. OCTA is confirmed to be a valuable tool for noninvasive diagnosing and monitoring of these patients. In particular, we found that microvascular changes in both SCP and DCP could be reliably highlighted by means of OCTA before the appearance of clinical signs of DR at fundoscopy. In our series, the temporal sectors appeared to be more significantly reduced compared to the other subfields thus possibly representing a primary site of pathology. Cohort studies are needed to further evaluate the potential of OCTA for the screening of DR in children with type 1 diabetes, for improving the treatment of diabetes-related ocular disease and to understand the relevance of intraocular early signs in the progression of the systemic disease.

Data Availability

The data used to support the findings of this study are available from the corresponding author upon request.

Conflicts of Interest

The authors declare that there is no conflict of interest regarding the publication of this paper.

Supplementary Materials

Tables S1 and S2 report the vascular densities of the SCP and DCP plexus for the right and left eyes of patients with type 1 diabetes and healthy controls. Table S3 shows the correlations between predictors and the superficial and deep vascular densities. *(Supplementary Materials)*

References

[1] S. J. Zborovski and F. H. Mahmud, "Paediatric type 1 diabetes 2018: clinical and research insights," *Paediatrics & Child Health*, vol. 23, no. 3, pp. 198–202, 2018.

[2] M. M. Geloneck, B. J. Forbes, J. Shaffer, G. S. Ying, and G. Binenbaum, "Ocular complications in children with diabetes mellitus," *Ophthalmology*, vol. 122, no. 12, pp. 2457–2464, 2015.

[3] B. S. Olsen, A. K. Sjølie, P. Hougaard et al., "The significance of the prepubertal diabetes duration for the development of retinopathy and nephropathy in patients with type 1 diabetes," *Journal of Diabetes and its Complications*, vol. 18, no. 3, pp. 160–164, 2004.

[4] M. Cahill, D. Wallace, S. Travers et al., "Detection and prevalence of early diabetic retinopathy in juvenile diabetics with diabetes for 10 years or more," *Eye*, vol. 14, no. 6, pp. 847–850, 2000.

[5] T. LeCaire, M. Palta, H. Zhang, C. Allen, R. Klein, and D. D'Alessio, "Lower-than-expected prevalence and severity of retinopathy in an incident cohort followed during the first 4-14 years of type 1 diabetes: the Wisconsin Diabetes Registry Study," *American Journal of Epidemiology*, vol. 164, no. 2, pp. 143–150, 2006.

[6] C. E. Kullberg, M. Abrahamsson, H. J. Arnqvist, K. Finnström, J. Ludvigsson, and VISS Study Group, "Prevalence of retinopathy differs with age at onset of diabetes in a population of patients with type 1 diabetes," *Diabetic Medicine*, vol. 19, no. 11, pp. 924–931, 2002.

[7] A. Kernell, I. Dedorsson, B. Johansson et al., "Prevalence of diabetic retinopathy in children and adolescents with IDDM. A population-based multicentre study," *Diabetologia*, vol. 40, no. 3, pp. 307–310, 1997.

[8] G. T. Lueder, J. Silverstein, and Academy of Pediatrics Section on Ophthalmology and Section on Endocrinology, "Screening for retinopathy in the pediatric patient with type 1 diabetes mellitus," *Pediatrics*, vol. 116, no. 1, pp. 270–273, 2005.

[9] G. A. Lutty, "Effects of diabetes on the eye," *Investigative Opthalmology & Visual Science*, vol. 54, no. 14, pp. ORSF81–ORSF87, 2013.

[10] A. Shahlaee, W. A. Samara, J. Hsu et al., "In vivo assessment of macular vascular density in healthy human eyes using optical coherence tomography angiography," *American Journal of Ophthalmology*, vol. 165, pp. 39–46, 2016.

[11] J. M. Simonett, F. Scarinci, F. Picconi et al., "Early microvascular retinal changes in optical coherence tomography angiography in patients with type 1 diabetes mellitus," *Acta Ophthalmologica*, vol. 95, no. 8, pp. e751–e755, 2017.

[12] A. Carnevali, R. Sacconi, E. Corbelli et al., "Optical coherence tomography angiography analysis of retinal vascular plexuses and choriocapillaris in patients with type 1 diabetes without diabetic retinopathy," *Acta Diabetologica*, vol. 54, no. 7, pp. 695–702, 2017.

[13] F. Scarinci, F. Picconi, P. Giorno et al., "Deep capillary plexus impairment in patients with type 1 diabetes mellitus with no signs of diabetic retinopathy revealed using optical coherence tomography angiography," *Acta Ophthalmologica*, vol. 96, no. 2, pp. e264–e265, 2018.

[14] N. Takase, M. Nozaki, A. Kato, H. Ozeki, M. Yoshida, and Y. Ogura, "Enlargement of foveal avascular zone in diabetic eyes evaluated by en face optical coherence tomography angiography," *Retina*, vol. 35, no. 11, pp. 2377–2383, 2015.

[15] T. E. de Carlo, A. T. Chin, M. A. Bonini Filho et al., "Detection of microvascular changes in eyes of patients with diabetes but not clinical diabetic retinopathy using optical coherence tomography angiography," *Retina*, vol. 35, no. 11, pp. 2364–2370, 2015.

[16] J. Gołębiewska, A. Olechowski, M. Wysocka-Mincewicz et al., "Optical coherence tomography angiography vessel density in children with type 1 diabetes," *PLoS One*, vol. 12, no. 10, article e0186479, 2017.

[17] K. C. Donaghue, R. P. Wadwa, L. A. Dimeglio et al., "Microvascular and macrovascular complications in children and adolescents," *Pediatric Diabetes*, vol. 15, no. S20, pp. 257–269, 2014.

[18] WHO Multicentre Growth Reference Study Group, *WHO child growth standards: lengt height-for-age, weight-for-age, weight-for-length, weight-for-height and body mass index-for-age: methods and development*, World Health Organization, Geneva, 2006.

[19] E. Cacciari, S. Milani, A. Balsamo et al., "Italian cross-sectional growth charts for height, weight and BMI (2 to

20 yr)," *Journal of Endocrinological Investigation*, vol. 29, no. 7, pp. 581–593, 2006.

[20] J. M. Tanner and R. H. Whitehouse, "Clinical longitudinal standards for height, weight, height velocity, weight velocity, and stages of puberty," *Archives of Disease in Childhood*, vol. 51, no. 3, pp. 170–179, 1976.

[21] C. M. Baker-Smith, S. K. Flinn, J. T. Flynn et al., "Diagnosis, evaluation, and management of high blood pressure in children and adolescents," *Pediatrics*, vol. 142, no. 3, p. e20182096, 2018.

[22] Expert Panel on Integrated Guidelines for Cardiovascular Health and Risk Reduction in Children and Adolescents and National Heart, Lung, and Blood Institute, "Expert panel on integrated guidelines for cardiovascular health and risk reduction in children and adolescents: summary report," *Pediatrics*, vol. 128, Supplement, pp. S213–S256, 2011.

[23] J. W. Hardin and J. M. Hilbe, *Generalized Linear Models and Extensions*, Stata Press, College Station TX, 2018.

[24] L. E. Papke and J. M. Wooldridge, "Econometric methods for fractional response variables with an application to 401(k) plan participation rates," *Journal of Applied Econometrics*, vol. 11, no. 6, pp. 619–632, 1996.

[25] S. Y. Wang, C. A. Andrews, W. H. Herman, T. W. Gardner, and J. D. Stein, "Incidence and risk factors for developing diabetic retinopathy among youths with type 1 or type 2 diabetes throughout the United States," *Ophthalmology*, vol. 124, no. 4, pp. 424–430, 2017.

[26] I. C. Han, M. Tadarati, K. D. Pacheco, and A. W. Scott, "Evaluation of macular vascular abnormalities identified by optical coherence tomography angiography in sickle cell disease," *American Journal of Ophthalmology*, vol. 177, pp. 90–99, 2017.

[27] R. W. Beck, R. M. Bergenstal, T. D. Riddlesworth et al., "Validation of time in range as an outcome measure for diabetes clinical trials," *Diabetes Care*, vol. 42, no. 3, pp. 400–405, 2019.

[28] J. Lu, X. Ma, J. Zhou et al., "Association of time in range, as assessed by continuous glucose monitoring, with diabetic retinopathy in type 2 diabetes," *Diabetes Care*, vol. 41, no. 11, pp. 2370–2376, 2018.

Research Article

Melatonin Affects Mitochondrial Fission/Fusion Dynamics in the Diabetic Retina

Janet Ya-An Chang,[1,2] Fei Yu,[1] Liheng Shi,[1] Michael L. Ko,[1] and Gladys Y.-P. Ko [1,2,3]

[1]*Department of Veterinary Integrative Biosciences, Texas A&M University, College Station, Texas, USA*
[2]*Interdisciplinary Toxicology Program, Texas A&M University, College Station, Texas, USA*
[3]*Texas A&M Institute of Neuroscience, Texas A&M University, College Station, Texas, USA*

Correspondence should be addressed to Gladys Y.-P. Ko; gko@cvm.tamu.edu

Mitochondrial fission and fusion are dependent on cellular nutritional states, and maintaining this dynamics is critical for the health of cells. Starvation triggers mitochondrial fusion to maintain bioenergetic efficiency, but during nutrient overloads (as with hyperglycemic conditions), fragmenting mitochondria is a way to store nutrients to avoid waste of energy. In addition to ATP production, mitochondria play an important role in buffering intracellular calcium (Ca^{2+}). We found that in cultured 661W cells, a photoreceptor-derived cell line, hyperglycemic conditions triggered an increase of the expression of dynamin-related protein 1 (DRP1), a protein marker of mitochondrial fission, and a decrease of mitofusin 2 (MFN2), a protein for mitochondrial fusion. Further, these hyperglycemic cells also had decreased mitochondrial Ca^{2+} but increased cytosolic Ca^{2+}. Treating these hyperglycemic cells with melatonin, a multifaceted antioxidant, averted hyperglycemia-altered mitochondrial fission-and-fusion dynamics and mitochondrial Ca^{2+} levels. To mimic how people most commonly take melatonin supplements, we gave melatonin to streptozotocin- (STZ-) induced type 1 diabetic mice by daily oral gavage and determined the effects of melatonin on diabetic eyes. We found that melatonin was not able to reverse the STZ-induced systemic hyperglycemic condition, but it prevented STZ-induced damage to the neural retina and retinal microvasculature. The beneficial effects of melatonin in the neural retina in part were through alleviating STZ-caused changes in mitochondrial dynamics and Ca^{2+} buffering.

1. Introduction

Mitochondria are dynamic organelles that constantly divide and fuse, and maintaining a proper equilibrium in this dynamics is critical in healthy cells [1, 2]. Under starvation, mitochondria can fuse with each other to maintain bioenergetic efficiency [3]. When there is a nutrient overload, fragmenting mitochondria is a way to store nutrients to avoid energy waste [4, 5]. Hence, the number and shape of mitochondria within a cell are tightly associated with cellular metabolism [6]. Mitochondrial fission requires recruiting dynamin-related protein 1 (DRP1) from the cytosol to the outer mitochondrial surface, whereas mitofusin 2 (MFN2) on the outer mitochondrial membrane coordinates with the protein optic atrophy 1 (OPA1) on the inner membrane to

regulate mitochondrial fusion [7, 8]. Most mitochondria in the retina are located in the photoreceptors, and mitochondria are a major intracellular source of reactive oxygen species (ROS), a by-product of the mitochondrial respiratory chain [9]. As photoreceptors have the highest metabolic rate and consume more oxygen, they generate more ROS than other retinal cells [10].

In addition to ATP production, mitochondria play an important role to buffer intracellular calcium (Ca^{2+}). When the cytosolic Ca^{2+} concentration is elevated due to stimulation, mitochondria along with the endoplasmic reticulum (ER) take up and store Ca^{2+} [11]. Mitochondria also prevent Ca^{2+} depletion in the ER by extruding Ca^{2+} to the cytoplasm [12, 13]. In retinal photoreceptors, mitochondria act as mediators to regulate Ca^{2+} uptake in the outer segment and cell

body [14]. The mitochondrial calcium uniporter (MCU) is a highly selective Ca^{2+} channel located in the inner membrane of mitochondria, which allows for the passage of Ca^{2+} into the matrix, and it is primarily responsible for mitochondrial storage of intracellular Ca^{2+} [15–17].

Oxidative stress is a major culprit in the pathogenesis of many metabolic diseases including diabetic retinopathy (DR) [18]. Thus, controlling the source of oxidative stress is critical in DR management. Diabetic retinopathy is a dual disorder with microvascular complications and retinal degeneration [19]. As for the role of mitochondria and ROS in DR, retinal endothelial cells isolated from type 2 diabetic patients have increased mitochondrial fission and ROS overproduction [20], and the retina from DR patients also shows downregulated mitochondrial fusion [21]. Historically, DR has been investigated and treated as a complication of the vasculature [22, 23]. However, increasing evidence shows that retinal neural dysfunction precedes any microvascular complication [24]. In animal models, pharmacological or genetic induction of photoreceptor death in early diabetes dampens the generation of ROS and stops the progression of DR [25], suggesting that photoreceptors are the major source of intraocular oxidative stress under diabetic insults and contribute to the vascular lesions and pathogenesis of early DR [9, 26]. Previously, we found that in the streptozotocin- (STZ-) induced diabetic retina, calcium homeostasis is impaired, and signaling pathways that are involved in calcium homeostasis are downregulated [27]. However, it is not known whether the impaired calcium homeostasis under diabetic stress is in part due to the damage to mitochondrial Ca^{2+} buffering. Furthermore, whether the balance of mitochondrial fission/fusion dynamics is impaired in photoreceptors under hyperglycemic stress is not clear.

Melatonin is a strong antioxidant that can scavenge a variety of ROS, including hydroxyl radical, H_2O_2, O^{2-}, singlet oxygen, peroxynitrite anion, nitric oxide, and hypochlorous acid [28], and activate other antioxidative enzymes, such as glutathione peroxidase and superoxide dismutase [28]. Melatonin is able to prevent oxidative stress caused by mitochondrial fission [29, 30] and reverse mitochondrial damage by upregulating mitochondrial fusion [31]. Melatonin not only attenuates tight junction breakdown in the brain [32], but it also decreases retinal injury [33]. Furthermore, melatonin is able to reduce hepatic mitochondrial damage in both STZ- and obesity-induced diabetic rats [34, 35]. However, in diabetic patients, reports on intraocular melatonin are controversial. In diabetic patients, melatonin levels in the blood and retina are significantly decreased [36], which is correlated with increased insulin resistance [37]. On the contrary, increased melatonin is found in the aqueous humor of diabetic patients [38]. In the United States, melatonin can be self-administered and easily purchased without a doctor's prescription. About 0.7% of Americans use melatonin as a supplement, double that of 5 years ago [39]. Since there are contradicting reports on melatonin's action in retinal neurons [40–42], we aimed to clarify the efficacy of melatonin in preventing retinal dysfunction in early diabetes.

2. Materials and Methods

2.1. Cell Culture.
Mammalian 661W cells were originally derived from a mouse retinal tumor and characterized as a cone-photoreceptor cell line, since they express cone-specific opsins, transducin, and arrestin [43, 44]. The 661W cells were obtained from Dr. Al-Ubaidi (University of Houston) and cultured in Dulbecco's modified Eagle's medium (DMEM) supplemented with 10% Fetal Bovine Serum (FBS), 1% Glutamax, and 1% antibiotics at 37°C and 5% CO_2. Cultured 661W cells were treated with high glucose (HG, 30 mM) for different durations to examine any signal transduction changes. Some HG-treated cells were treated with melatonin (100 μM) concurrently to determine the effect of melatonin on HG-induced changes.

2.2. Western Immunoblotting.
Cell lysates were collected and prepared as described previously [45, 46]. Briefly, 661W cells were harvested and lysed in a Tris lysis buffer (in mM): 50 Tris, 1 EGTA, 150 NaCl, 1% Triton X-100, 1% β-mercaptoethanol, 50 NaF, and 1 Na_3VO_4, pH 7.5. Samples were separated on 10% sodium dodecyl sulfate-polyacrylamide gels by electrophoresis and transferred to nitrocellulose membranes. The primary antibodies used in this study were DRP1 (1:1000; Cell Signaling Technology, Danvers, MA, USA), MFN2 (1:1000 Abcam, Cambridge, MA, USA), MCU (1:1000 Abcam), and actin (loading control; 1:1000, Cell Signaling Technology). Blots were visualized using appropriate secondary antibodies (Cell Signaling Technology) at 1:1000 conjugated to horseradish peroxidase and an enhanced chemiluminescence (ECL) detection system (Pierce, Rockford, IL, USA). Band intensities were quantified by densitometry using Scion Image (NIH, Bethesda, MD, USA).

2.3. Calcium Imaging in Living Cells.
The 661W cells were cultured on cover glass chambered slides (Nunc Lab-Tek; Thermo Fisher Scientific, Waltham, MA, USA) with the same medium described above. After treatment with HG or HG/melatonin for 24 hours, cells were directly loaded with 2 μM Fluo-4 (Thermo Fisher Scientific) and 2 μM rhodamine-2 (Rhod-2; Thermo Fisher Scientific) for 30 mins at 37°C for cytosolic and mitochondrial Ca^{2+} imaging [47, 48]. After washing, new culture medium was added, and then fluorescent images were taken under identical settings, including the light intensity, exposure time, and magnification. The average fluorescent intensity per pixel for each image was quantified without any modification using the luminosity channel of the histogram function of Photoshop 6.0 (Adobe Systems, San Jose, CA, USA). A total of 8 to 11 cell images from each group were analyzed from 3 different sets of experiments [45, 46].

2.4. Animals.
Four-week-old wild-type (WT) male C57BL/6J mice were purchased from the Jackson Laboratory (Bar Harbor, ME, USA). All animal experiments were approved by the Institutional Animal Care and Use Committee of Texas A&M University. Mice were housed under temperature- and humidity-controlled conditions with 12:12 h light-dark cycles. All mice were given food and water *ad libitum*.

2.5. Diabetes Induction and Melatonin Treatment. At 5 weeks of age (body weight around 20 g), mice were randomly assigned to control or STZ-diabetic groups. The STZ-diabetic mice were given intraperitoneal (i.p.) injections of STZ (100 mg/kg body weight (b.w.)) for three consecutive days. STZ was first dissolved in 0.05 M citric buffer (pH 4.5; 10 mg/ml), and each mouse was injected at a dose of 200 μl per 20 g b.w. The nondiabetic controls were given i.p. injections of citric buffer (same volume). The blood glucose levels were monitored once a week using a Clarity glucometer (Diagnostic Test Group, Boca Raton, FL, USA) during the daytime at Zeitgeber time (ZT) 10. One week post STZ injections, mice with a blood glucose level higher than 250 mg/dl were considered to be diabetic. At this time, half of the STZ-diabetic mice were given 10 mg/kg b.w. melatonin by oral gavage daily right before the room lights turned off for three months, while the other half were given H_2O. Freshly prepared melatonin was mixed in H_2O (2 mg/ml), and each mouse was given 100 μl melatonin solution per 20 g b.w. Electroretinogram (ERG) recordings were used to record retinal light responses, and fluorescein angiography (FA) was used to monitor retinal vasculature changes for all mice monthly. STZ-diabetic mice were sacrificed after 3 months of melatonin treatments, and the eyes were fixed for further analyses.

2.6. In Vivo Electroretinogram (ERG). The ERG retinal light responses were recorded as described previously [46]. Mice were dark-adapted for a minimum of 3 hours and anesthetized with an i.p. injection of Avertin (2% 2,2,2-tribromoethanol, 1.25% tert-amyl alcohol; Fisher Scientific, Pittsburgh, PA, USA) solution (12.5 mg/ml) at a dose of 500 μl per 25 g of body weight. Pupils were dilated using a single drop of 1% tropicamide/2.5% phenylephrine mixture for 5 minutes. Mice were placed on a heating pad to maintain their body temperature at 37°C. The ground electrode was placed on the tail, and the reference electrode was placed under the skin in the cheek below the eye. A thin drop of Goniovisc (Hub Pharmaceuticals, Rancho Cucamonga, CA, USA) was applied to the cornea surface to keep it moist, and a threaded recording electrode conjugated to a minicontact lens (OcuScience, Henderson, NV, USA) was placed on top of the cornea. All preparatory procedures were done under a dim red light, and the light was turned off during the recording. A portable ERG device (OcuScience) was used to measure dark-adapted ERG recordings at light intensities of 0.1, 0.3, 1, 3, 10, and 25 candelas·second/meter^2 (cd·s/m^2). Responses to 4 light flashes were averaged at the lower light intensities (0.1, 0.3, 1.0, and 3.0 cd·s/m^2), whereas only 1 light flash was applied for the higher light intensities (10 and 25 cd·s/m^2). A 1-minute recovery period was programmed between different light intensities. The amplitudes and implicit times of the a- and b-waves were recorded and analyzed using the ERGView 4.4 software (OcuScience). Both eyes were included in the analyses.

2.7. Fluorescein Angiography (FA). Mice were anesthetized with an i.p. injection of Avertin (12.5 mg/ml) at a dose of 500 μl per 25 g of body weight. The pupils were dilated using a single drop of 1% tropicamide/2.5% phenylephrine mixture for 5 minutes. Immediately following pupil dilation, 10% sodium fluorescein (Akorn, Lake Forest, IL, USA) was i.p. injected at a dose of 50 μl per 25 g of body weight. Images were taken using an iVivo Funduscope for small animals (OcuScience). The vascular parameters were further analyzed using Photoshop 6.0 (Adobe Systems) and AngioTool, an analytical software developed by the US National Institutes of Health/National Cancer Institute (Bethesda, MD, USA). Areas of 289×289 pixels in the peripheral retinal region (800 pixels from the optic nerve) were cropped using Photoshop and used to analyze the microvascular density using AngioTool. The primary retinal arteries and veins were not included in the analyses.

2.8. Immunofluorescent Staining. Mouse eyes were excised and prepared as previously described [46]. Briefly, the eyes were fixed with Zamboni fixative and processed for paraffin sectioning (4 μm). Each glass slide contained single paraffin sections from the control (CON), STZ, and STZ plus melatonin (STZ+MEL) groups. After deparaffinization and antigen retrieval, sections were washed in phosphate-buffered saline (PBS), blocked with 10% goat serum for 2 hours at room temperature, and then incubated overnight with primary antibodies at 4°C. On the next day, sections were washed with PBS several times and incubated with fluorescent-conjugated secondary antibodies for 2 hours at room temperature and mounted with ProLong Gold antifade reagent containing 4′,6′-diamidino-2-phenylindole (DAPI; Invitrogen/Life Technologies, Grand Island, NY, USA). The primary antibodies used were DRP1, MFN2, and MCU. The secondary antibodies used were Alexa Fluor 488 goat anti-rabbit immunoglobulin G (IgG; 1 : 150 dilution; Molecular Probes/Life Technologies, Grand Island, NY, USA) and Cy5 goat anti-mouse IgG (1 : 150 dilution; Abcam). Images were obtained using a Zeiss Stallion digital imaging workstation equipped with a Zeiss Axiovert 200M microscope (Carl Zeiss AG, Oberkochen, Germany). Fluorescent images from each group were taken under identical parameters, including the same exposure time and magnification. Image analysis included the whole retina (from the photoreceptor outer segment to the ganglion cell layer), photoreceptor inner segments ("photoreceptors"), and the inner retina (from the inner nuclear layer to ganglion cell layer). The averaged fluorescence intensity per pixel for each image was quantified without any modification using the luminosity channel of the histogram function in Photoshop 6.0 (Adobe Systems), and the green or red fluorescence intensities were measured on a brightness scale from 0 to 255. A total of 3 to 5 retinal sections from each group were processed for immunostaining and image analyses. The fluorescent intensities of the control (CON) were arbitrarily set at 1 for each slide. N represents the number of mice from each group.

2.9. Statistical Analyses. All data are presented as mean ± standard error of the mean (SEM). Origin 8.6 software (OriginLab, Northampton, MA, USA) was used for statistical analyses. One-way analysis of variance (ANOVA) followed by Fisher's post hoc test was used for statistical

analyses among all experimental groups. Both eyes from the same animal were used in the analyses, and "n" indicates the number of animals per group. Throughout, $p < 0.05$ was regarded as significant.

3. Results

3.1. High Glucose (HG) Induces Changes in Mitochondrial Fission/Fusion Dynamics and Intracellular Calcium Storage in Photoreceptor-Derived Cells. Since photoreceptors are the largest cell population in the mouse retina and are the major source of intraocular oxidative stress in the diabetic retina [9], we used cultured 661W cells, a photoreceptor-derived murine cell line [44], to understand how hyperglycemia affects mitochondrial fission/fusion dynamics and whether melatonin is able to protect photoreceptors from hyperglycemia-induced damage in mitochondria. The cultured 661W cells were treated with high glucose (HG, additional 30 mM added into the culture medium) for 4, 6, 16, and 24 hours. Compared to the control (CON) treated with H_2O (vehicle), treatments with HG upregulated DRP1 expression significantly from 6 to 24 hours but downregulated the expression of MFN2 from 6 to 24 hours in a time-dependent manner (Figure 1), indicating that HG induced mitochondrial fission but dampened the fusion process in cultured 661W cells. Treatments with HG also decreased the MCU expression in a time-dependent manner (Figure 1), indicating that HG might decrease the mitochondrial Ca^{2+} pool. Treatment with melatonin (100 μM) concurrently with HG for 24 h was able to avert HG-caused increase of DRP1 and decrease of MCU (Figure 1), suggesting that melatonin might have protective actions against hyperglycemia-induced changes in mitochondrial fission-fusion dynamics and in decreased mitochondrial Ca^{2+} buffering capacity.

3.2. High Glucose- (HG-) Induced Decreases in the Mitochondrial Ca^{2+} Pool Are Alleviated by Melatonin Treatments. Cultured retinal neurons [49] or retinal endothelial cells [50] treated with HG for a few days have an increase in cytosolic (intracellular) Ca^{2+}, which can further lead to morphological changes in mitochondria [51] and cell apoptosis [50]. We postulated that HG-caused increase of cytosolic Ca^{2+} in part was due to the decrease of MCU (Figure 1), meaning mitochondria would have decreased capacity to store Ca^{2+}. To verify this hypothesis, we used Fluo-4 [52] and Rhod-2 [53] to differentiate between cytosolic and mitochondrial Ca^{2+}, respectively. Compared to the control (CON) treated with H_2O, 661W cells treated with HG for 24 h had a higher Fluo-4 intensity with a decreased Rhod-2 intensity (Figure 2), reflecting that HG caused an increase of cytosolic Ca^{2+} but a decrease of mitochondrial Ca^{2+}. The HG-induced decrease of the mitochondrial Ca^{2+} pool might partially contribute to the increased cytosolic Ca^{2+}. We found that melatonin was able to prevent HG-caused decrease of MCU (Figure 1), indicating that melatonin might be able to alleviate HG-caused changes in the mitochondrial Ca^{2+} buffering ability. Melatonin treatment prevented HG-caused decreases in mitochondrial

Ca^{2+} storage (Figure 2), but it did not completely dampen HG-induced increases in cytosolic Ca^{2+}. These results (Figures 1 and 2) illustrate that HG-caused decrease of MCU dampened the mitochondrial capability to store Ca^{2+}, and melatonin was able to prevent this impairment through an upregulation of MCU.

3.3. Melatonin Once-a-Day Oral Supplement Does Not Prevent STZ-Induced Diabetic Conditions Systemically. We used STZ injections to induce type 1 diabetes in this study. Mice were randomly assigned to four groups: the control (CON) injected with citric buffer, STZ-injected (STZ), melatonin-treated (MEL), and STZ-injected with daily melatonin treatments through oral gavage (STZ+MEL). Instead of providing melatonin in drinking water at all times or in daily intraperitoneal injections or by subdermal implants, which were used in published reports on the *in vivo* effects of melatonin, we administered 10 mg/kg b.w. of melatonin through oral gavage once daily to mimic the most commonly used intake route in humans. This dosage is equivalent to 0.7 mg/kg b.w. of humans [54], which is within the range of taking melatonin as a preventative treatment for cancer tumorigenesis [55] or management of insomnia [56, 57]. We administered melatonin once daily to mice right before the room light turned off (immediately before Zeitgeber time 12) to avoid circadian phase-shifting of the mice, as melatonin synthesis begins in the evening and continues throughout most of the nocturnal phase [58]. We monitored the body weights and blood glucose levels in mice before and after the STZ injections. Compared to the CON or MEL, STZ-induced diabetic mice had slower body weight gains (Figure 3(a)), and they developed diabetic hyperglycemia (above 250 mg/dl) within one month after the STZ injections (Figure 3(b)). Daily treatments with melatonin in STZ mice (STZ+MEL) did not improve the slow weight gain (Figure 3(a)). Chronic treatments with melatonin seemed to further worsen the hyperglycemic condition in STZ-diabetic mice (Figure 3(b)). Hence, daily melatonin treatment through oral gavage was not effective in controlling systemic glycemia in STZ-induced diabetic mice.

3.4. Dark-Adapted Retinal Light Responses Are Decreased in Diabetic Mice Three Months after STZ Injections. Distorted color vision and delayed retinal light responses are among the first clinical signs of retinal dysfunction in early stage diabetic patients without DR [59, 60]. We previously reported that the retinal light responses are delayed in obese mice that were given a high-fat diet for only one month, even though at this point these mice still have normal blood glucose levels [46]. This result verifies that under prediabetic conditions, the physiology of the neural retina might have been compromised. Melatonin treatments through either intraperitoneal injections [61] or subcutaneous implantation of melatonin pellets [33] in STZ-diabetic rats improve STZ-induced reduction of retinal light responses. We next examined at what point does the STZ-induced hyperglycemic condition cause retinal dysfunction and whether melatonin treatments through daily oral gavage might have the same beneficial
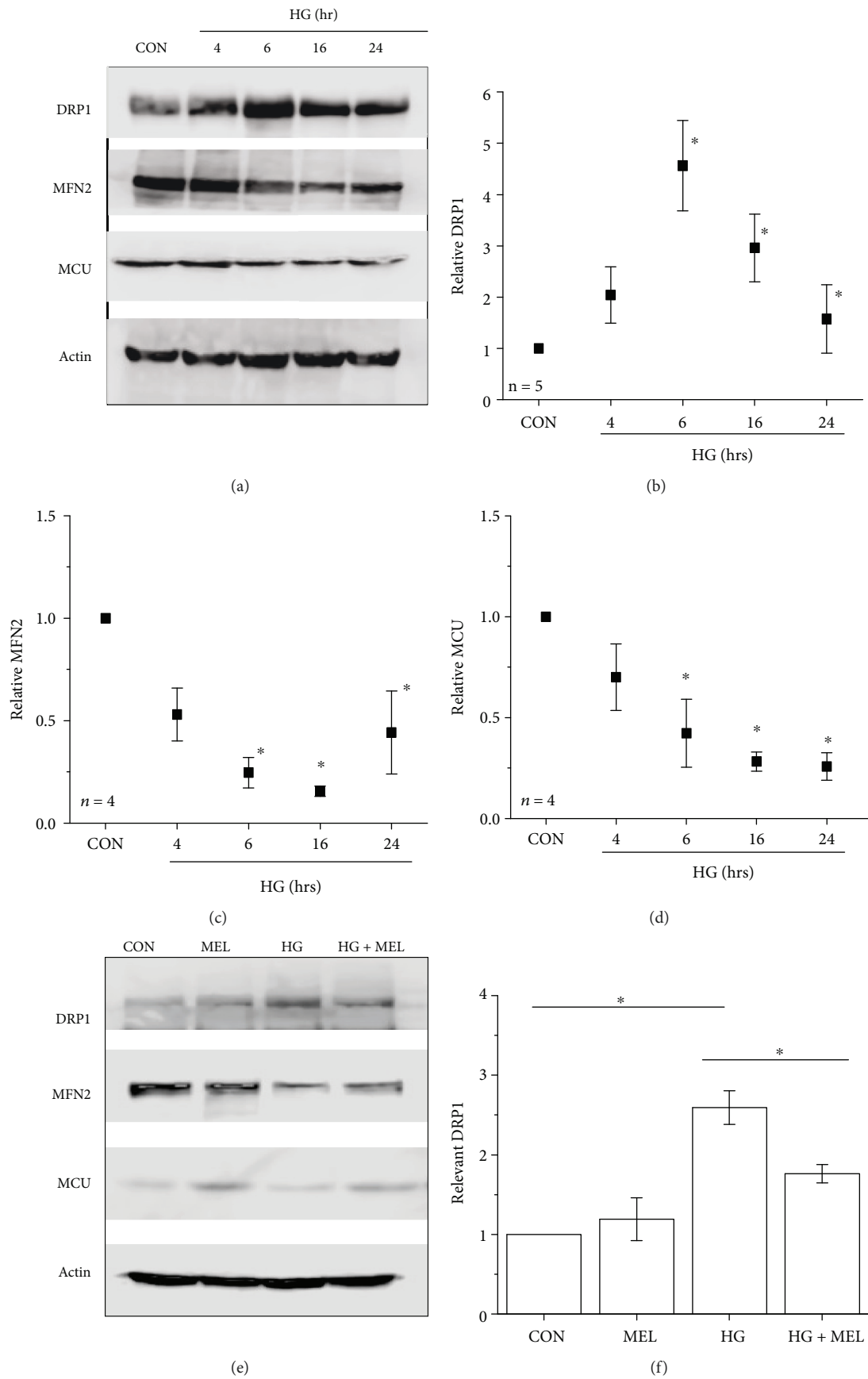
(a)

(b)

(c)
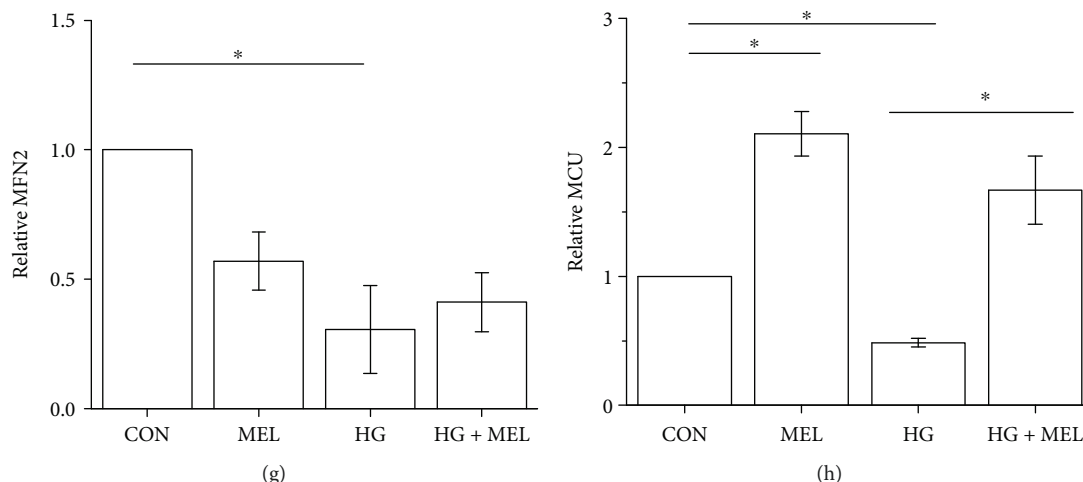
(d)

(e)

(f)

Figure 1: Continued.

FIGURE 1: High glucose induces changes in mitochondrial fission/fusion dynamics in cultured 661W cells. Cultured 661W cells were acutely exposed to high-glucose conditions (HG; 30 mM) for 4, 6, 16, or 24 h (a-d) and collected for Western blotting of DRP1 (b), MFN2 (c), and MCU (d). The control (c) cells were treated with H_2O. (e-g) Cultured 661W cells were treated with 0.01% ethanol (vehicle) as the control (CON), melatonin (MEL, 100 μM; dissolved in 0.01% ethanol), HG (30 mM), or a combination of melatonin and HG (HG+MEL) for 24 h. Cells were then collected and processed for Western blotting analysis of DRP1 (f), MFN2 (g), and MCU (h). The experiments were repeated at least four times (n = 4-5). $^*p < 0.05$.

effects as other routes by using ERG recordings to measure retinal light responses monthly.

Mice were first dark adapted for at least 3 h prior to the ERG recordings with stimulations of various light intensities at 0.1, 0.3, 1, 3, 10, and 25 cd·s/m^2 (Figures 4 and 5). The ERG a-wave reflects the light responses from the photoreceptors, while the b-waves reflect the inner retinal light responses [62]. The ERG implicit times reflect how fast the neural retina responds to light flashes [63]. One month after STZ injections, STZ-injected mice without melatonin treatments (STZ) had delayed retinal light responses, as their implicit times were longer compared to the non-STZ mice (Figures 4 and 5). This delayed light response in the STZ mice continued at 2- and 3-month post STZ injections, along with significantly lower light responses as reflected by decreased a- and b-wave ERG amplitudes (Figures 4(c)–4(f) and 5(c)–5(f)), indicating that chronic hyperglycemic conditions negatively impact retinal light responses. Treatments with melatonin for 3 months (MEL) seemed to increase the retinal light responses in nondiabetic mice, and melatonin treatments (STZ+MEL) appeared to prevent STZ-induced dampening of inner retinal light responses (b-wave) by this time, since the ERG b-wave amplitudes of the STZ+MEL group were similar to that of the control (CON; Figure 5(e); % denotes a statistical significance between STZ and STZ +MEL). Hence, through once daily oral gavage treatments for 3 months, melatonin appears to have protective effects on retinal light responses against STZ-induced diabetes.

3.5. Melatonin Appears to Prevent the Development of STZ-Induced Microvascular Complications. We previously reported that high-fat diet-induced diabetic mice have increased microvascular complications including increased vascular permeability (shown as increased vascular areas) and acellular microvasculature in the peripheral retina at 6-

7 months after the high-fat diet regimen [46, 64, 65]. There is increased vascular permeability in STZ-induced diabetic mice [66]. Even though melatonin appeared to have a temporary and mild effect on retinal light responses of diabetic mice (STZ+MEL; Figures 4 and 5), we next examined whether melatonin had any protective effect on STZ-induced microvascular changes. We employed fluorescein angiography (FA), a tool that reveals changes in the ocular vasculature and can indicate vascular permeability in the eye [67], with AngioTool (NIH) to visualize and quantify the ocular vessels (Figure 6). We previously did not find any major vascular changes in the central retina in obesity-induced diabetic animals [46, 64, 65]. As such, we focused on vascular changes in the peripheral retina. These STZ mice (3 months after STZ injections) had an increase in vascular area and average vessel length (Figure 6), which echoes a previous finding that there is an increase in ocular vascular permeability at 3 months after STZ injections [66]. Daily treatments with melatonin had a dampening effect in STZ-induced increases in vascular area and average vessel length (Figure 6). As daily oral gavage of melatonin (MEL) did not affect body weight, blood glucose levels (Figure 3), or retinal light responses (Figures 4 and 5), unexpectedly, melatonin alone (MEL) appears to increase the vascular area (Figure 6), even though treatments with melatonin in STZ mice (STZ+MEL) decreased the vascular area and average vessel length. We also observed "venous beading" in 3 of the 6 STZ mice at 3 months post STZ injections (Figure 6(d), STZ, red rectangle). Venous beading is a microvascular abnormality often observed in the eyes of patients with nonproliferative DR [68]. Venous beading was not observed in the control (CON), MEL, or STZ+MEL mice, indicating that melatonin treatments might avert venous beading in STZ-diabetic mice. Thus, treatments with melatonin might be able to prevent the STZ-induced microvascular complications in the retina.
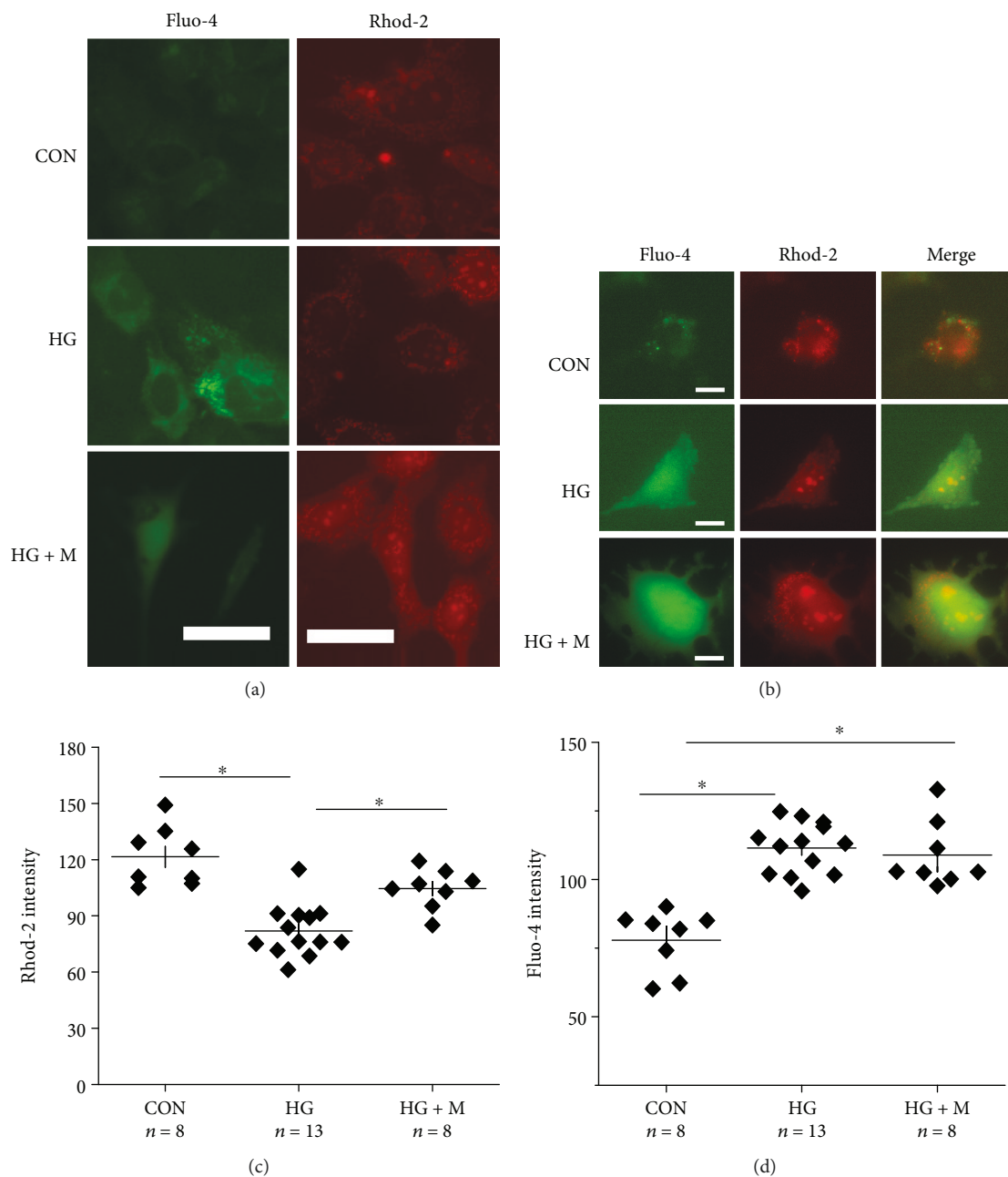
Fluo-4   Rhod-2

CON

HG

HG + M

(a)

Fluo-4   Rhod-2   Merge

CON

HG

HG + M

(b)

(c)

(d)

Figure 2: Melatonin treatments alleviate HG-induced decreases in mitochondrial Ca^{2+} buffering. Calcium-imaging of cultured 661W cells after 24 h of treatments with H_2O (CON), HG, or HG+melatonin (HG+M). Cells were loaded with Fluo-4 and Rhod-2 for cytosolic and mitochondrial Ca^{2+} imaging, respectively. Scale bar = 20 μm in (a) and 10 μm in (b). The Rhod-2 (c) and Fluo-4 (d) fluorescent intensities indicating mitochondrial (c) and cytosolic (d) Ca^{2+} were quantified. The experiments were repeated at least three times. $^*p < 0.05$.

3.6. Melatonin Administration Alleviates the STZ-Disturbed Mitochondrial Fission-and-Fusion Dynamics and Calcium Buffering in the Diabetic Retina. As mentioned previously, mitochondria undergo fission processes when cells are under nutrient overload in cultures [4, 5]. We showed that when 661W cells are cultured in high-glucose conditions (Figure 1), there was an increase of DRP1 and decrease of MFN2 indicating an increase of mitochondrial fission but a decrease in fusion. Since melatonin might have a protective effect in diabetic retinas, we examined whether the mitochondrial fission-and-fusion dynamics in the retina might

be altered under chronic hyperglycemic conditions with a focus on the mitochondrial changes in the retina from STZ mice with or without melatonin treatments. Interestingly, we found that there was no significant change in the mitochondrial fission process in the retina measured by the immunostaining of DRP1 in the STZ-diabetic mouse retina (STZ) compared to the control (CON), and treatment with melatonin in STZ mice (STZ+MEL) did not have any impact on the retinal DRP1 expression (Figure 7). However, the mitochondrial fusion process measured by the immunostaining of MFN2 is significantly decreased in the STZ-diabetic
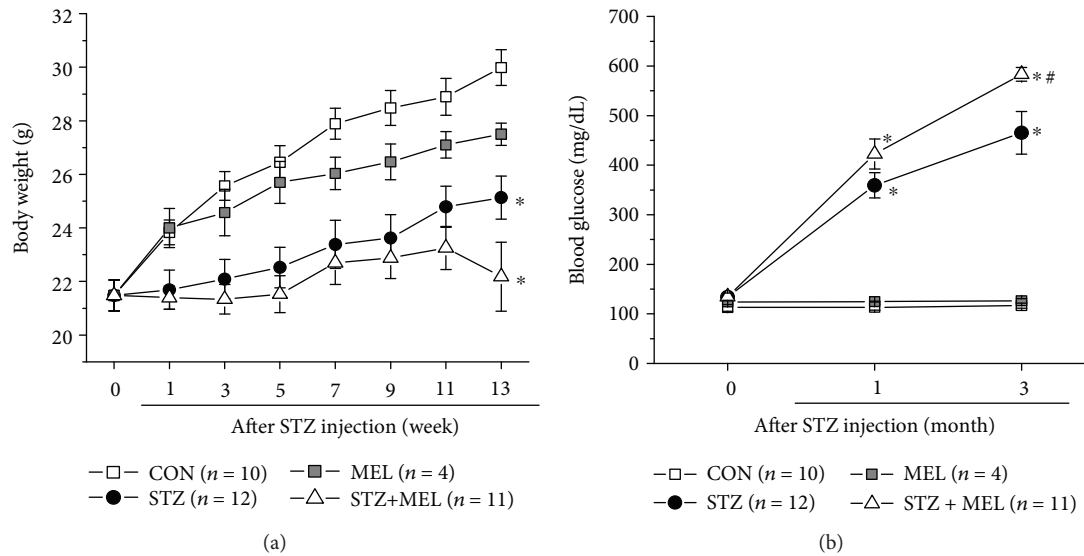
(a)

(b)

FIGURE 3: Daily treatments with melatonin did not improve STZ-induced diabetic conditions in body weights and systemic hyperglycemia. One week after STZ injections, some STZ-injected mice were given daily melatonin via oral gavage (STZ+MEL). (a) STZ-induced diabetic mice (STZ) with or without melatonin treatments gained weight more slowly starting 1 week after STZ injections compared to the control mice injected with citric buffer (CON). Three months after melatonin treatment, the average body weights of STZ+MEL mice or STZ mice were lower than those of the control mice (*). There was no statistical difference between the CON and melatonin-treated (MEL) groups. (b) The STZ and STZ+MEL mice had significantly higher systemic blood glucose levels than the CON or MEL (*). The blood glucose levels of STZ+MEL mice were higher than those of STZ mice (#) after 3 months post-STZ injection. * denotes a statistical significance compared to the control mice (CON); # denotes a statistical significance compared to the STZ mice. *, #$p < 0.05$.

mouse retina, and the decrease was more profound in the photoreceptors than in the inner retina, but the MFN2 level in the STZ mouse retina treated with melatonin (STZ +MEL) was similar to that of the control (CON), indicating that melatonin might prevent STZ-induced decrease of mitochondrial fusion in the retina.

In diabetic cardiomyocytes, mitochondrial Ca^{2+} is decreased by 40%, and the buffering capacity of mitochondria is altered [69]. Since STZ mouse retinas had altered levels of the mitochondrial fusion protein MFN2, we next examined whether the expression of MCU was also altered, since MCU is responsible for storing intracellular Ca^{2+} in the mitochondria [15, 16]. Similar to the cultured 661W cells that were under hyperglycemic conditions which had decreased MCU and mitochondrial Ca^{2+} pools (Figures 1 and 2), we found that the protein expression of MCU was decreased in the STZ mouse retinas (photoreceptors as well as the inner retina), but treatments with melatonin in these mice (STZ+MEL) were able to prevent the STZ-induced loss of MCU in photoreceptors as well as the inner retina (Figure 7), implying that melatonin treatments could protect or recover mitochondrial Ca^{2+} buffering ability in the diabetic retina.

4. Discussion

Maintaining proper mitochondrial fission/fusion dynamics is critical for keeping cells healthy. When there is a nutrient overload, such as in hyperglycemic or diabetic conditions, it causes an imbalance in mitochondrial dynamics and leads to oxidative stress. Melatonin is an antioxidant and is also

known to inhibit proangiogenic factors, relieve oxidative stress and inflammation [61, 70, 71], and rescue retinal damage in diabetic animals [33, 61, 72]. Melatonin is able to prevent oxidative stress caused by chemically induced mitochondrial fission [29, 30] and reverse ROS-induced mitochondrial damage by upregulating mitochondrial fusion [31], but we report here for the first time that melatonin is able to prevent hyperglycemia-caused decrease of mitochondrial fusion and Ca^{2+} pool both in vitro and in vivo. Even though there are multiple protein complexes involved in the mitochondrial fission/fusion dynamics and Ca^{2+} buffering, we selected key players that are essential for these processes (DRP1, MFN2, and MCU) to investigate the effects of melatonin in hyperglycemia-caused changes in mitochondrial function, as well as the protective effect of melatonin in STZ-induced diabetic retinas. As overexpression of MCU can restore the damage caused by hyperglycemia-associated oxidative stress in cardiomyocytes [73], our data showed that melatonin prevented hyperglycemia-caused decreases of MCU in cultured 661W cells and STZ-diabetic retinas, which implies that melatonin treatments could decrease the damage caused by diabetes-induced oxidative stress in part through protecting mitochondria Ca^{2+} buffering ability in the retina.

Interestingly, we found that daily melatonin treatment through oral gavage was not effective in controlling systemic glycemia in STZ-induced diabetic mice (Figure 3), which echoes previously published data using subcutaneous implants of melatonin pellets to treat STZ-induced diabetic rats [33]. The melatonin-insulin antagonism might explain the ineffectiveness of chronic melatonin treatments on controlling systemic glucose levels. Healthy rats given melatonin

Figure 4: Dark-adapted ERG a-wave amplitudes and implicit times recorded at one, two, and three months after STZ injections. The dark-adapted ERG a-wave amplitudes (a, c, e) and implicit times (b, d, f) in the control (CON), STZ-injected (STZ), melatonin-treated (MEL), and STZ-injected and melatonin-treated (STZ+MEL) mice at 1 month (a, b), 2 months (c, d), and 3 months (e, f) after the STZ injections. * denotes a statistical significance between CON and STZ; # denotes a statistical significance between MEL and STZ+MEL; $ denotes a statistical significance between CON and MEL; *$p < 0.05$.
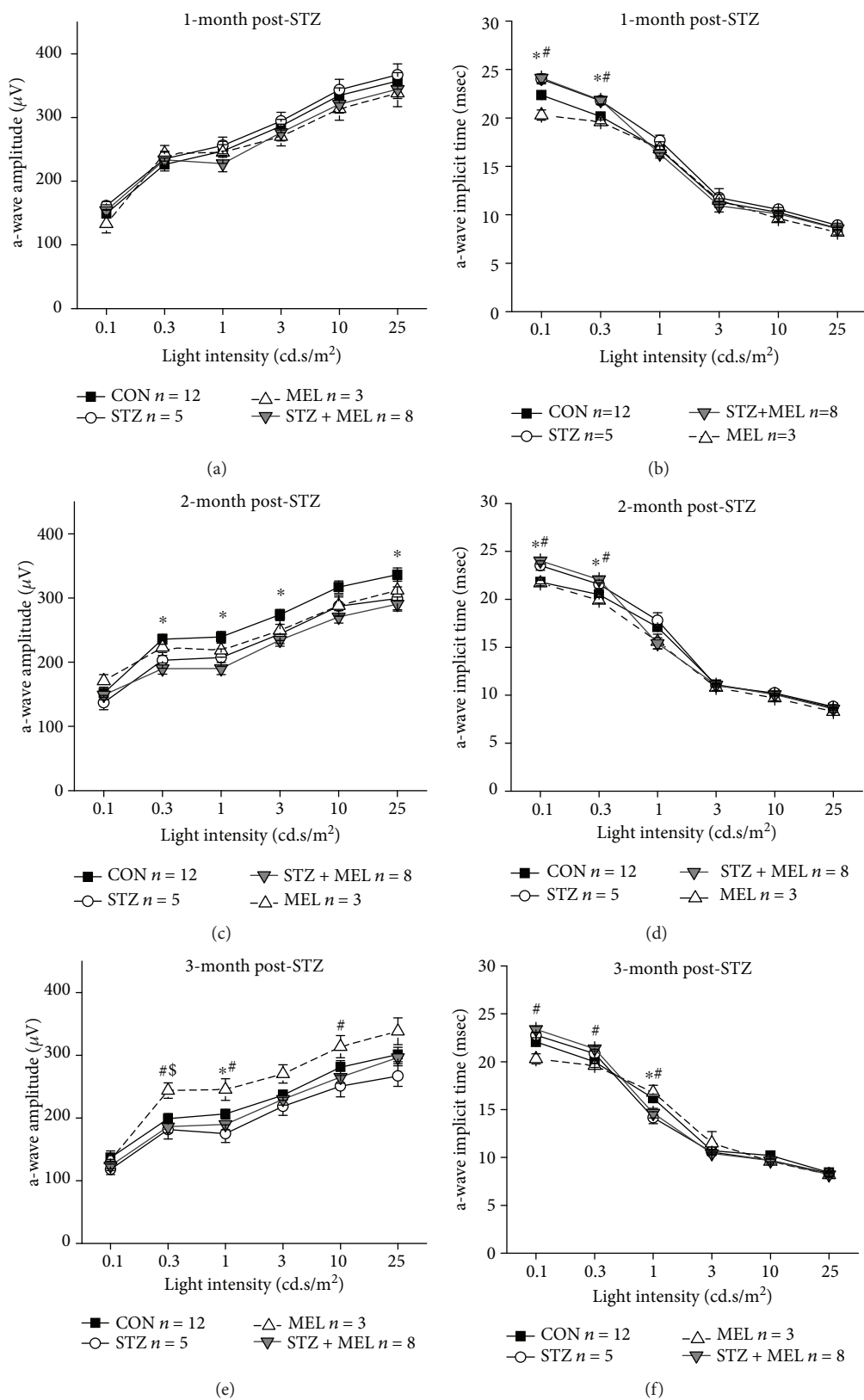
FIGURE 5: Dark-adapted ERG b-wave amplitudes and implicit times recorded at one, two, and three months after STZ injections. The dark-adapted ERG b-wave amplitudes (a, c, e) and implicit times (b, d, f) in the control (CON), STZ-injected (STZ), melatonin-treated (MEL), and STZ-injected and melatonin-treated (STZ+MEL) mice at 1 month (a, b), 2 months (c, d), and 3 months (e, f) after the STZ injections. $*$ denotes a statistical significance between CON and STZ; # denotes a statistical significance between MEL and STZ+MEL; $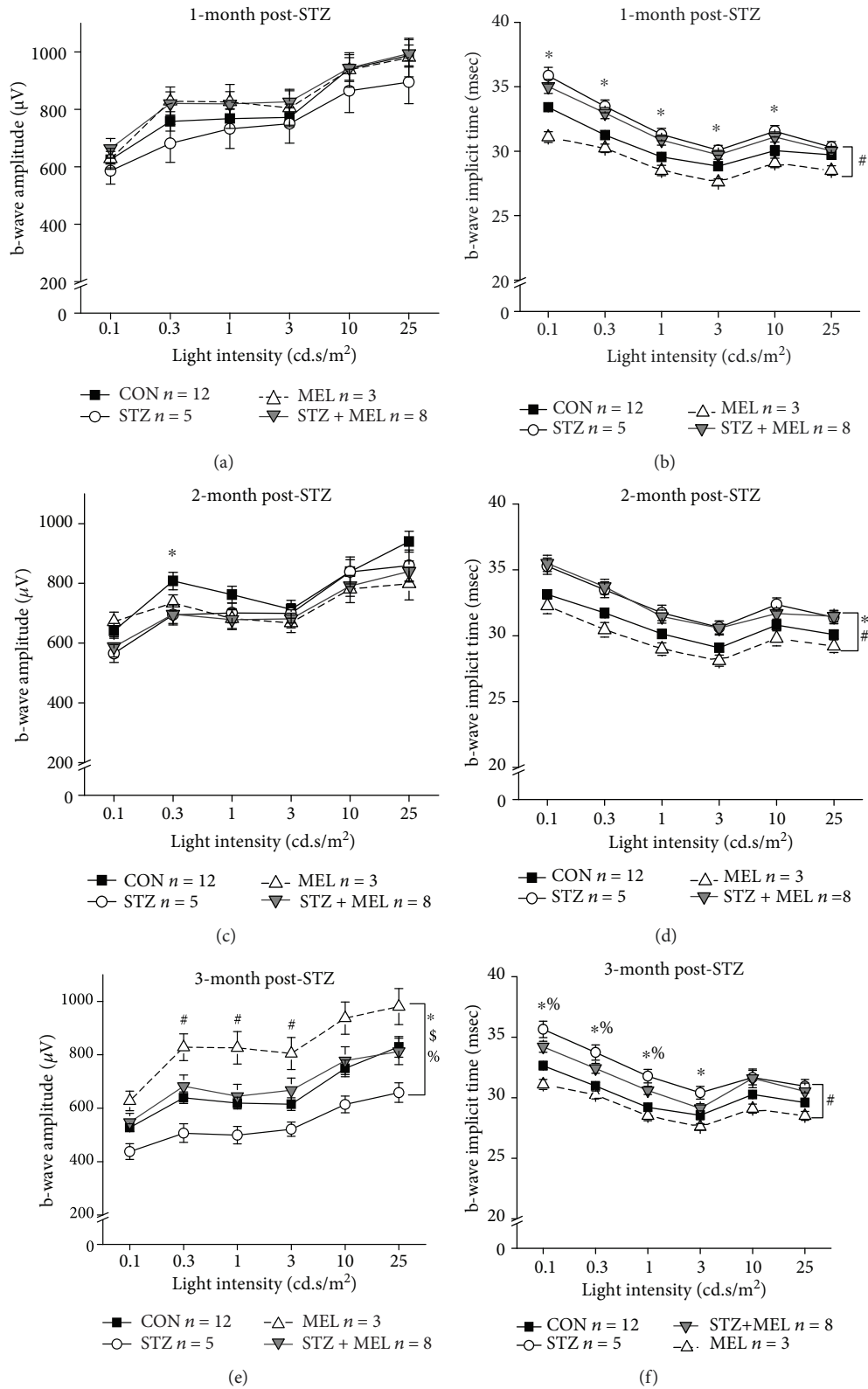 denotes a statistical significance between CON and MEL; % denotes a statistical significance between STZ and STZ+MEL; $*p < 0.05$.

(a)

(b)

(c)

(d)
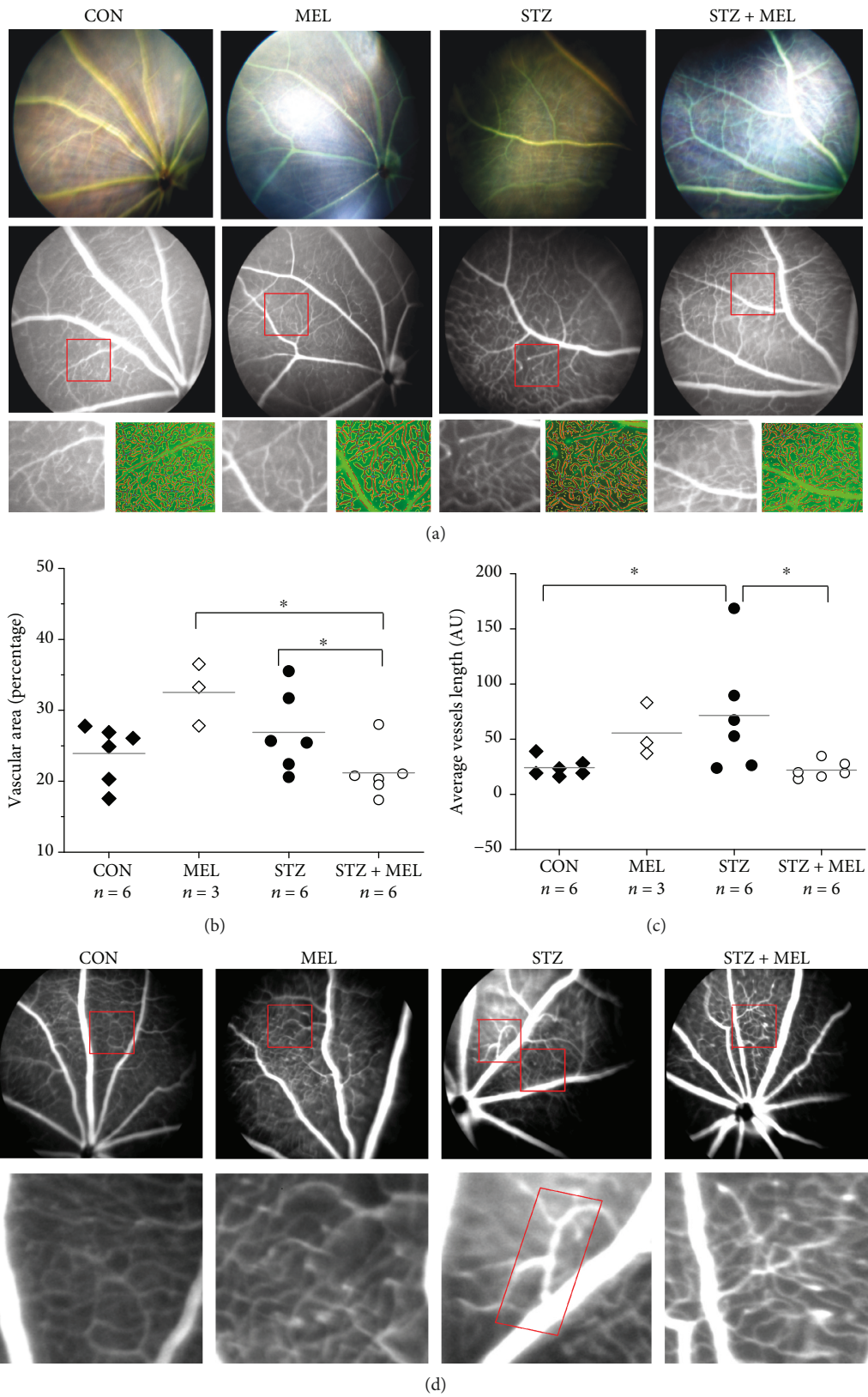
FIGURE 6: Melatonin treatments appear to prevent the development of microvascular complications. (a) Fluorescein angiography was used to visualize the intraocular vasculature in mice. AngioTool was used to determine the (b) percentage of vascular area to the retinal area and (c) the average vessel length. "AU" is the arbitrary unit used in the AngioTool software. The vascular area (percentage) and the average vessel length in STZ+MEL mice are significantly less than those in the STZ mice (*). (d) Venous beading (rectangle) was observed in STZ mice. *$p < 0.05$.

FIGURE 7: Daily melatonin treatments prevent STZ-induced changes in mitochondrial fusion and Ca^{2+} uniporter proteins. The immunofluorescent images of DRP1, MFN2, and MCU in the neural retinas from three groups are shown. The analyzed data of relative changes in fluorescent intensities of the whole retina (second row), the photoreceptors (IS only; third row), and the inner retina (from INL to GL; third row) are shown. The fluorescent intensities of the control (CON) were arbitraril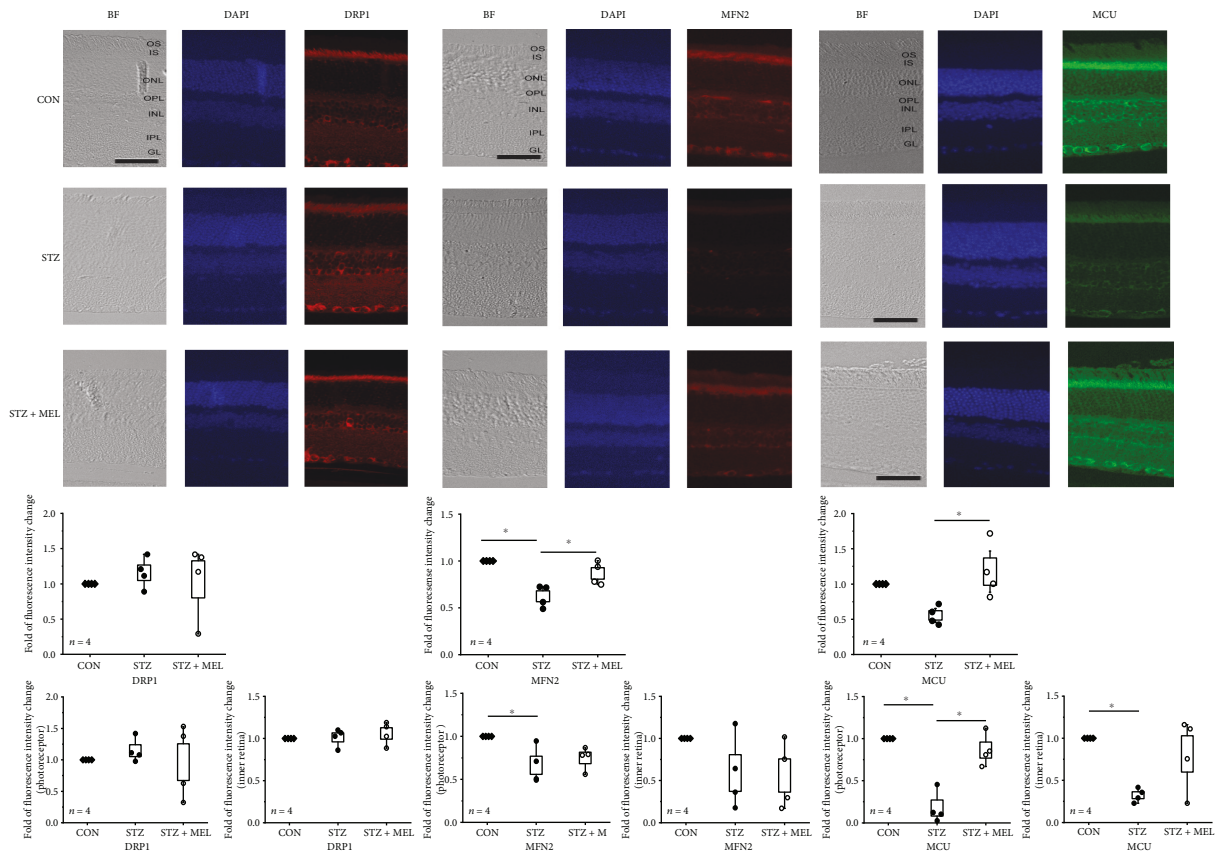y set at 1 for each slide. Each datum point is the average of relative fluorescent intensities (multiple images) from a single mouse. There is no apparent change of DRP1 in the STZ mouse retina (STZ) compared to the control (CON). Melatonin does not have an impact on DRP1 in STZ mouse retinas (STZ+MEL). The STZ mouse retina (STZ) has an apparent decrease in MFN2 compared to both CON and melatonin-treated (STZ+MEL) groups in the photoreceptors. The STZ mouse retina (STZ) also has a significantly decreased MCU expression compared to the melatonin (STZ +MEL) group in the photoreceptors and inner retina. BF = Bright field. DAPI stained nuclei. Scale bar = 50 μm. OS: photoreceptor outer segments; IS: photoreceptor inner segments; ONL: outer nuclear layer; OPL: outer plexiform layer; INL: inner nuclear layer; IPL: inner plexiform layer; GL: ganglion cell layer. $^{*}p < 0.05$.

through drinking water for 3 months have decreased serum insulin but increased corticosterone in addition to altered metabolic profiles [74]. If exogenous melatonin further decreases systemic insulin in STZ-diabetic mice that already secrete extremely low insulin [75], it would lead to a failure to control systemic glycemia.

Diabetic retinopathy is a dual disorder with microvascular complications and retinal degeneration [19]. Monthly ERG recordings showed that retinal light responses changed in mice at 1-month post-STZ injections as their implicit times increased, which shows that the health of the neural retina might have been compromised before any detectable vascular complications. However, one potential concern is the effect of STZ itself. Streptozotocin is a well-known chemical that induces type 1 diabetes in animals through targeting the islet cells, but it is also toxic to the neural retina [76]. Within a month after STZ injections, there is transient cell apoptosis and upregulated glial activation in the neural

retina, but these abnormalities quickly return to normal in the subsequent 2-4 months [77]. Further retinal degeneration and acellular capillaries are observed at least 6 months after the STZ injections [77]. This indicates that STZ might have a transient toxic effect on the neural retina within the first few weeks of injections, which is also reflected in our overall ERG a- and b-wave amplitudes. However, the decreased b-wave amplitudes and increased implicit times after 3 months of STZ injections might indicate that hyperglycemic conditions worsen the retinal light responses.

We found that melatonin treatments had a protective effect on the neural retina particularly after 3 months of treatments. Previous studies using daily intraperitoneal (i.p.) injections of melatonin (10 mg/kg) [61] or melatonin pellet implants (20 mg) [33] to treat STZ-induced diabetic rats demonstrated that these treatments for 3 months clearly alleviate the STZ-induced decreases in ERG a- and b-wave amplitudes back to the normal levels of nondiabetic rats,

which are similar to our results. However, treatment with melatonin alone for 3 months significantly enhanced ERG a- and b-wave amplitudes in mice (Figures 4 and 5) but not in rats [33]. There are two possible explanations for the discrepancy between our results and previous reports on the effects of melatonin on retinal light responses. First, the retinal sensitivity to melatonin treatments is species-dependent. As such, rats might be more responsive to melatonin than the mouse strain (C57BL/6J) that was used in our study. The C57BL/6J is the most used mouse strain to study retinal function since it does not carry genes that cause retinal degeneration. However, C57BL/6J is melatonin-deficient, since this mouse strain lacks serotonin-N-acetyltransferase and hydroxyindole-O-methyl-transferase, two enzymes needed for the synthesis of melatonin from serotonin [78], and it is not clear whether the retinal expression of melatonin receptors in C57BL6J is similar to that of other melatonin-proficient animals [79]. It is possible that the retina of melatonin-proficient animals (such as rats) might respond to exogenous melatonin more effectively compared to that of melatonin-deficient animals. Second, the routes of treatments and the dosages between our current study (oral) and previous reports (i.p. [61] or subcutaneous implantation [33]) are different. We strived to mimic the most common route of human intakes of melatonin (orally, once a day) at a comparable dosage. Thus, it is possible that our overall melatonin dosage absorbed by the animals was not as much compared to those in previous reports.

We also found that melatonin had a protective effect on the retinal microvasculature. We used FA to chronologically monitor the vascular changes, and increases in average vessel length were observed in mice at 3 months post STZ injections. Even though we did not specifically perform vascular permeability assays, changes in FA could indicate vascular permeability in the eye [67]. Venous beading was observed in 50% of the STZ-diabetic mice, but STZ mice treated with melatonin (STZ+MEL) did not have venous beading despite their diabetic status. Melatonin treatments also dampened STZ-induced increases in average vessel length, which indicates that melatonin treatments might prevent vascular permeability in diabetic animals. This indicates that at our dosage via oral gavage, melatonin might have direct effects on the microvasculature, in which the molecular action of melatonin on the microvasculature requires further investigation.

The ATP level is critical in regulating mitochondrial dynamics [45]. In cultured retinal cells, treatment with HG elevates the extracellular ATP, where the release of ATP is involved in the inflammation process [80]. We found that treatments with HG elevated DRP1 and dampened MFN2 in cultured 661W photoreceptors, and the level of MFN2 was also decreased in the STZ-diabetic retina. Mitochondrial fission and fusion play a crucial role in regulating energy expenditure and oxidative metabolism. Tissue-specific ablation of MFN2 in the liver impairs insulin signaling and increases hepatic gluconeogenesis and endoplasmic reticulum (ER) stress [81]. We found that melatonin treatments were able to prevent the STZ-induced decrease of MFN2 in the retina and the HG-caused elevation of DRP1 in cultured

661W cells. These data imply that melatonin is able to avert diabetes-induced decreases in mitochondrial fusion and HG-caused increases of mitochondrial fission. One possible mechanism is that melatonin blocks the translocation of DRP1 into mitochondria to prevent their fission [82]. Hence, melatonin could alleviate hyperglycemia-induced changes in mitochondrial dynamics.

In diabetic pancreases [83] and hearts [84], mitochondria function is disturbed due to the downregulation of MCU. Our data confirmed that the expression of MCU was decreased in HG-treated 661W cells and STZ-diabetic retinas. Further, hyperglycemia decreased the mitochondrial calcium buffering capability in these cells. Treatment with melatonin prevented HG-caused decreases in mitochondrial Ca^{2+} in part through increasing the MCU expression. The decrease of retinal mitochondrial Ca^{2+} buffering ability affects the mitochondrial dynamics [85] and potentially worsens the progression of DR [86]. Thus, our data provide evidence that melatonin is able to recover hyperglycemia-induced decrease of mitochondrial Ca^{2+} pools by increasing the expression of MCU. However, melatonin treatments did not dampen the HG-induced increase of cytosolic Ca^{2+}. Since the overall cytosolic Ca^{2+} depends on the calcium influx through various calcium channels in the plasma membrane, the calcium ATPase in the plasma membrane to extrude intracellular Ca^{2+}, the mitochondrial Ca^{2+} pool, and the ER Ca^{2+} storage, we postulate that melatonin is not able to recover all of the components regulating intracellular calcium homeostasis.

Whether the effect of melatonin on mitochondria is through its antioxidant property or through its receptors remains to be determined, since the interaction between melatonin and its receptors depends on the exposure dosage, duration, and cell types. Treatment with melatonin (100-1000 nM) prevents H_2O_2-induced photoreceptor death in part through melatonin receptors [87]. When an ovary cell line is exposed to a lower concentration of melatonin (400 pM) for 8 hours, an increase in type 1 melatonin (MT1) receptor binding sites occurs [88]. However, treating the same ovary cells at a higher concentration of melatonin (1 μM) for 5 hours desensitizes the MT1 receptors and inhibits phosphoinositide hydrolysis and the subsequent signal transduction cascade [89]. Intraperitoneal injections with 10 mg/kg melatonin cause melatonin to accumulate in the mitochondria much more than in the cytosol, which is not mediated by the MT1 or MT2 receptors on the plasma membrane [90]. This result implies that melatonin at higher concentrations could act directly in the mitochondria, in which we showed that melatonin alone affected MCU and MFN2. Melatonin might also directly act inside the cells as a scavenger of reactive oxygen species or to rescue mitochondria when cells are under oxidative stress. However, MT1 receptors appear to be expressed in the mitochondria isolated from brain lysates [91], and mitochondria also have the ability to synthesize melatonin in brain neurons [92]. Thus, whether the action of melatonin on mitochondria in photoreceptors is mediated by the mitochondrial MT1 receptors remains to be determined.

Taken together, we showed that melatonin is able to avert hyperglycemia-induced changes in mitochondrial dynamics and Ca^{2+} storage in cultured 661W cells. We demonstrated that neural retinal dysfunction might precede any detectable microvascular complications in type 1 diabetes. While the efficacy of melatonin in treating human diabetes still requires more in-depth studies, using an equivalent daily dosage of melatonin (0.7 mg/kg b.w.) taken orally might have a protective effect against diabetes-induced retinal dysfunction and prevent diabetic microvascular complications.

Data Availability

The data (numbers, images, and Western blots) used to support the findings of this study are included within the article. The raw/quantified data used to support the findings of this study are available from the corresponding author upon request.

Conflicts of Interest

The authors declare no competing financial interests.

Authors' Contributions

Janet Ya-An Chang was involved in the experimental design; performed the experiments; was responsible for all data acquisition, analyses, and interpretation as well as writing the manuscript. Fei Yu assisted with experiments, data analyses, and writing of the manuscript. Liheng Shi assisted with data analysis. Michael Ko assisted with editorial work, revisions, and approval of the manuscript. In addition to supervising the project, Gladys Ko was involved in providing the experimental materials and animals, the experimental design, data analyses and interpretation, writing, editing, revision of the text, and approval of the manuscript.

Acknowledgments

References

[1] I. Scott and R. J. Youle, "Mitochondrial fission and fusion," *Essays in Biochemistry*, vol. 47, pp. 85–98, 2010.

[2] H. Sesaki and R. E. Jensen, "Division versus fusion: Dnm1p and Fzo1p antagonistically regulate mitochondrial shape," *The Journal of Cell Biology*, vol. 147, no. 4, pp. 699–706, 1999.

[3] L. C. Gomes and L. Scorrano, "Mitochondrial elongation during autophagy: a stereotypical response to survive in difficult times," *Autophagy*, vol. 7, no. 10, pp. 1251–1253, 2011.

[4] M. Liesa and O. S. Shirihai, "Mitochondrial dynamics in the regulation of nutrient utilization and energy expenditure," *Cell Metabolism*, vol. 17, no. 4, pp. 491–506, 2013.

[5] E. Schrepfer and L. Scorrano, "Mitofusins, from mitochondria to metabolism," *Molecular Cell*, vol. 61, no. 5, pp. 683–694, 2016.

[6] M. O. Dietrich, Z. W. Liu, and T. L. Horvath, "Mitochondrial dynamics controlled by mitofusins regulate Agrp neuronal activity and diet-induced obesity," *Cell*, vol. 155, no. 1, pp. 188–199, 2013.

[7] H. Chen, S. A. Detmer, A. J. Ewald, E. E. Griffin, S. E. Fraser, and D. C. Chan, "Mitofusins Mfn1 and Mfn2 coordinately regulate mitochondrial fusion and are essential for embryonic development," *The Journal of Cell Biology*, vol. 160, no. 2, pp. 189–200, 2003.

[8] Y. J. Lee, S. Y. Jeong, M. Karbowski, C. L. Smith, and R. J. Youle, "Roles of the mammalian mitochondrial fission and fusion mediators Fis1, Drp1, and Opa1 in apoptosis," *Molecular Biology of the Cell*, vol. 15, no. 11, pp. 5001–5011, 2004.

[9] Y. Du, A. Veenstra, K. Palczewski, and T. S. Kern, "Photoreceptor cells are major contributors to diabetes-induced oxidative stress and local inflammation in the retina," *Proceedings of the National Academy of Sciences of the United States of America*, vol. 110, no. 41, pp. 16586–16591, 2013.

[10] D.-Y. Yu and S. J. Cringle, "Oxygen distribution and consumption within the retina in vascularised and avascular retinas and in animal models of retinal disease," *Progress in Retinal and Eye Research*, vol. 20, no. 2, pp. 175–208, 2001.

[11] L. Contreras, I. Drago, E. Zampese, and T. Pozzan, "Mitochondria: the calcium connection," *Biochimica et Biophysica Acta (BBA) - Bioenergetics*, vol. 1797, no. 6-7, pp. 607–618, 2010.

[12] J. Santo-Domingo and N. Demaurex, "Calcium uptake mechanisms of mitochondria," *Biochimica et Biophysica Acta (BBA) - Bioenergetics*, vol. 1797, no. 6-7, pp. 907–912, 2010.

[13] D. E. Clapham, "Calcium signaling," *Cell*, vol. 131, no. 6, pp. 1047–1058, 2007.

[14] M. M. Giarmarco, W. M. Cleghorn, S. R. Sloat, J. B. Hurley, and S. E. Brockerhoff, "Mitochondria maintain distinct Ca^{2+} pools in cone photoreceptors," *The Journal of Neuroscience*, vol. 37, no. 8, pp. 2061–2072, 2017.

[15] Y. Kirichok, G. Krapivinsky, and D. E. Clapham, "The mitochondrial calcium uniporter is a highly selective ion channel," *Nature*, vol. 427, no. 6972, pp. 360–364, 2004.

[16] V. Paupe and J. Prudent, "New insights into the role of mitochondrial calcium homeostasis in cell migration," *Biochemical and Biophysical Research Communications*, vol. 500, no. 1, pp. 75–86, 2018.

[17] D. De Stefani, A. Raffaello, E. Teardo, I. Szabo, and R. Rizzuto, "A forty-kilodalton protein of the inner membrane is the mitochondrial calcium uniporter," *Nature*, vol. 476, no. 7360, pp. 336–340, 2011.

[18] F. B. Giacco and M. Brownlee, "Oxidative stress and diabetic complications," *Circulation Research*, vol. 107, no. 9, pp. 1058–1070, 2010.

[19] Y. Alvarez, K. Chen, A. L. Reynolds, N. Waghorne, J. J. O'Connor, and B. N. Kennedy, "Predominant cone photoreceptor dysfunction in a hyperglycaemic model of non-proliferative diabetic retinopathy," *Disease Models & Mechanisms*, vol. 3, no. 3-4, pp. 236–245, 2010.

[20] S. M. Shenouda, M. E. Widlansky, K. Chen et al., "Altered mitochondrial dynamics contributes to endothelial dysfunction in diabetes mellitus," *Circulation*, vol. 124, no. 4, pp. 444–453, 2011.

[21] Q. Zhong and R. A. Kowluru, "Diabetic retinopathy and damage to mitochondrial structure and transport machinery," *Investigative Ophthalmology & Visual Science*, vol. 52, no. 12, pp. 8739–8746, 2011.

[22] S. Colberg, R. J. Sigal, B. Fernhall et al., "Exercise and type 2 diabetes: the American College of Sports Medicine and the American Diabetes Association: joint position statement," *Diabetes Care*, vol. 33, no. 12, pp. e147–e167, 2010.

[23] T. S. Kern and R. L. Engerman, "Microvascular metabolism in diabetes," *Metabolism*, vol. 35, no. 4, pp. 24–27, 1986.

[24] N. C. Cho, G. L. Poulsen, J. N. Ver Hoeve, and T. M. Nork, "Selective loss of S-cones in diabetic retinopathy," *Archives of Ophthalmology*, vol. 118, no. 10, pp. 1393–1400, 2000.

[25] A. Maeda and K. Palczewski, "Retinal degeneration in animal models with a defective visual cycle," *Drug Discovery Today: Disease Models*, vol. 10, no. 4, pp. e163–e172, 2013.

[26] S. G. Jarrett and M. E. Boulton, "Consequences of oxidative stress in age-related macular degeneration," *Molecular Aspects of Medicine*, vol. 33, no. 4, pp. 399–417, 2012.

[27] L. Shi, M. L. Ko, C. C. Y. Huang et al., "Chicken embryos as a potential new model for early onset type I diabetes," *Journal Diabetes Research*, vol. 2014, article 354094, 10 pages, 2014.

[28] R. J. Reiter, D. X. Tan, C. Osuna, and E. Gitto, "Actions of melatonin in the reduction of oxidative stress. a review," *Journal of Biomedical Science*, vol. 7, no. 6, pp. 444–458, 2000.

[29] J. I. Chuang, I. L. Pan, C. Y. Hsieh, C. Y. Huang, P. C. Chen, and J. W. Shin, "Melatonin prevents the dynamin-related protein 1-dependent mitochondrial fission and oxidative insult in the cortical neurons after 1-methyl-4-phenylpyridinium treatment," *Journal of Pineal Research*, vol. 61, no. 2, pp. 230–240, 2016.

[30] W. Suwanjang, A. Y. Abramov, K. Charngkaew, P. Govitrapong, and B. Chetsawang, "Melatonin prevents cytosolic calcium overload, mitochondrial damage and cell death due to toxically high doses of dexamethasone-induced oxidative stress in human neuroblastoma SH-SY5Y cells," *Neurochemistry International*, vol. 97, pp. 34–41, 2016.

[31] H. Pei, J. Du, X. Song et al., "Melatonin prevents adverse myocardial infarction remodeling via Notch1/Mfn2 pathway," *Free Radical Biology & Medicine*, vol. 97, pp. 408–417, 2016.

[32] J. Chen, G. Chen, J. Li et al., "Melatonin attenuates inflammatory response-induced brain edema in early brain injury following a subarachnoid hemorrhage: a possible role for the regulation of pro-inflammatory cytokines," *Journal of Pineal Research*, vol. 57, no. 3, pp. 340–347, 2014.

[33] E. M. Salido, M. Bordone, A. de Laurentiis et al., "Therapeutic efficacy of melatonin in reducing retinal damage in an experimental model of early type 2 diabetes in rats," *Journal of Pineal Research*, vol. 54, no. 2, pp. 179–189, 2013.

[34] H. Elbe, M. Esrefoglu, N. Vardi, E. Taslidere, E. Ozerol, and K. Tanbek, "Melatonin, quercetin and resveratrol attenuates oxidative hepatocellular injury in streptozotocin-induced diabetic rats," *Human & Experimental Toxicology*, vol. 34, no. 9, pp. 859–868, 2015.

[35] A. Agil, M. El-Hammadi, A. Jiménez-Aranda et al., "Melatonin reduces hepatic mitochondrial dysfunction in diabetic obese rats," *Journal of Pineal Research*, vol. 59, no. 1, pp. 70–79, 2015.

[36] D. do Carmo Buonfiglio, R. A. Peliciari-Garcia, F. G. do Amaral et al., "Early-stage retinal melatonin synthesis impairment in streptozotocin-induced diabetic Wistar rats," *Investigative Ophthalmology & Visual Science*, vol. 52, no. 10, pp. 7416–7422, 2011.

[37] C. J. McMullan, E. S. Schernhammer, E. B. Rimm, F. B. Hu, and J. P. Forman, "Melatonin secretion and the incidence of type 2 diabetes," *JAMA*, vol. 309, no. 13, pp. 1388–1396, 2013.

[38] E. Aydin and S. Sahin, "Increased melatonin levels in aqueous humor of patients with proliferative retinopathy in type 2 diabetes mellitus," *International Journal of Ophthalmology*, vol. 9, no. 5, pp. 721–724, 2016.

[39] T. C. Clarke, L. I. Black, B. J. Stussman, P. M. Barnes, and R. L. Nahin, "Trends in the use of complementary health approaches among adults: United States, 2002–2012," in *National Health Statistics Reports*, pp. 1–16, National Center for Health Statistics, 2015.

[40] A. Wiechmann and W. O'Steen, "Melatonin increases photoreceptor susceptibility to light-induced damage," *Investigative Ophthalmology & Visual Science*, vol. 33, no. 6, pp. 1894–1902, 1992.

[41] K. Baba, N. Pozdeyev, F. Mazzoni et al., "Melatonin modulates visual function and cell viability in the mouse retina via the MT1 melatonin receptor," *Proceedings of the National Academy of Sciences of the United States of America*, vol. 106, no. 35, pp. 15043–15048, 2009.

[42] A. F. Wiechmann, C. F. Chignell, and J. E. Roberts, "Influence of dietary melatonin on photoreceptor survival in the rat retina: an ocular toxicity study," *Experimental Eye Research*, vol. 86, no. 2, pp. 241–250, 2008.

[43] E. Tan, X. Q. Ding, A. Saadi, N. Agarwal, M. I. Naash, and M. R. Al-Ubaidi, "Expression of cone-photoreceptor-specific antigens in a cell line derived from retinal tumors in transgenic mice," *Investigative Ophthalmology & Visual Science*, vol. 45, no. 3, pp. 764–768, 2004.

[44] M. R. Al-Ubaidi, R. L. Font, A. B. Quiambao et al., "Bilateral retinal and brain tumors in transgenic mice expressing simian virus 40 large T antigen under control of the human interphotoreceptor retinoid-binding protein promoter," *The Journal of Cell Biology*, vol. 119, no. 6, pp. 1681–1687, 1992.

[45] J. Y.-A. Chang, L. Shi, M. L. Ko, and G. Y. P. Ko, "Circadian regulation of mitochondrial dynamics in retinal photoreceptors," *Journal of Biological Rhythms*, vol. 33, no. 2, pp. 151–165, 2018.

[46] A. J. Kim, J. Y. A. Chang, L. Shi, R. C. A. Chang, M. L. Ko, and G. Y. P. Ko, "The effects of metformin on obesity-induced dysfunctional retinas," *Investigative Ophthalmology & Visual Science*, vol. 58, no. 1, pp. 106–118, 2017.

[47] J. F. Burkeen, A. D. Womac, D. J. Earnest, and M. J. Zoran, "Mitochondrial calcium signaling mediates rhythmic extracellular ATP accumulation in suprachiasmatic nucleus astrocytes," *The Journal of Neuroscience*, vol. 31, no. 23, pp. 8432–8440, 2011.

[48] K. J. Spinelli and P. G. Gillespie, "Monitoring intracellular calcium ion dynamics in hair cell populations with Fluo-4 AM," *PLoS One*, vol. 7, no. 12, article e51874, 2012.

[49] T. O. S. Pereira, G. N. F. da Costa, A. R. S. Santiago, A. F. Ambrósio, and P. F. M. dos Santos, "High glucose enhances intracellular Ca^{2+} responses triggered by purinergic stimulation in retinal neurons and microglia," *Brain Research*, vol. 1316, pp. 129–138, 2010.

[50] J. Li, P. Wang, S. Yu, Z. Zheng, and X. Xu, "Calcium entry mediates hyperglycemia-induced apoptosis through Ca^{2+}/calmodulin-dependent kinase ll in retinal capillary endothelial cells," *Molecular Vision*, vol. 18, pp. 2371–2379, 2012.

[51] S. Deheshi, B. Dabiri, S. Fan, M. Tsang, and G. L. Rintoul, "Changes in mitochondrial morphology induced by calcium or rotenone in primary astrocytes occur predominantly through

ros-mediated remodeling," *Journal of Neurochemistry*, vol. 133, no. 5, pp. 684–699, 2015.

[52] K. R. Gee, K. A. Brown, W. N. U. Chen, J. Bishop-Stewart, D. Gray, and I. Johnson, "Chemical and physiological characterization of fluo-4 Ca^{2+}-indicator dyes," *Cell Calcium*, vol. 27, no. 2, pp. 97–106, 2000.

[53] E. Boitier, R. Rea, and M. R. Duchen, "Mitochondria exert a negative feedback on the propagation of intracellular Ca^{2+} waves in rat cortical astrocytes," *The Journal of Cell Biology*, vol. 145, no. 4, pp. 795–808, 1999.

[54] A. B. Nair and S. Jacob, "A simple practice guide for dose conversion between animals and human," *Journal of Basic and Clinical Pharmacy*, vol. 7, no. 2, pp. 27–31, 2016.

[55] M. Rondanelli, M. A. Faliva, S. Perna, and N. Antoniello, "Update on the role of melatonin in the prevention of cancer tumorigenesis and in the management of cancer correlates, such as sleep-wake and mood disturbances: review and remarks," *Aging Clinical and Experimental Research*, vol. 25, no. 5, pp. 499–510, 2013.

[56] N. Buscemi, B. Vandermeer, R. Pandya et al., "Melatonin for treatment of sleep disorders: summary," in *AHRQ Evidence Report Summaries*, Agency for Healthcare Research and Quality (US), Rockville, MD, USA, 2004.

[57] R. B. Costello, C. V. Lentino, C. C. Boyd et al., "The effectiveness of melatonin for promoting healthy sleep: a rapid evidence assessment of the literature," *Nutrition Journal*, vol. 13, no. 1, p. 106, 2014.

[58] S. Benloucif and M. L. Dubocovich, "Melatonin and light induce phase shifts of circadian activity rhythms in the C3H/HeN mouse," *Journal of Biological Rhythms*, vol. 11, no. 2, pp. 113–125, 1996.

[59] C. Feitosa-Santana, G. V. Paramei, M. Nishi, M. Gualtieri, M. F. Costa, and D. F. Ventura, "Color vision impairment in type 2 diabetes assessed by the D-15d test and the Cambridge Colour Test," *Ophthalmic and Physiological Optics*, vol. 30, no. 5, pp. 717–723, 2010.

[60] M. McFarlane, T. Wright, D. Stephens, J. Nilsson, and C. A. Westall, "Blue flash ERG PhNR changes associated with poor long-term glycemic control in adolescents with type 1 diabetes," *Investigative Ophthalmology & Visual Science*, vol. 53, no. 2, pp. 741–748, 2012.

[61] T. Jiang, Q. Chang, J. Cai, J. Fan, X. Zhang, and G. Xu, "Protective effects of melatonin on retinal inflammation and oxidative stress in experimental diabetic retinopathy," *Oxidative Medicine and Cellular Longevity*, vol. 2016, Article ID 3528274, 13 pages, 2016.

[62] L. H. Pinto, B. Invergo, K. Shimomura, J. S. Takahashi, and J. B. Troy, "Interpretation of the mouse electroretinogram," *Documenta Ophthalmologica*, vol. 115, no. 3, pp. 127–136, 2007.

[63] K. T. Brown, "The eclectroretinogram: its components and their origins," *Vision Research*, vol. 8, no. 6, pp. 633–677, 1968.

[64] R. C. A. Chang, L. Shi, C. C. Y. Huang et al., "High-fat diet-induced retinal dysfunction," *Investigative Ophthalmology & Visual Science*, vol. 56, no. 4, pp. 2367–2380, 2015.

[65] L. Shi, A. J. Kim, R. C. A. Chang et al., "Deletion of miR-150 exacerbates retinal vascular overgrowth in high-fat-diet induced diabetic mice," *PLoS One*, vol. 11, no. 6, article e0157543, 2016.

[66] R. Robinson, V. A. Barathi, S. S. Chaurasia, T. Y. Wong, and T. S. Kern, "Update on animal models of diabetic retinopathy: from molecular approaches to mice and higher mammals," *Disease Models & Mechanisms*, vol. 5, no. 4, pp. 444–456, 2012.

[67] R. Rajagopal, G. W. Bligard, S. Zhang, L. Yin, P. Lukasiewicz, and C. F. Semenkovich, "Functional deficits precede structural lesions in mice with high-fat diet-induced diabetic retinopathy," *Diabetes*, vol. 65, no. 4, pp. 1072–1084, 2016.

[68] M. Ibrahim, P. Turkcuoglu, R. Channa et al., "Retinal and choroidal manifestations in bartonellosis, Lyme disease, and syphilis," in *Retinal and Choroidal Manifestations of Selected Systemic Diseases*, pp. 105–137, Springer, 2013.

[69] J. Suarez, Y. Hu, A. Makino, E. Fricovsky, H. Wang, and W. H. Dillmann, "Alterations in mitochondrial function and cytosolic calcium induced by hyperglycemia are restored by mitochondrial transcription factor A in cardiomyocytes," *American Journal of Physiology-Cell Physiology*, vol. 295, no. 6, pp. C1561–C1568, 2008.

[70] C. C. Lo, S. H. Lin, J. S. Chang, and Y. W. Chien, "Effects of melatonin on glucose homeostasis, antioxidant ability, and adipokine secretion in ICR mice with NA/STZ-induced hyperglycemia," *Nutrients*, vol. 9, no. 11, 2017.

[71] G. Özdemir, Y. Ergün, S. Bakariş, M. Kılınç, H. Durdu, and E. Ganiyusufoğlu, "Melatonin prevents retinal oxidative stress and vascular changes in diabetic rats," *Eye*, vol. 28, no. 8, pp. 1020–1027, 2014.

[72] S. Mehrzadi, M. Motevalian, M. Rezaei Kanavi, I. Fatemi, H. Ghaznavi, and M. Shahriari, "Protective effect of melatonin in the diabetic rat retina," *Fundamental & Clinical Pharmacology*, vol. 32, no. 4, pp. 414–421, 2018.

[73] J. Diaz-Juarez, J. Suarez, F. Cividini et al., "Expression of the mitochondrial calcium uniporter in cardiac myocytes improves impaired mitochondrial calcium handling and metabolism in simulated hyperglycemia," *American Journal of Physiology-Cell Physiology*, vol. 311, no. 6, pp. C1005–C1013, 2016.

[74] B. Bojková, P. Orendáš, L. Friedmanová et al., "Prolonged melatonin administration in 6-month-old Sprague-Dawley rats: metabolic alterations," *Acta Physiologica Hungarica*, vol. 95, no. 1, pp. 65–76, 2008.

[75] E. Peschke, S. Wolgast, I. Bazwinsky, K. Ponicke, and E. Muhlbauer, "Increased melatonin synthesis in pineal glands of rats in streptozotocin induced type 1 diabetes," *Journal of Pineal Research*, vol. 45, no. 4, pp. 439–448, 2008.

[76] P. M. Martin, P. Roon, T. K. Van Ells, V. Ganapathy, and S. B. Smith, "Death of retinal neurons in streptozotocin-induced diabetic mice," *Investigative Ophthalmology & Visual Science*, vol. 45, no. 9, pp. 3330–3336, 2004.

[77] R. A. Feit-Leichman, R. Kinouchi, M. Takeda et al., "Vascular damage in a mouse model of diabetic retinopathy: relation to neuronal and glial changes," *Investigative Ophthalmology & Visual Science*, vol. 46, no. 11, pp. 4281–4287, 2005.

[78] G. Tosini and M. Menaker, "The clock in the mouse retina: melatonin synthesis and photoreceptor degeneration," *Brain Research*, vol. 789, no. 2, pp. 221–228, 1998.

[79] M. L. Dubocovich, M. A. Rivera-Bermudez, M. J. Gerdin, and M. I. Masana, "Molecular pharmacology, regulation and function of mammalian melatonin receptors," *Frontiers in Bioscience*, vol. 8, no. 4, pp. d1093–d1108, 2003.

[80] G. Costa, T. Pereira, A. M. Neto, A. J. Cristóvão, A. F. Ambrósio, and P. F. Santos, "High glucose changes extracellular adenosine triphosphate levels in rat retinal cultures," *Journal of Neuroscience Research*, vol. 87, no. 6, pp. 1375–1380, 2009.

[81] D. Sebastian, M. I. Hernandez-Alvarez, J. Segales et al., "Mitofusin 2 (Mfn2) links mitochondrial and endoplasmic reticulum function with insulin signaling and is essential for normal glucose homeostasis," *Proceedings of the National Academy of Sciences of the United States of America*, vol. 109, no. 14, pp. 5523–5528, 2012.

[82] M. Li, H. Pi, Z. Yang et al., "Melatonin antagonizes cadmium-induced neurotoxicity by activating the transcription factor EB-dependent autophagy-lysosome machinery in mouse neuroblastoma cells," *Journal of Pineal Research*, vol. 61, no. 3, pp. 353–369, 2016.

[83] A. I. Tarasov, F. Semplici, M. A. Ravier et al., "The mitochondrial Ca^{2+} uniporter MCU is essential for glucose-induced ATP increases in pancreatic β-cells," *PLoS One*, vol. 7, no. 7, article e39722, 2012.

[84] J. Suarez, F. Cividini, B. T. Scott et al., "Restoring mitochondrial calcium uniporter expression in diabetic mouse heart improves mitochondrial calcium handling and cardiac function," *Journal of Biological Chemistry*, vol. 293, no. 21, pp. 8182–8195, 2018.

[85] G. Szabadkai, A. M. Simoni, K. Bianchi et al., "Mitochondrial dynamics and Ca^{2+} signaling," *Biochimica et Biophysica Acta (BBA) - Molecular Cell Research*, vol. 1763, no. 5-6, pp. 442–449, 2006.

[86] R. A. Kowluru and M. Mishra, "Therapeutic targets for altering mitochondrial dysfunction associated with diabetic retinopathy," *Expert Opinion on Therapeutic Targets*, vol. 22, no. 3, pp. 233–245, 2018.

[87] A. Sánchez-Bretaño, K. Baba, U. Janjua, I. Piano, C. Gargini, and G. Tosini, "Melatonin partially protects 661W cells from H_2O_2-induced death by inhibiting Fas/FasL-caspase-3," *Molecular Vision*, vol. 23, pp. 844–852, 2017.

[88] M. I. Masana, P. A. Witt-Enderby, and M. L. Dubocovich, "Melatonin differentially modulates the expression and function of the hMT_1 and hMT_2 melatonin receptors upon prolonged withdrawal," *Biochemical Pharmacology*, vol. 65, no. 5, pp. 731–739, 2003.

[89] R. S. MacKenzie, M. A. Melan, D. K. Passey, and P. A. Witt-Enderby, "Dual coupling of MT_1 and MT_2 melatonin receptors to cyclic AMP and phosphoinositide signal transduction cascades and their regulation following melatonin exposure," *Biochemical Pharmacology*, vol. 63, no. 4, pp. 587–595, 2002.

[90] C. Venegas, J. A. García, G. Escames et al., "Extrapineal melatonin: analysis of its subcellular distribution and daily fluctuations," *Journal of Pineal Research*, vol. 52, no. 2, pp. 217–227, 2012.

[91] X. Wang, A. Sirianni, Z. Pei et al., "The melatonin MT1 receptor axis modulates mutant huntingtin-mediated toxicity," *The Journal of Neuroscience*, vol. 31, no. 41, pp. 14496–14507, 2011.

[92] Y. Suofu, W. Li, F. G. Jean-Alphonse et al., "Dual role of mitochondria in producing melatonin and driving GPCR signaling to block cytochrome c release," *Proceedings of the National Academy of Sciences of the United States of America*, vol. 114, no. 38, pp. E7997–E8006, 2017.